CHARACTERIZATION OF THE STRUCTURAL CHANGES IN HOT ROLLED AND ANNEALED IRON ALUMINIDE BASE ALLOYS

A Thesis Submitted
in Partial Fulfillment of the Requirements
for the Degree of
MASTER OF TECHNOLOGY

by

PIYUSH SRIVASTAVA

to the

DEPARTMENT OF MATERIALS AND METALLURGICAL ENGINEERING
INDIAN INSTITUTE OF TECHNOLOGY, KANPUR
FEBRUARY, 1996

MME-1996-M-SRI-CHA

CERTIFICATE

This is to certify that the work contained in the thesis entitled "**CHARACTERIZATION OF THE STRUCTURAL CHANGES IN HOT ROLLED AND ANNEALED Fe_3Al BASE ALLOYS**" by **Piyush Srivastava**, has been carried out under my supervision and that this work has not been submitted elsewhere for a degree.

(Prof. R. K. Ray)
Materials & Metallurgical Engg. Dept.
Indian Institute of Technology
Kanpur

ACKNOWLEDGEMENT

I express my sincere gratitude to Professor R.K. Ray for his valuable guidance, unbounded willingness to cooperate and constant encouragement throughout the course of present work.

I am also thankful to Prof. S. Bhargava for his help at various stages of experiment.

Help of various kinds rendered by Dr.S. Ghosh Chowdhury, Mr. S. Suwas, Mr. B. Bhattacharya, Mr. H. C. Srivastava and Dr. R. R. Nagarajan is gratefully acknowledged.

I would like to thank my friends Sanjeev Kumar Shukla, Neeraj Mathur and Bhanu Pratap Srivastava for their help in the experimental work. Thanks are owed to all my friends whose company and affection I have got during my stay.

Last but not the least, thanks are due to Mr. K. P. Mukherjee, Mr. P. K. Paul, Mr. Umashanker Singh, Mr. K. K. Malhotra, Mr. Awasthi, Dr. M.N. Mangole, Mr. Srivastava and all other technical staff for their assistance at various stages of my work.

PIYUSH SRIVASTAVA

ABSTRACT

Three alloys with composition Fe - 28% Al, Fe - 28% Al - 5% Cr and Fe - 28% Al - 5% Cr - 5% Zr - 0.05% C were subjected to controlled hot rolling. These were further subjected to various annealing treatments. Both the as hot rolled as well as the annealed alloys were characterised using various techniques namely XRD, DSC, SEM and optical microscopy. While Fe - 28% Al and Fe - 28% Al - 5% Cr alloys are single phase materials, Fe - 28% Al - 5% Cr - 5% Zr - 0.05% C alloy has a dual phase microstructure. Addition of Zr to the Fe - Al - Cr base alloy to the formation of the Fe_3Zr phase. Zr addition also seems to have strong grain refining effect on the base alloy. Recrystallization in all three alloys begins at around 550^{o}C. Annealing treatment do not appear to remove the through - thickness anisotropy which is present in the alloys right from the hot rolling stage. They are found only to change the nature of this anisotropy. The least amount of anisotropy is obtained in case of the Fe - 28% Al - 5% Cr alloy in both as hot rolled as well as annealed conditions follwed by air cooling.

CONTENTS

CHAPTER		PAGE
I.	**INTRODUCTION**	1
II.	**LITERATURE REVIEW**	
	2.1 Iron Aluminides: A General Survey	4
	2.1.1 Improving Room Temp. Ductility	4
	2.1.2 Improving High Temp. Strength	8
	2.1.3 Commercialization of Iron Aluminides	11
	2.2 Fe - Al System	14
	2.3 Fe - Al - Cr System	16
	2.4 Fe - Al - Zr System	16
	2.5 Mechanical Properties of Fe_3Al Alloys.	16
	2.5.1 Effect of Cr Addition	31
	2.5.2 Rolling Texture in Fe-Al-Cr Alloy	31
	2.5.3 Effect of Zr Addition alongwith Cr	32
III.	**EXPERIMENTAL PROCEDURE**	
	3.1 Materials and Initial Treatments	36
	3.2 Heat Treatment	38
	3.3 Specimen Preparation	38
	3.3.1 For X-ray Analysis	38
	3.3.2 For Optical Microscopy	38
	3.3.3 For SEM	39
	3.3.4 For Differential Scanning Chalorimetry	39
	3.4 Characterization Methods	39
	3.4.1 X-ray Diffraction	39
	3.4.2 Microscopy (Optical and SEM)	40
	3.4.3 Differential Scanning Chalorimetry	40

CHAPTER		PAGE
IV.	**RESULTS**	
	4.1 Results of Optical Microscopy	42
	4.1.1 Fe-28% Al Alloy	42
	4.1.2 Fe-28% Al-5% Cr Alloy	47
	4.1.3 Fe-28% Al-5% Cr-5% Zr-0.05% C Alloy	47
	4.2 Results of X-ray Studies	57
	4.2.1 Standard X-ray Diffraction tables for Fe_3Al, FeAl, Fe_3Zr and α-Fe.	57
	4.2.2 X-ray Diffraction Tables for Alloys subjected to heat treatments at 400°C, 600°C, 800°C and 950°C respectively for 1 hour (only rolling plane)	59
	4.2.3 Fe-28% Al Alloy	71
	4.2.4 Fe-28% Al - 5% Cr Alloy	85
	4.2.5 Fe-28% Al-5% Cr -5% Zr-0.05% C Alloy	99
	4.3 Results of SEM and EDAX Analysis	114
	4.4 Results of Differential Scanning Chalorimetry	121
V.	**DISCUSSION**	126
VI.	**CONCLUSIONS**	131
	REFERENCES	133

LIST OF TABLES

Table		Page
1.1	Important Aluminides and their Relevant Properties.	3
2.1	Effect of Test Environment on Room-Temperature Properties of Binary Fe_3Al.	6
2.2	Potential Applications of Iron Aluminides.	13
2.3	Effect of Recrystallization on Room Temperature Tensile Properties of Fe_3Al Alloy.	28
4.1	Standard X-ray diffraction table for Fe_3Al alloy.	57
4.2	Standard X-ray diffraction table for FeAl alloy.	57
4.3	Standard X-ray diffraction table for Fe_3Zr alloy.	58
4.4	Standard X-ray diffraction table for α - Fe alloy.	58
4.5 (a-e)	X-ray diffraction tables for Fe -28% Al alloy in as received condition as well as after subjecting them to annealing treatments at 400°C, 600°C, 800°C and 950°C respectively for 1 hour (followed by air cooling).	59
4.6 (a-e)	X-ray diffraction tables for Fe-28% Al-5% Cr alloy in as received condition as well as after subjecting them to annealing treatments at 400°C, 600°C, 800°C and 950°C respectively for 1 hour (followed by air cooling).	63
4.7 (a-e)	X-ray diffraction tables for Fe - 28% Al-5% Cr - 5% Zr - 0.05% C alloy in as received condition as well as after subjecting them to annealing treatments at 00°C, 600°C, 800°C and 950°C respectively for 1 hour (followed by air cooling).	67
4.8	Tables for X-ray diffraction data for Fe-28% Al alloy on rolling plane in as received condition as well as after subjecting this alloy to various annealing treatments.	71
4.9	Tables for X-ray diffraction data for Fe-28% Alalloy on mid plane in as received condition as well as after subjecting this alloy to various annealing treatments.	75

Table		Page
4.10	Tables for X-ray diffraction data for Fe-28% Al-5% Cr alloy on rolling plane in as received condition as well as after subjecting this alloy to various annealing treatments.	85
4.11	Tables for X-ray diffraction data for Fe-28% Al-5% Cr alloy on mid plane in as received condition as well as after subjecting this alloy to various annealing treatments.	89
4.12	Tables for X-ray diffraction data for Fe-28% Al-5% Cr -5% Zr -0.05% C alloy on rolling plane in as received condition as well as after subjected this alloy to various annealing treatments.	99
4.13	Tables for X-ray diffraction data for Fe-28% Al-5% Cr -5% Zr -0.05% C alloy on mid plane in as received condition as well as after subjected this alloy to various annealing treatments.	104
4.14	Atomic percentages of various elements in the matix phase in Fe-28% Al-5% Cr-5% Zr-0.05% C alloy subjected to various annealing treatments.	118
4.15	Atomic percentages of various elements in the precipitate phase in Fe-28% Al-5% Cr-5% Zr-0.05% Calloy subjected to various annealing treatments.	119

LIST OF FIGURES

Figure		Page
2.1	Effect of Ternay Concentrations on $T_c^{DO_3\text{-}B2}$.	10
2.2	Fe - Al phase diagram.	15
2.3	Ordered Crystal Structures in Fe - Al System.	17
2.4	Ranges of Ordered α_1 and α_2 phases.	18
2.5	Variation of Order - Disorder Reaction Temperature as a function of Cr content along the Cr_3Al - Fe_3Al section.	19
2.6	Variation of Order - Disorder Reaction Temperature as a function of Cr content along the Cr_3Al - Fe_3Al section.	20
2.7	Isothermal Section at 900°C of Al-Zr- Fe System.	21
2.8	Variation of yield strength and Elongation with Aluminum Content.	24
2.9	Schematic DO_3 Superlattice Dislocations.	25
2.10	Yield Strength vs. Test Temperature for Unalloyed Fe_3Al.	26
2.11	The Dependence of the Flow Stress of Fe_3Al on Test Temperature.	26
2.12	Yield Stress vs. Temperature curves for Alloyed Fe_3Al shown with respective Alloy contents and $DO_3 \longrightarrow$ B2 Transition Temperature (T_c).	27
2.13	Charpy Impact Properties of Fe - 16at% Al based Alloys ((1) and (2)) and Fe - 28% at% Al based Alloy (3) in wrought condition.	29
2.14	True Stress - True Strain Curve for Large - grained Fe - 40% Al as a Function of Temperature.	29
2.15	Effect of Alloying additions to reduce the Environmental effect of Fe-Al Alloys.	33
2.16 (a-c)	Effect of Cr Addition on 0.2% Yield Strength, Ultimate Tensile Strength and Rupture Strength in Fe - Al Alloy.	34

Figure		Page
3.1	Figure showing dimensions of specimen used and different planes viz. RP, TP, LP etc.	37
4.1 (a-d)	Optical Micrographs of as received Fe-28% Al Alloy.	43
4.2 (a-d)	Optical Micrographs on RP of Fe - 28% Al Alloy in heat treated condition (for 1 hour).	44
4.3 (a-d)	Optical Micrographs on RP of Fe - 28% Al Alloy in heat treated condition (for 10 hours follwed by AC).	45
4.4 (a-d)	Optical Micrographs on RP of Fe - 28% Al Alloy in heat treated condition (for 10 hours follwed by WQ).	46
4.5 (a-d)	Optical Micrographs of as received Fe-28% Al-5% Cr Alloy.	48
4.6 (a-d)	Optical Micrographs on RP of Fe - 28% Al - 5% Cr Alloy in heat treated condition (for 1 hour).	49
4.7 (a-d)	Optical Micrographs on RP of Fe - 28% Al - 5% Cr Alloy in heat treated condition (for 10 hours follwed by AC).	50
4.8 (a-d)	Optical Micrographs on RP of Fe - 28% Al- 5% Cr Alloy in heat treated condition (for 10 hours follwed by WQ).	51
4.9 (a-d)	Optical Micrographs of as received Fe-28% Al- 5% Cr - 5% Zr - 0.05% C Alloy.	53
4.10 (a-d)	Optical Micrographs on RP of Fe - 28% Al - 5% Cr - 5% Zr - 0.05% C Alloy in heat treated condition (for 1 hour).	54
4.11 (a-d)	Optical Micrographs on RP of Fe - 28% Al - 5% Cr - 5% Zr - 0.05% C Alloy in heat treated condition (for 10 hours follwed by AC).	55
4.12 (a-d)	Optical Micrographs on RP of Fe - 28% Al-5% Cr - 5% Zr - 0.05% C Alloy in heat treated condition (for 10 hours follwed by WQ).	56
4.13	X-ray diffraction patterns of Fe-28% Al alloy on rolling plane in as received condition as well as in heat treated condition (for 1 hour).	61
4.14	X-ray diffraction patterns of Fe-28% Al - 5% Cr alloy on rolling plane in as received condition as well as in heat treated condition (for 1 hour).	65

Figure		Page
4.15	X-ray diffraction patterns of Fe-28% Al - 5% Cr-5% Zr - 0.05% C alloy on rolling plane in as received condition as well as in heat treated condition (for 1 hour).	70
4.16	X-ray diffraction patterns of Fe-28% Al alloy on rolling plane in as received condition as well as in heat treated condition (for 10 hours followed by AC).	79
4.17	X-ray diffraction patterns of Fe-28% Al alloy on rolling plane in as received condition as well as in heat treated condition (for 10 hours followed by WQ).	80
4.18	X-ray diffraction patterns of Fe-28% Al alloy on mid plane in as received condition as well as in heat treated condition (for 10 hours followed by AC).	81
4.19	X-ray diffraction patterns of Fe-28% Al alloy on mid plane in as received condition as well as in heat treated condition (for 10 hours followed by WQ).	82
4.20	X-ray diffraction patterns of Fe-28% Al-5% Cr alloy on rolling plane in as received condition as well as in heat treated condition (for 10 hours followed by AC).	92
4.21	X-ray diffraction patterns of Fe-28% Al-5% Cr alloy on rolling plane in as received condition as well as in heat treated condition (for 10 hours followed by WQ).	93
4.22	X-ray diffraction patterns of Fe-28% Al-5% Cr alloy on mid plane in as received condition as well as in heat treated condition (for 10 hours followed by AC).	94
4.23	X-ray diffraction patterns of Fe-28% Al-5% Cr alloy on mid plane in as received condition as well as in heat treated condition (for 10 hours followed by WQ).	95
4.24	X-ray diffraction patterns of Fe-28% Al-5% Cr- 5% Zr-0.05% C alloy on rolling plane in as received condition as well as in heat treated condition (for 10 hours followed by AC).	109

Figure		Page
4.25	X-ray diffraction patterns of Fe-28% Al-5% Cr- 5% Zr-0.05% C alloy on rolling plane in as received condition as well as in heat treated condition (for 10 hours followed by WQ).	110
4.26	X-ray diffraction patterns of Fe-28% Al-5% Cr- 5% Zr-0.05% C alloy on mid plane in as received condition as well as in heat treated condition (for 10 hours followed by AC).	111
4.27	X-ray diffraction patterns of Fe-28% Al-5% Cr- 5% Zr - 0.05% C alloy on mid plane in as received condition as well asin heat treated condition (for 10 hours followed by WQ).	112
4.28 (a,b)	Scanning Electron Micrographs of Alloys in as received condition.	115
4.29	Scanning electron micrograph showing alignment second phase particles of Fe - 28% Al -5% Cr - 5% Zr - 0.05% C alloy.	115
4.30 (a-d)	Scanning electron micrographs of annealed Fe - 28% Al - 5% Cr - 5% Zr - 0.05% C alloy samples taken on rolling plane.	116
4.31 (a-d)	Scanning electron micrographs of annealed Fe - 28% Al - 5% Cr - 5% Zr - 0.05% C alloy samples taken on mid plane.	117
4.32 (a-c)	DSC plots for all three alloys in as received condition.	123

CHAPTER I

INTRODUCTION

As a result of the recent activities on high temperature alloy development, intermetallic compounds including a number of aluminides such as those of Ni, Fe and Ti have received considerable attention. These ordered alloys possess a number of promising properties for structural applications at elevated temperatures in hostile environments. First, they are capable of forming protective oxide films which give excellent oxidation and corrosion resistance. Second, they generally possess attractive high temperature strength such as increase in yield strength with increasing temperatures (anomalous yielding behaviour). Third, they commonly have low material density and high melting point. Fourth, they are normally structurally stable because of slow diffusional processes in ordered lattices. Some of the important aluminides with their properties have been mentioned in Table 1.1.

In spite of their superiority over conventional superalloys, both costwise as well as propertywise, these aluminides have not been exploited commercially. It has been attributed to poor room temperature ductility and low high temperature strength of these aluminides. Recent studies on aluminides have been done mostly on these two accounts. It has been reported that various techniques like ternary additions (with Zr and Cr) and microalloying (with boron, carbon etc.) improve their mechanical properties to a great

extent. In addition to these, microstructural modifications via various heat treatments and rolling texture modifications are also helpful to a great extent. Currently, a great deal of research is going on to make these techniques commercially viable.

Not much work has been done to elucidate the hot rolling textures of Fe_3Al base alloys. Since these materials have a promise to be used in the sheet form, an idea of their hot rolling texture is very important to have. With this idea in mind, the present work was undertaken.

TABLE 1.1

Important Aluminides and Their Relevent Properties

Alloy	Crystal Structure	Melting Point (^{o}C)	Density g/cm^3	Yield Strength (MPa)	Young's Modulus ($\times 10^3$ MPa)
Ni_3Al	LI_2 (Ordered fcc)	1390	7.5	250-500	178.6
NiAl	B2 (Ordered bcc)	1640	5.9	250-475	294.4
Fe_3Al	DO_3 (Ordered bcc)	1540	6.7	385-392	140.7
FeAl	B2 (Ordered bcc)	1250	5.6	360-380	260.6
Ti_3Al	DO_{19} (Ordered hcp)	1600	4.2	700-990	144.8
TiAl	LI_o (Ordered tetragonal)	1460	3.9	400-650	175.8

CHAPTER II

LITERATURE REVIEW

2.1 IRON ALUMINIDES : A GENERAL SURVEY

Iron aluminides have been of interest since 1930's when their excellent oxidation resistance was first noted (due to protective layer of Al_2O_3). However development of these alloys have been limited. It is due to:

a) poor room temperature ductility and brittle fracture,

b) low high temperature strength and fracture toughness.

2.1.1 Improving Room Temperature Ductility

Possible causes of brittleness in intermetallics include:

i) Insufficient number of deformation modes

ii) High yield strength or hardness due to difficulty in generation and glide of dislocation

iii) Poor cleavage strength or low surface energy

iv) Planar slip and localized deformation

v) High strain rate sensitivity (which promotes brittle crack propagation at crack tips), and

vi) Grain boundary "weakness", a classic example of this is Ni_3Al which is ductile in single crystal form and brittle in polycrystalline form.

A key question that arises here is whether the brittleness in ordered intermetallics results from intrinsic factors or it results from extrinsic factors. Earlier it was thought that Fe_3Al alloys are intrinsically brittle. However, it has been pointed out

that interaction of H_2O vapour in air with Al in the alloy is a major contributor to low room temperature ductility of Fe_3Al and FeAl alloys. The extent of environmental effect on binary Fe_3Al is illustrated in Table 2.1. Mechanism proposed for this brittleness is hydrogen embrittlement which is

$$2Al + 3H_2O \longrightarrow Al_2O_3 + 6H$$

This atomic hydrogen induces classic hydrogen embrittlement at crack tips i.e. atomic hydrogen generated at crack tip, is transported into specimen during stressing producing a brittle cleavage fracture [2]. Segregation of impurities to grain boundaries is considered unlikely to be the principal source of brittleness.

As it is well known that contact of moisture present in air with Al in aluminides leads to hydrogen embrittlement, an oil film on the specimen surface can prevent contact of moisture in air with Al on alloy surface and, thus, can reduce or eliminate the hydrogen embrittlement [1].

Apart from above, it is also established that the ordered alloy (Fe - 28% Al) is most sensitive to environmental embrittlement whereas the disordered alloy (Fe - 16% Al) is least sensitive. In case it is not possible to reduce Al content from 28%, addition of small amount of Cr leads to improvement in ductility, especially in two phase alloy containing α solid solution and ordered DO_3 phase. One possible reason for such improvement may be more uniform distribution of ductile α solid solution around each of the ordered phase particles. Further addition of small amount of grain refiners such as Zr/C leads to marginal improvement in ductility.

Table 2.1: Effect of Test Environment on Room Temperature properties of Binary Fe_3Al.

Test Environment	Elongation (%)	Strength (MPa)	
		0.2% Yield	Ultimate Tensile
Air	3.7	279	514
Vacuum (10^{-4}Pa)	12.4	316	813
Oxygen	11.7	298	888
H_2O Vapor	2.1	322	439

Ductility can also be improved by microstructural modifications. Highly elongated structure, with minimum transverse grain boundaries, is most resistant to hydrogen diffusion, resulting in its highest ductility. The increased recrystallization increases the number of transverse boundaries which increases the hydrogen diffusion and results in lower ductility.

In case of Fe_3Al alloys, it has been established that DO_3 structure is more environmentally sensitive than B2 structure. Hence,B2 structure of these alloys is more ductile [1].

Although ordering leads to reduction in ductility in FeCo - 2% V (B2 type structure) alloy, its effect is negligible in Fe_3Al alloys [3].

It is being tried to improve ductility of iron aluminides through such diverse techniques as grain refinement through thermomechanical treatments, microalloying with B and various rapid solidification techniques.

Ni_3Al when doped with B shows a lot of improvement in room temperature ductility. As original brittleness is not shown by single crystal, it was thought to be a grain boundary phenomenon. It was actually shown that B indeed segregates to the grain boundaries and dislocations can apparently propagate across the boundaries more easily in presence of Boron [19].

However grain boundaries never display their brittleness when subjected to stress. The dislocation configuration within grains have a considerable influence on how such stresses are distributed. The propagation of dislocations across the grain boundaries may also be related to the behaviour of grain boundary

dislocations. TEM studies by Yen. et. al. [19] on B doped and undoped Ni_3Al show the following prominent features in alloys containing boron:

i) Boron free alloys contain some extended dislocations

ii) Boron removes all stacking faults

iii) Improved ductility is observed in B doped Ni rich aluminides.

The relative importance of dislocation behaviour within the grains as well as at the grain boundaries is not well understood.

The effect of boron is to strengthen the grain boundaries so that it can withstand the stresses induced by a planar array of dislocations. Planar slip during deformation is a characteristic of intermetallics and ordered alloys where super lattice dislocations can be visualised as two unit dislocations that move together, separated by a strip of antiphase boundary. This unique dislocation structure implies that cross slip is restricted and thus there is less likelihood of accommodative slip processes at the grain boundaries.

2.1.2 Improving High Temperature Strength

Reducing hydrogen embrittlement by elimination of moisture i.e. using vacuum or oxygen environment leads to significant improvement in UTS [Table 2.1]. Coating with oil leads to similar effects.

Considerable efforts have been made to improve high temperature strength of iron aluminides by alloying it with ternary elements like Ti and Si and today it is well established that many ternary solutes provide this strengthening. One reason why ternary solute additions may be beneficial to high temperature

strength is that they help stabilise the DO_3 ordered structure to temperature well above 550°C (the critical temperature for DO_3 - B2 transformation $T_c^{DO_3\text{-}B2}$ in binary Fe_3Al). There is evidence for a positive correlation between solute induced increase in high temperature strength and the corresponding solute induced increase in $T_c^{DO_3\text{-}B2}$. Particularly large increases in $T_c^{DO_3\text{-}B2}$ of Fe_3Al have been reported for Ti, Si and Mo. Specifically the effect of Ti on $T_c^{DO_3\text{-}B2}$ is about 50 K/at%Ti, for Si additions in the dilute limit the increase is about 60 K/at% Si and for Mo additions the reported effects are 25, 30, 35 K/at% Mo. Situation is less clear for Cr additions. Fig. 2.1 shows effect of various alloying elements on $T_c^{DO_3\text{-}B2}$ [4].

Thus addition of 6 at% Mo and Ti in solid solution of Fe_3Al increases rupture life by six orders of magnitude at temperatures near 700°C. This increase is attributed to a large increase in activation energy for creep resulting from an increase in $T_c^{DO_3\text{-}B2}$.

Usually aluminides do not have high room temperature strength. A sharp rise in flow stress with temperature is observed during plastic deformation of most ordered alloys (particularly those with LI_2 structure e.g. Ni_3Al). However it is not possible to give single mechanism to explain the effect of alloying elements on aluminides. For example in Ni_3Al type aluminides, flow stress peak shifts towards higher temperature on alloying. In FeCo type alloy peak strength is associated with order - disorder transformation temperature and in Fe_3Al, it is related to temperature of transformation from one ordered structure to another. hardening rates compared to their disordered or partially

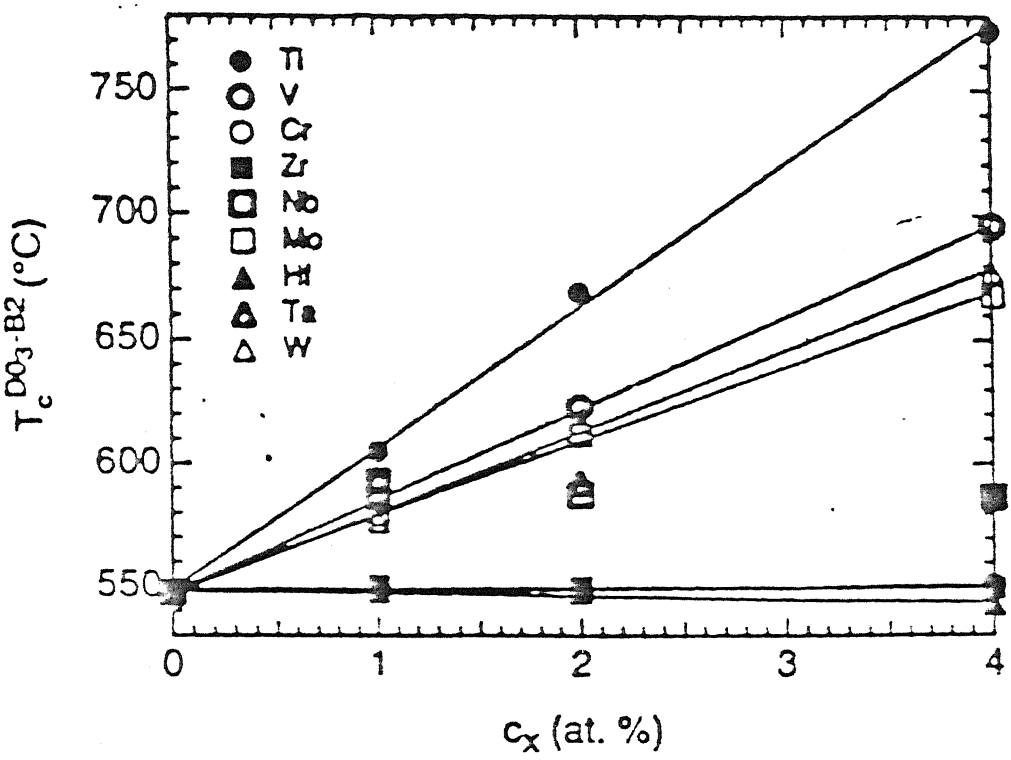

Fig. 2.1: Effect of Ternay Concentrations on $T_c^{DO_3\text{-}B2}$.

ordered counterparts can double with order at temperatures near 22°C, whereas lesser increments in rate are noted in other crystal structures. High straining rates induced by long range order may permit attainment of very high strength through cold working operations or thermomechanical treatments.

Efforts were made by Stoloff and Davies to correlate elevated temperature flow stress with long range order, but no certain trend could be observed except the fact that T_c was obtained at 550°C which corresponds to S = 0.3 where S is degree of long range order [3].

2.1.3 Commercialization of Iron Aluminides

Although iron aluminides show low RT ductility and low high temperature strength, these shortcomings can be overcome if certain precautions are followed. These shortcomings indeed have been overcome recently. Several sizes of pilot heats (7 to 230 kg) of the Fe_3Al based alloys have been melted by commercial vendors. The 2000 and 3000 kg heats are the largest heats melted by precision rolled products in Oak Ridge National Laboratory. Two iron aluminide production methods are described below, of which the first one is commercially more successful:

a) Air - melting is feasible for iron aluminide alloys. Reasonable care is needed in treating the melt charge and the selection of crucible material. Both the iron and aluminum need to be dried to minimise the generation of hydrogen because a large amount of hydrogen can be generated and dissolved in molten metal causing gas porosity in iron aluminides. Typical hydrogen levels in Fe_3Al alloy melted in air can be in the range of 3 to 4 ppm. This can be further reduced to approximately 2 ppm by blowing

argon through the melt. Vacuum melting of the alloy can yield hydrogen levels of approximately 1 ppm.

The high Al content of Fe_3Al based alloys allows excellent protection through the formation of a protective aluminum oxide slag. The aluminum oxide formation yields low levels of oxygen and nitrogen in the melt and also provides nearly 100% recovery of most of the alloying elements. Vacuum melting and electroslag remelting processes further reduce the O_2 and N_2 contents of Fe_3Al based alloys.

Melting in magnesia crucible showed a pick up of 20 ppm of Mg as opposed to 10 ppm of Mg observed in alumina crucible. The higher magnesium level, especially when segregated, can cause hot workability problems. The Mg levels can be reduced to 10 ppm by vacuum arc remelting process.

The Fe_3Al based alloys are castable into shapes by both sand and investment casting processes. The casting parameters such as type of sand, melt superheat, cooling rate and post cast treatments are not fully developed for sand castings. In case of investment castings, issues such as shell material, use of grain refiner, shell temperature, melt superheat, cooling rates and post cast heat treatments need additional work. Low room temperature ductility in the as cast condition is the primary concern in the handling and use of castings. Efforts are under way to improve the cast ductility and to find answers to some of questions raised above regarding casting process [1].

b) The other technique is called carbon deoxidation technique. Base materials of electrolytic iron and high purity pig Al are induction vacuum melted in high purity stabilised zirconia

crucible. After addition of 0.05% spectrographic carbon, the molten iron is held 10 minutes under an ultimate vacuum of 1 micron or less. The aluminum pig is added to the molten iron prior to casting into steel molds. The as cast grain size is critically dependent on pouring temperature. To minimise thermal shock and possible microcracking the ingots are stripped hot from molds and burried in vermiculite to ensure slow cooling [5].

Finally, Fe_3Al based alloys are hot workable with typical hot working temperature ranging between 900 and 1100^{o}C. The hot worked material can be warm finished at temperatures as low as 650^{o}C. The Fe - 16% Al alloys can also be cold finished with intermediate anneals at 800^{o}C. However, the Fe_3Al based alloys are not cold workable.

Potential applications of iron aluminides have been given in Table 2.2 [1].

Table 2.2: Potential Applications of Iron Aluminides.

Application	Component System
Heating elements	Toasters, stoves, ovens, cigarette lighters, and dryers.
Wrapping wire	Insulation wrapping for investment casting molds.
Regenerator disks	Automotive gas-turbine engines.
Hot-gas filters	Coal-gasification systems.
Tooling	Dies for superplastic forming of titanium-based alloys.
Shields	Coal-fired power plants to protect the superheater and reheater tubes.
Automotive	Exhaust manifolds, catalytic converters, and exhaust support hangers.
Molten metals	Sensor sheathing material for molten aluminum, zirconium, and cadmium.
Others	Components needing high-temperature sulfidation and oxidation resistance

2.2 THE IRON - ALUMINUM SYSTEM

The Fe-Al system has been depicted in Fig. 2.2. It has wide α-Fe range with maximum solubility of Al in Fe being 44% (approximately) at 1310^{o}C. At room temperature, this value corresponds to 18% (atomic %). Apart from α-Fe, it has various stable phases Fe_3Al, FeAl, $FeAl_2$, Fe_2Al_5 and $FeAl_3$ etc. of which the last three have a very small composition range. Out of all these phases, only $\alpha 2$ (or B2) and DO_3 ordered phases are of interest to us which have stoichiometric compositions FeAl and Fe_3Al respectively. γ-Fe and ϵ-phase having extremely small composition range are also formed. Direct transition from α-Fe to $\alpha 2$ (or B2) phase is possible over temperature range 612^{o}C to 1310^{o}C and composition range 22% to 45% Al. Similarly it can also be observed from this diagram that direct transition from B2 to DO_3 phase is possible over temperature range 200^{o}C to 552^{o}C and composition range 25% to 36% Al. From phase diagram, we get the following phases which are of interest to us:

i) Disordered solid solution α

ii) FeAl with an imperfectly ordered B2 structure

iii) Fe_3Al with perfectly ordered DO_3 structure

iv) Two phase regions α + DO_3 and α + B2

v) Three phase region α + B2 + DO_3.

From the crystal structures of B2 and DO_3 unit cells, we can observe that B2 structure of FeAl can be formed by ordering among nearest neighbours of α-phase. A further ordering among second nearest neighbour atoms produces the Fe_3Al phase (DO_3 structure) with a unit cell having twice the α-lattice parameter. DO_3 structure consists of 8 BCC unit cells which have 4 atoms of Al

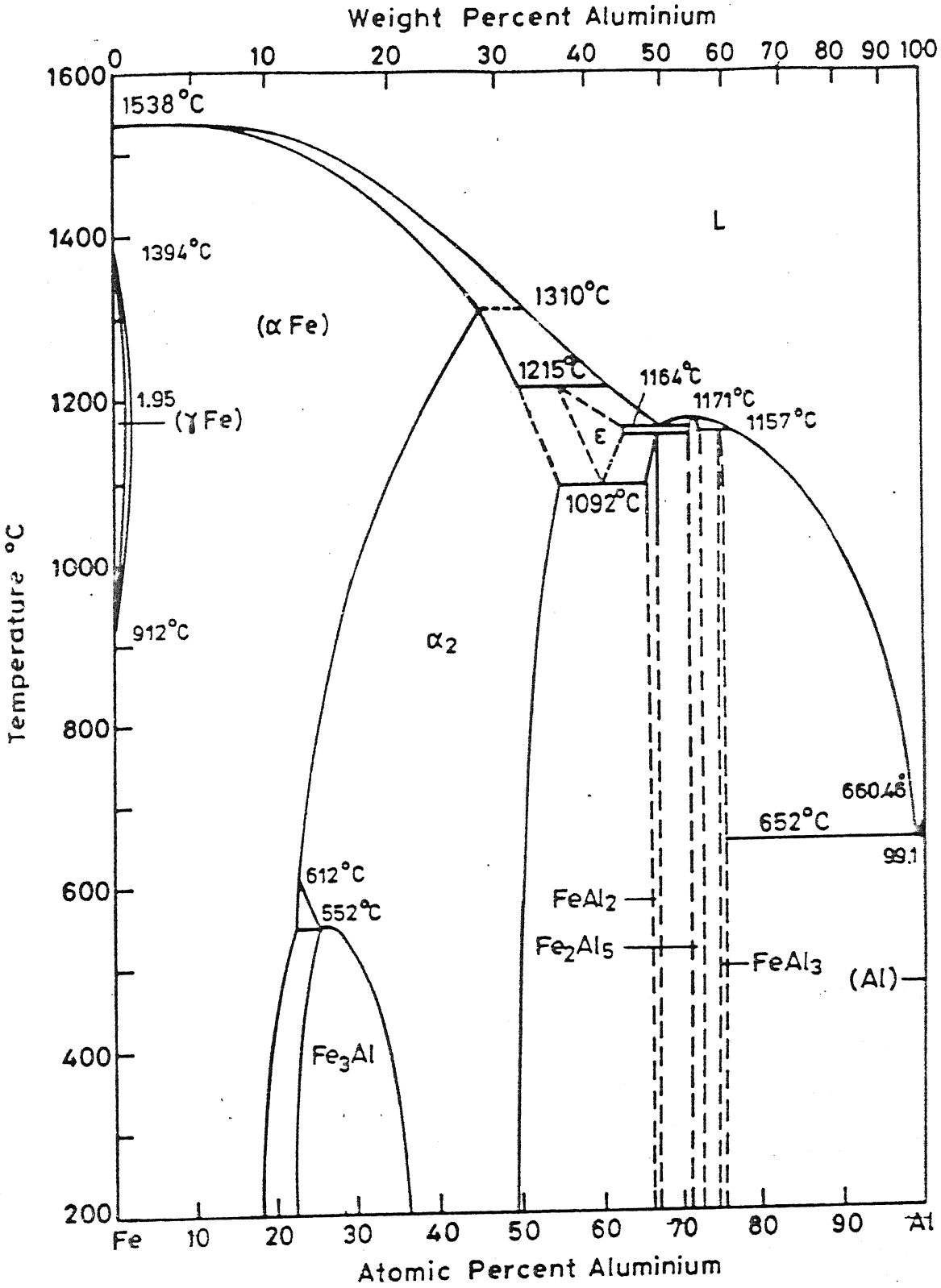

Fig. 2.2: Fe - Al phase diagram.

and 12 of Fe [Fig.2.3]. Disordered lattice is BCC while ordered one is FCC structure owing to tetrahedral arrangement of Al atoms. B2 unit cell have 8 corner atoms of one type and one central atoms of other type.

2.3 THE IRON - ALUMINUM - CHROMIUM SYSTEM

Fe - Al - Cr forms a ternary system. Sections of ternary phase diagram, which are of interest to us, are shown in Fig. 2.4, 2.5 and 2.6. Fig. 2.4 shows ranges of ordered $\alpha_1(Fe_3Al)$ and $\alpha_2(FeAl)$ phases while Fig.2.5 and 2.6 shows variation of order disorder temperature as a function of chromium content along the Cr_3Al - Fe_3Al section [20].

2.4 The Iron - Aluminum - Zirconium System:

Figure 2.7 shows isothermal section of ternary Fe - Al - Zr system at $900^{O}C$. Figure shows ranges of various phases viz. ZrAl, Zr_2Al_3, $ZrAl_2$, αZr, $Zr_{18}Fe_{59}Al_{23}$ etc. [21].

2.5 MECHANICAL PROPERTIES OF IRON - ALUMINUM ALLOYS

Various mechanical properties of iron aluminides based on Fe_3Al have been examined. From Fig.2.8 in which yield strength and elongation are plotted as a function % Al, it can be observed that yield strength maximum and ductility minimum are obtained near the stoichiometric composition of Fe_3Al. Kubaschewski [22] has shown that deformation mode of Fe - Al alloys changes from $\frac{1}{4}$ a_o<111> ordinary dislocations to superlattice paired dislocations of type $\frac{1}{4}$ a_o<111> in 24 - 28 at % Al range i.e. as Al content increases from 28%, latter type deformation mode prevails while if Al content is less than 24% it is the former that prevails. A schematic representation of possible DO_3 superlattice dislocations

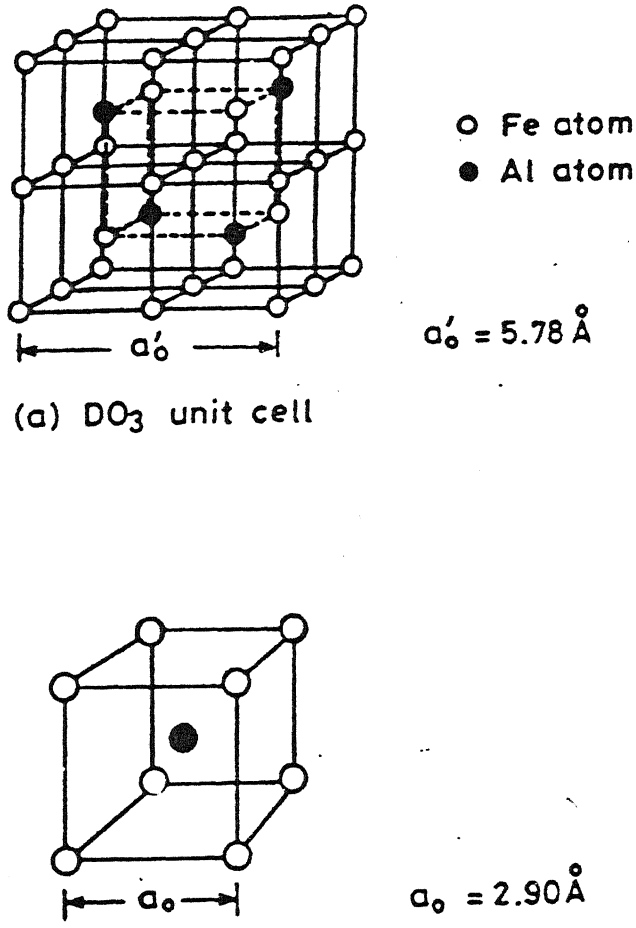

Fig. 2.3: Ordered Crystal Structures in Fe - Al System.

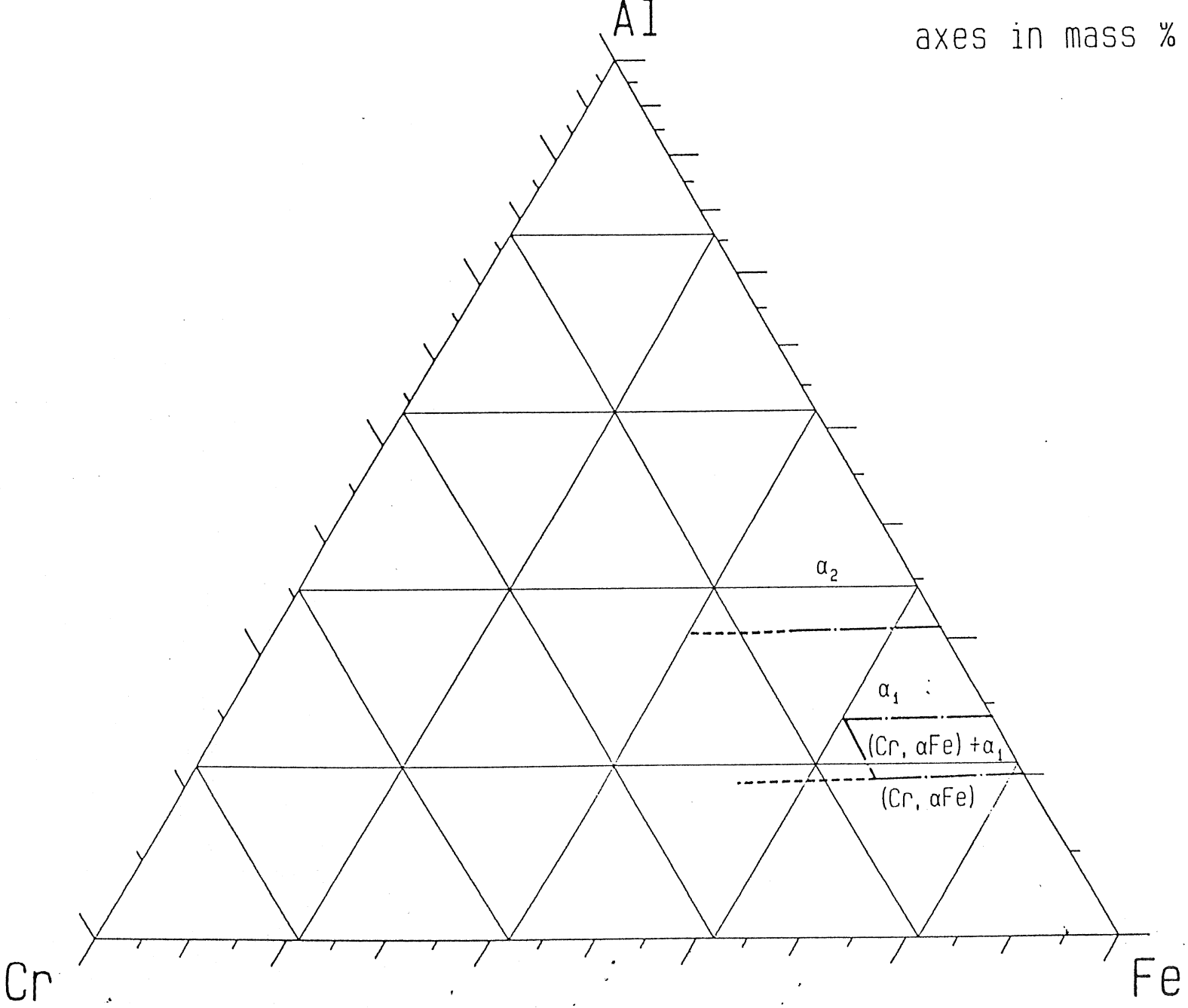
Al
axes in mass %
Cr
Fe
α_2
α_1
(Cr, αFe) + α_1
(Cr, αFe)

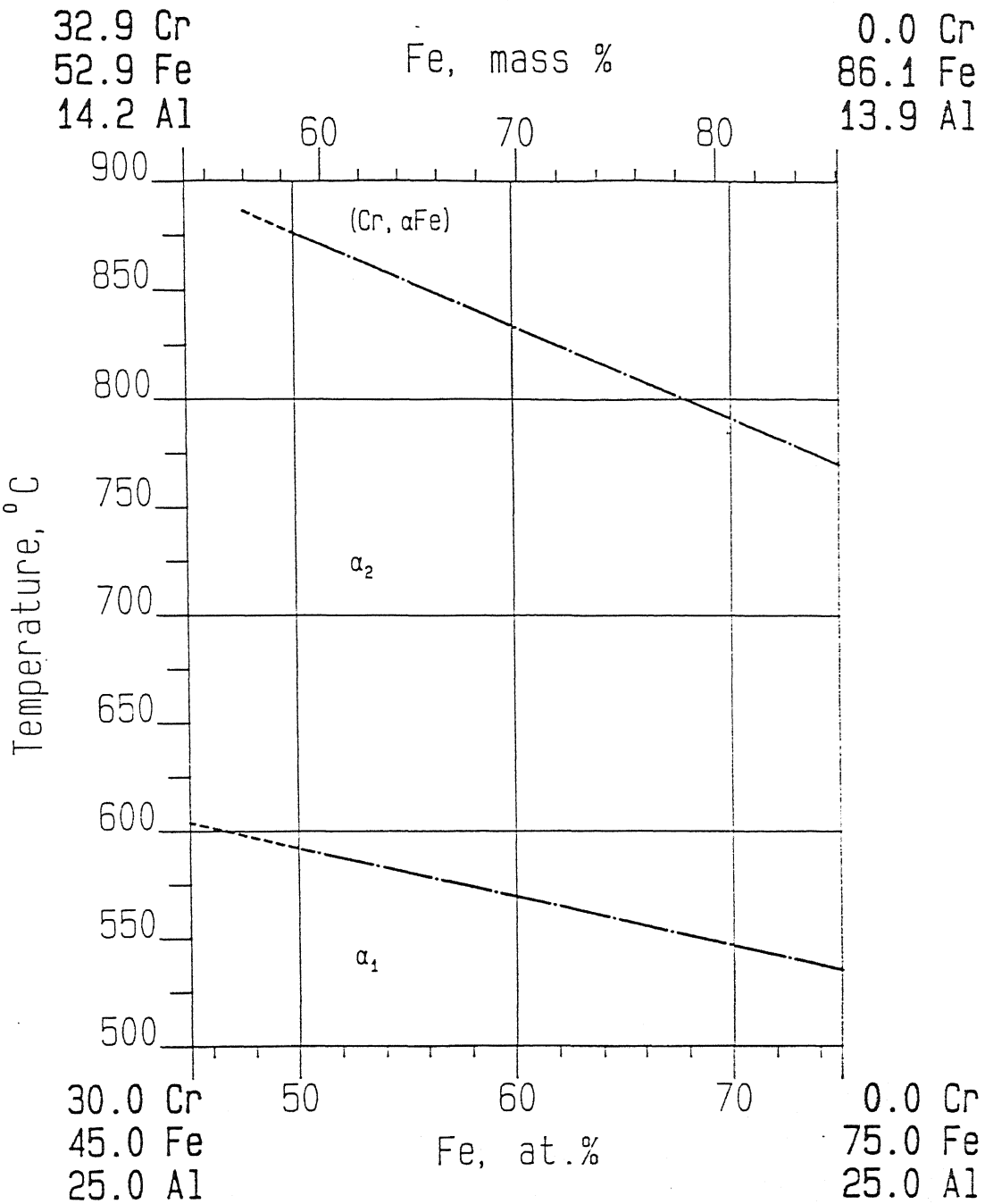

Fig. 2.5: Variation of Order - Disorder Reaction Temperature as a function of Cr content along the Cr_3Al - Fe_3Al section.

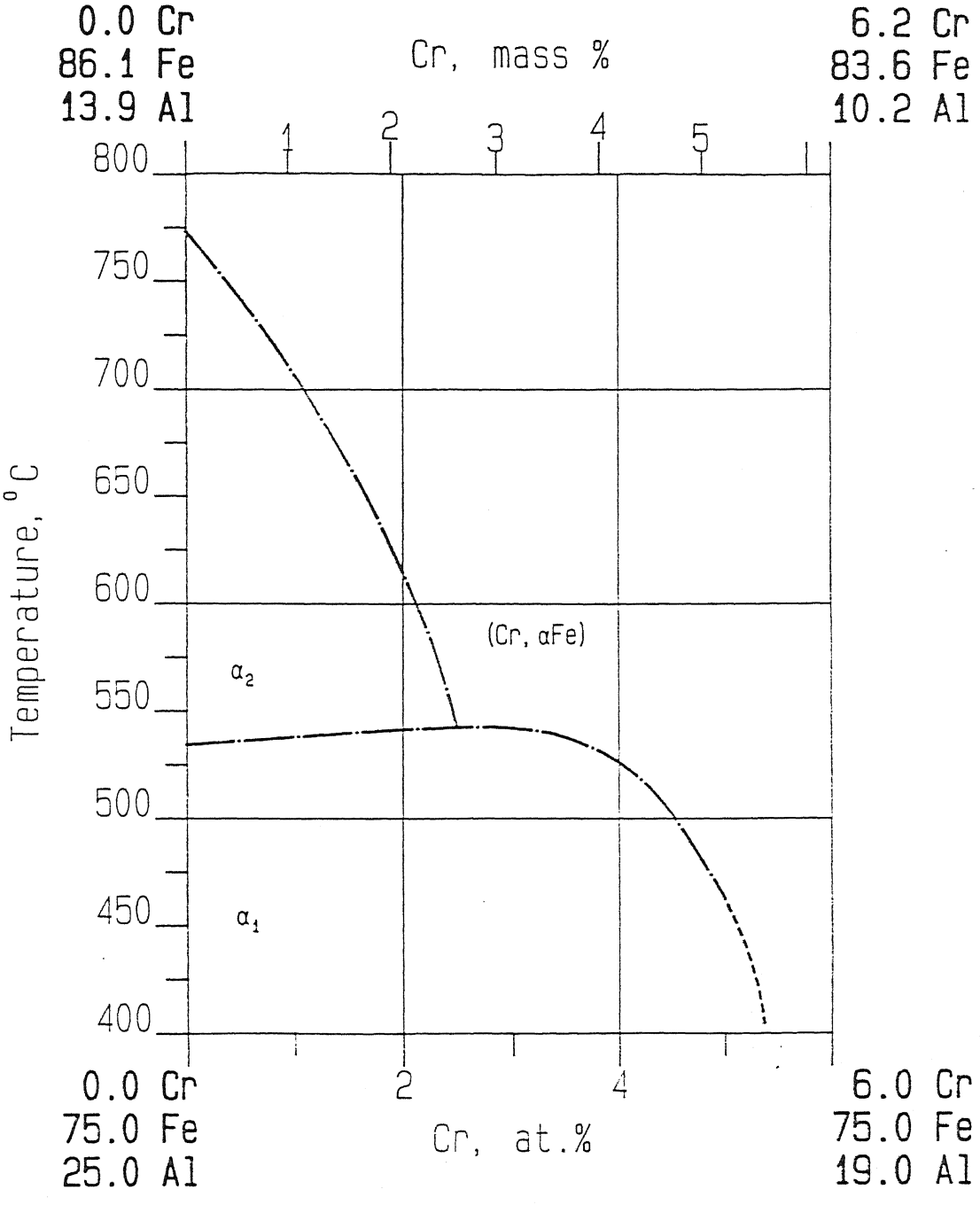

Fig. 2.6: Variation of Order - Disorder Reaction Temperature as a function of Cr content along the Cr_3Al - Fe_3Al section.

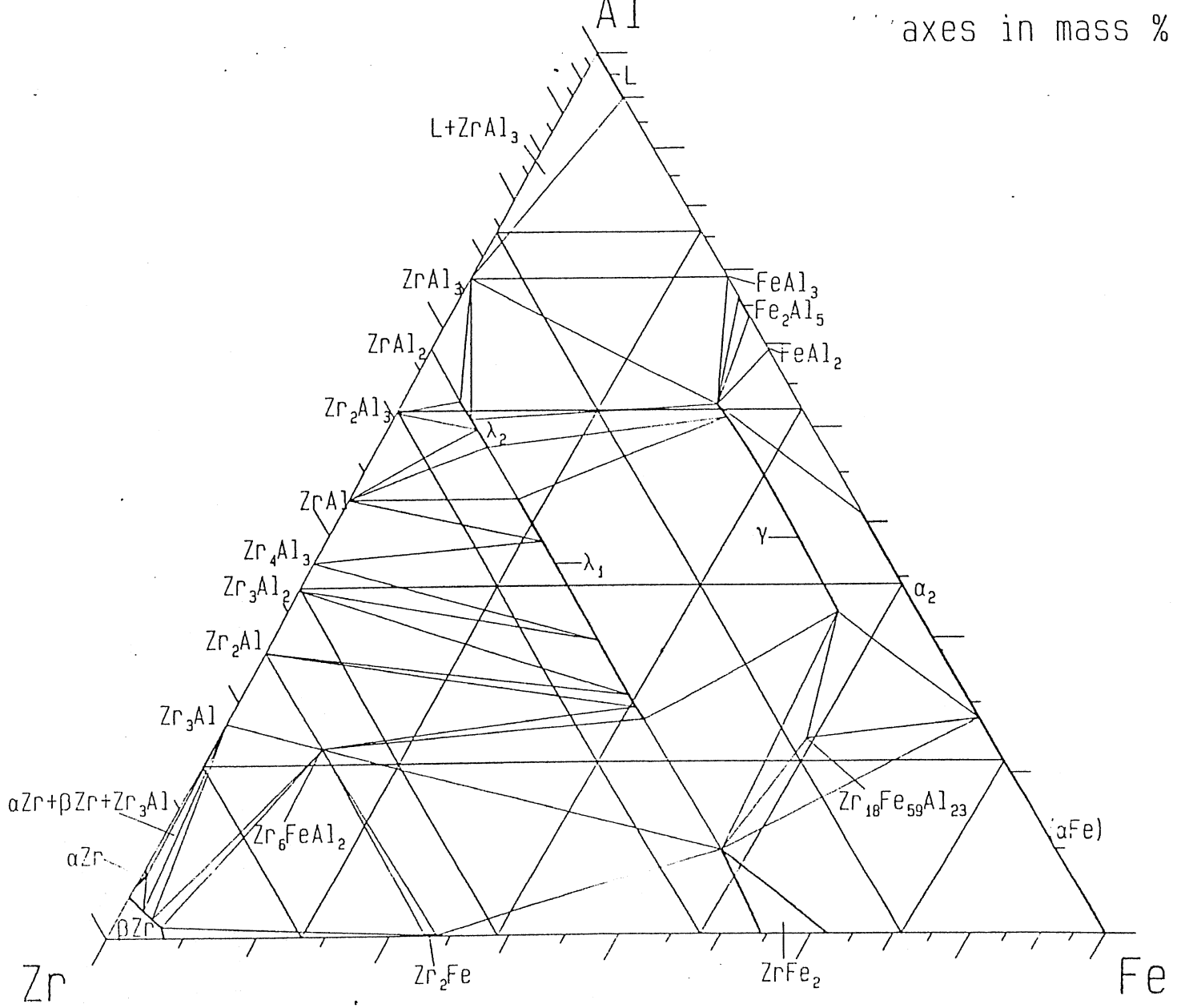

Fig. 2.7: Isothermal Section at 900°C of Al-Zr- Fe System.

and their imperfect variants is shown in Fig.2.9 [23]. In this figure ordinary dislocation of Type (e) and (f) which leave behind NNAPB and NNNAPB trails, predominate in room temperature deformation of alloys with less than 26% Al. Superlattice dislocation of type (b), which are associated with NNNAPB's only, and consists of two dislocation components and not four, are responsible for deformation in higher aluminum alloys. These observations have also been confirmed by various others including Marcinkowski [24] apart from Mendiratta et.al. [23].

The transition from higher yield strength value at 26% Al to lower one at 27% Al can be explained from the Fe - Al phase diagram. At 500^{o}C, this range of Al corresponds to boundary between DO_3 and α + DO_3 phase fields. As we move towards lower values of Al (less than 26%), we will end up in α + DO_3 region. Age hardening effect of α precipitated in DO_3 phase during ordering treatment at 500^{o}C is responsible for higher yield strength values at lower Al content alloys [27]. Higher yield strength of lower Al content alloys is caused by low mobility of dislocations coupled closely with APB's. Above 26 at%Al, the APB energy of <111> fault vector increases substantially and deformation is, therefore, by tightly coupled superlattice dislocations.

Variation of ductility vs. %Al is in reverse fashion to that of variation of yield strength i.e. ductility increases as atomic % of Al increases

Fig. 2.10 [31,6] given variation of yield strength with test temperature for four alloys having Al content 24%, 28%, 30% and 40% respectively. Behaviour at 24% Al is distinctly different from

that at 28 and 30% Al. As explained earlier, higher ambient strength of Fe - 24% Al is attributed to age hardening effect of α precipitates in DO_3 matrix. A distinct feature of Fe - (28 - 40)% Al is anomalous strength peak at around 550^{o}C which corresponds to second order transformation temperature from DO_3 to B2. This type of yield behaviour has been observed in many other ordered systems including CuZr [33], FeCo [34] etc. In Fe_3Al alloys, peak strength is associated with degree of long range order. Critical value of long range parameter S is found to be 0.5 irrespective of DO_3 to B2 transformation temperature. This has been shown by Handa et.al. [32] and Stoloff. et.al (Fig.2.11 9 [3]). DO_3 to B2 transformation temperature and correspondingly strength level improves with alloying (especially of Mo and Ti).This is obvious from Fig.2.12 [25,26].

McKamey et. al. [2] have studied the effect of recrystallization on strength (yield as well as fracture) and ductility. Results are summarized in Table 2.3. Increasing degree of recrystallization is associated with decreasing yield stress, fracture stress and elongation values.

Room temperature toughness is shown to decrease with increasing Al content. This have been shown by Charpy - impact energy versus temperature curve [Fig.2.13]. Micro addition of Y is also shown to improve charpy impact energy. McKamey [34] has reported improvement in the creep properties by alloying with Mo and B. Rupture life of 57.4 hours as compared to 1.6 hours for unalloyed Fe_3Al and percentage creep elongation of 24.9 as compared to 33.6 (tested at 207 MPa, 593^{o}C). Reduction in Carbon percentage is reported to increase impact resistance[5].

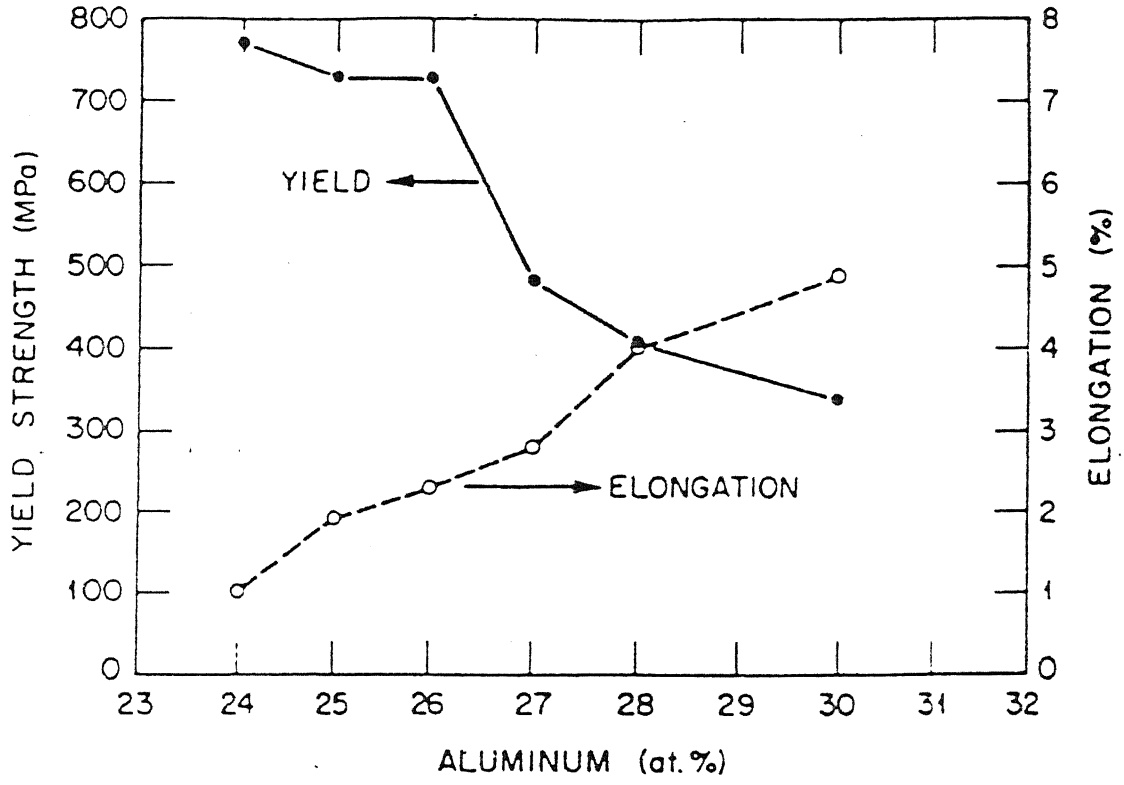

Fig. 2.8: Variation of yield strength and Elongation with Aluminum Content.

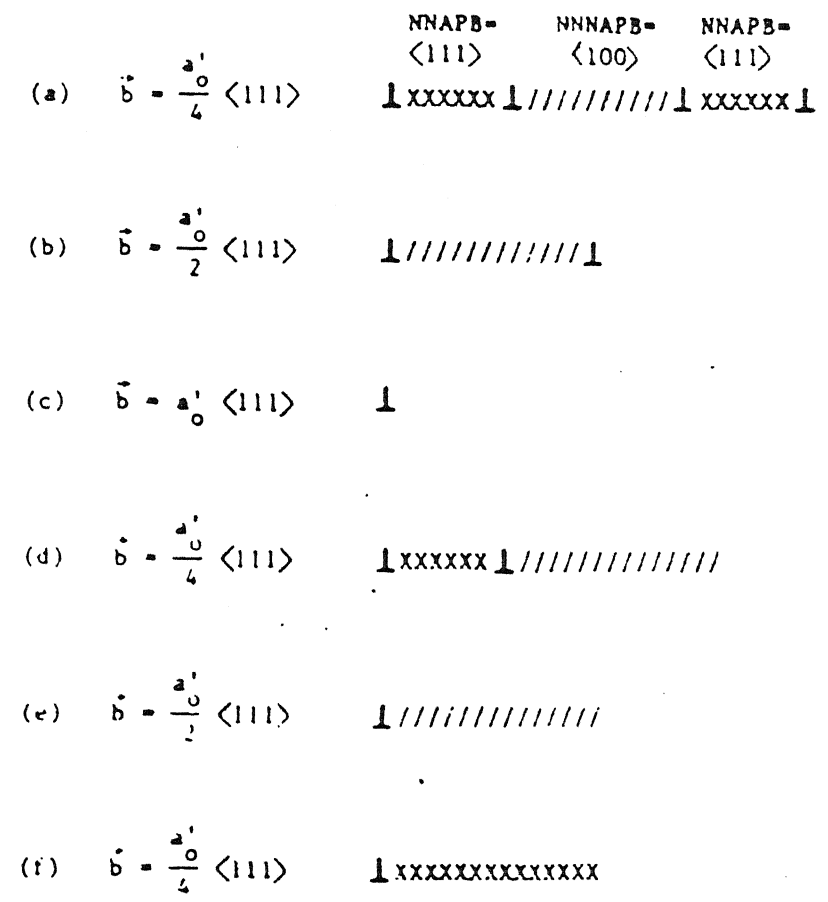

Fig. 2.9: Schematic DO_3 Superlattice Dislocations.

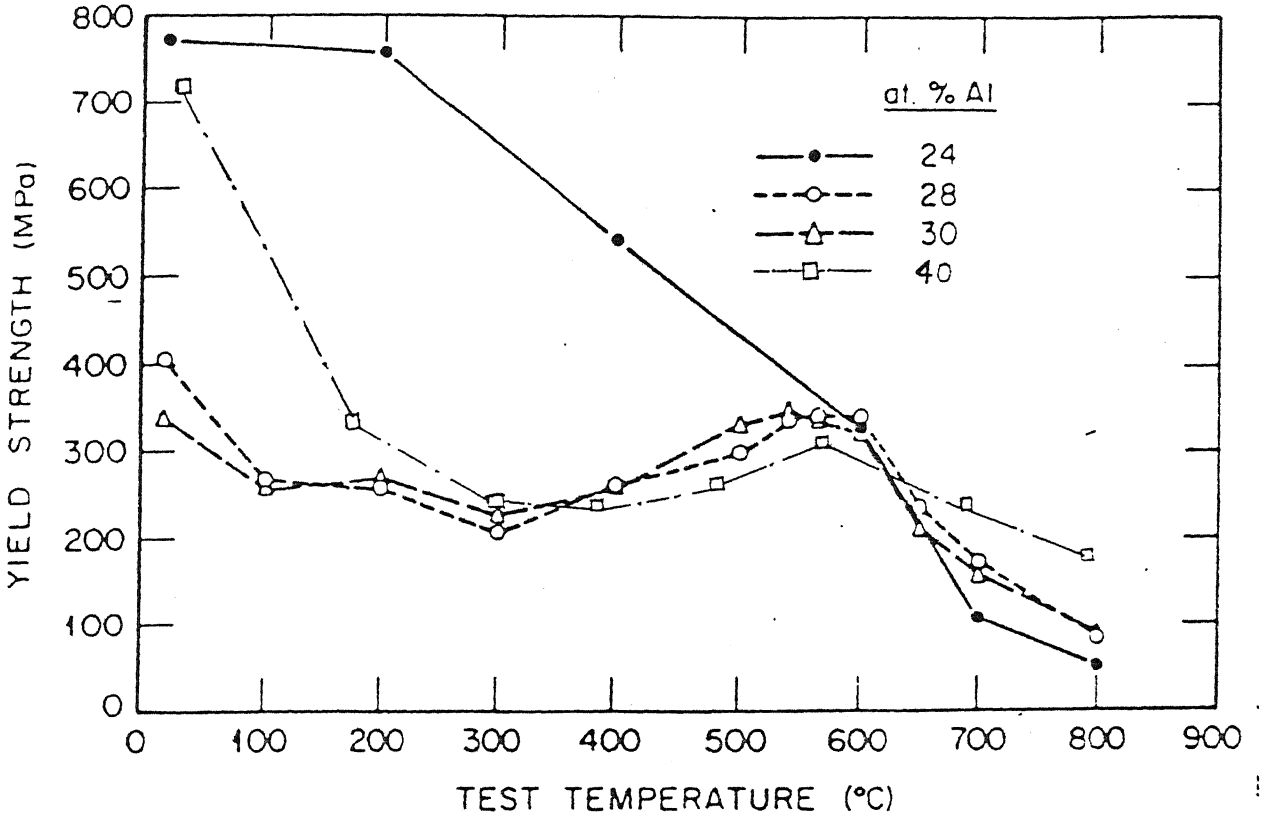

Fig. 2.10: Yield Strength vs. Test Temperature for Unalloyed Fe_3Al.

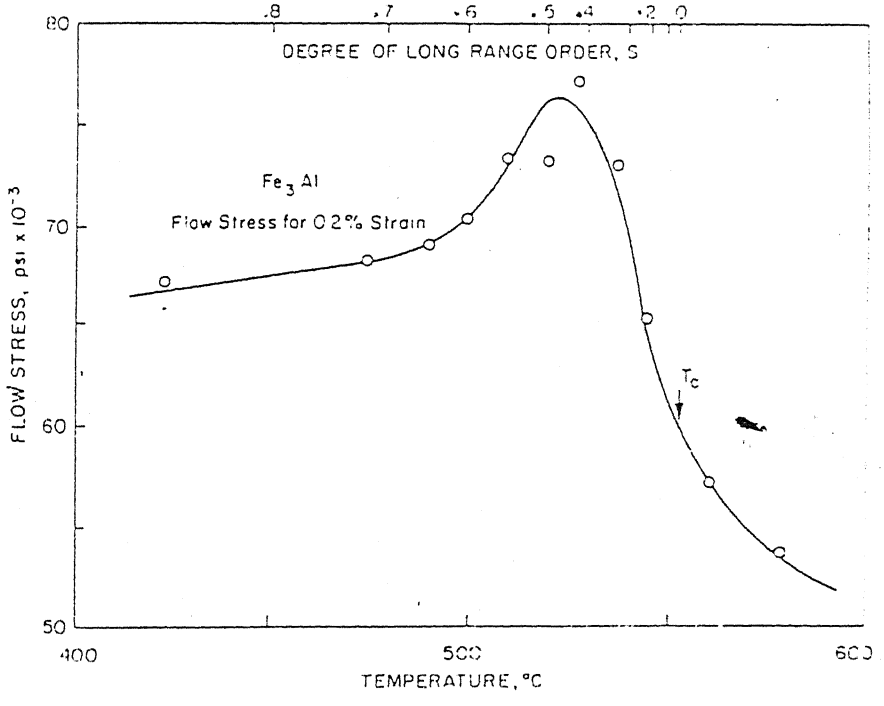

Fig. 2.11: The Dependence of the Flow Stress of Fe_3Al on Test Temperature.

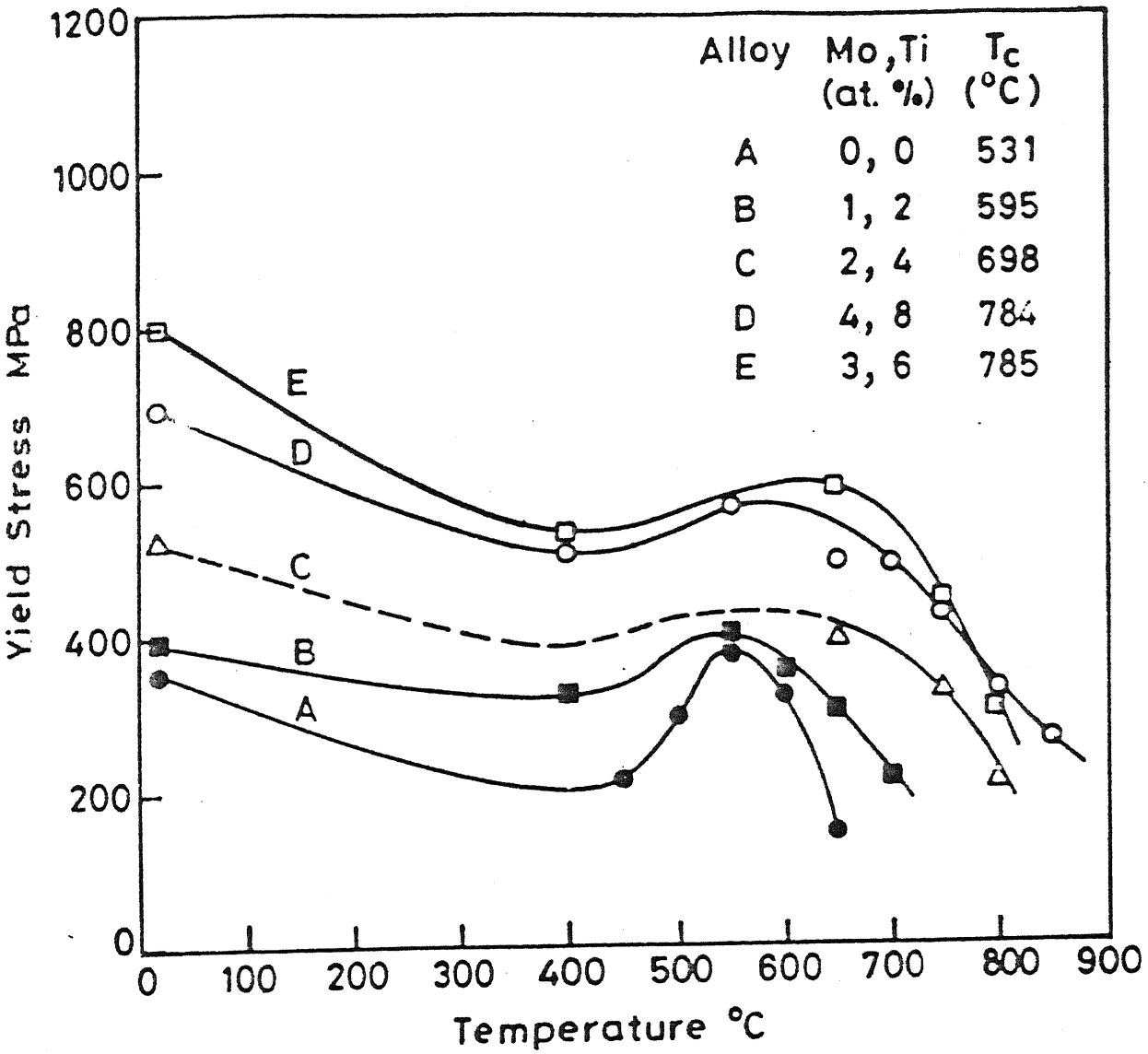

Fig. 2.12: Yield Stress vs. Temperature curves for Alloyed Fe_3Al shown with respective Alloy contents and $DO_3 \longrightarrow$ B2 Transition Temperature (T_c).

Table: 2-3
Effect of Recrystallization on Room Temperature Tensile Properties of a Fe_3Al Alloy[a]

Heat treatment[b] (h/°C)	Fraction recrystallized (%) (grain size, μm)	Yield stress (MPa)	Fracture stress (MPa)	Elongation (%)
1/550	0	550	760	5.4
1/650	0	543	807	8.1
1/750	10	479	736	8.0
1/850	20	453	670	6.4
1/1000	100 (41)	280	413	3.0
1/1100	100 (68)	279	450	4.0
0.5/750	<5	481	736	8.2
1/750	10	466	710	7.8
4/750	25	438	665	7.8
24/750	50 (20-30)	369	577	5.2
48/750	80 (20-60)	328	492	4.4
0.17/1000	100 (34)	288	439	3.6
0.5/1000	100 (36)	287	425	3.0
1/1000	100 (43)	274	436	3.2
4/1000	100 (45)	277	422	3.0

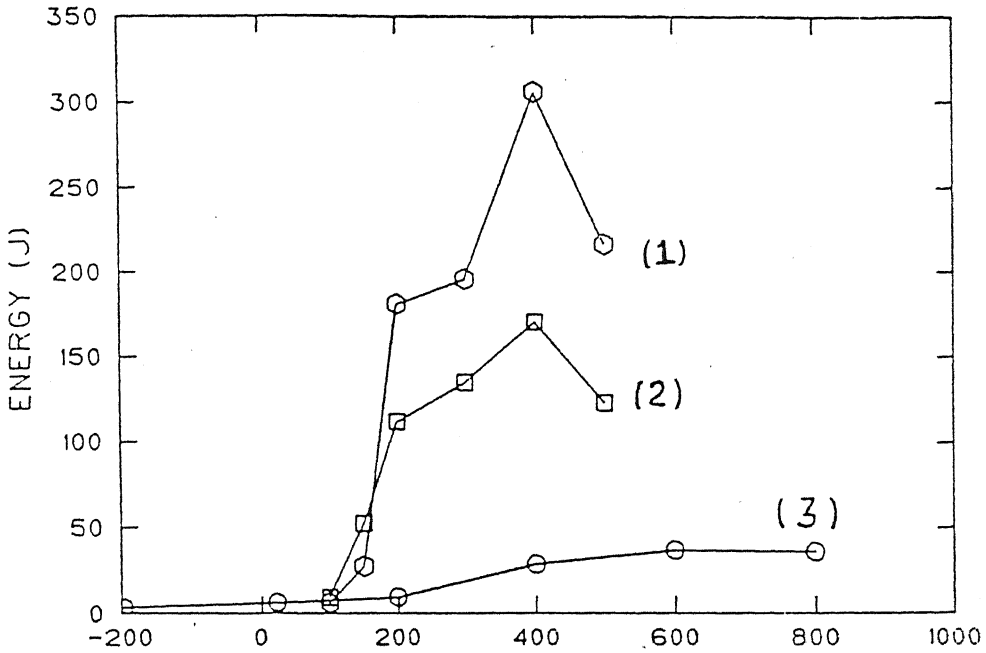

Fig. 2.13: Charpy Impact Properties of Fe - 16at% Al based Alloys ((1) and (2)) and Fe - 28% at% Al based Alloy (3) in wrought condition.

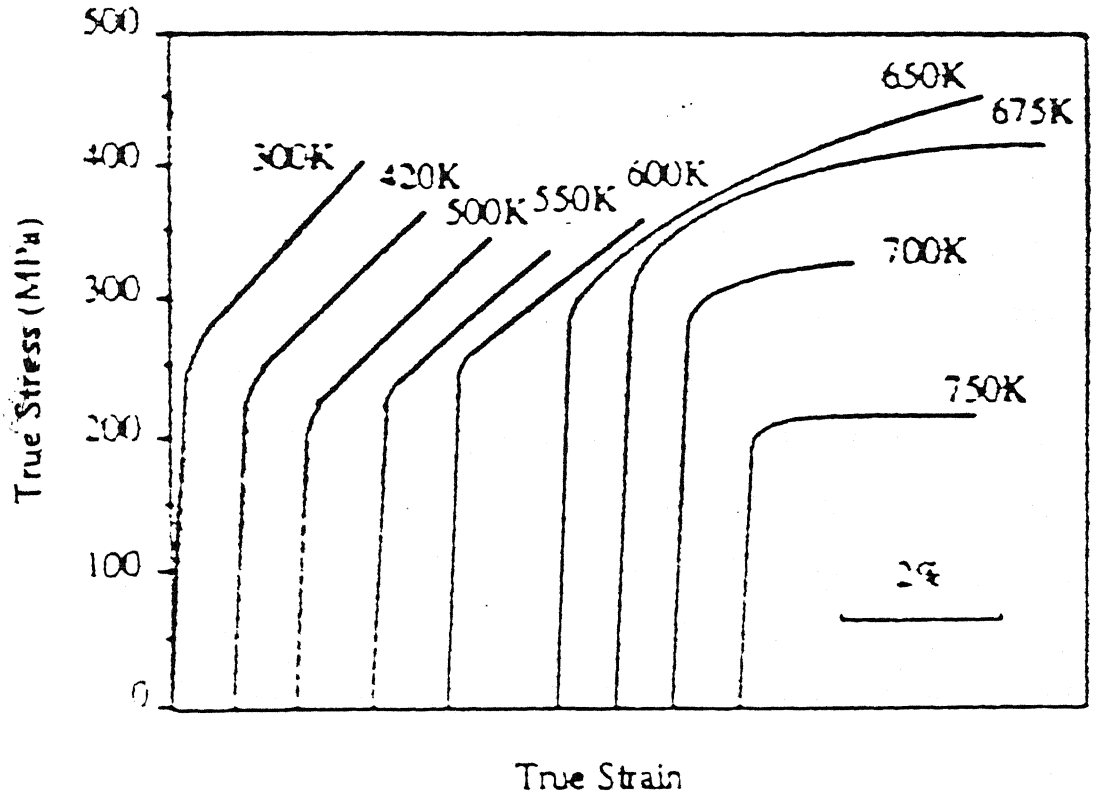

Fig. 2.14: True Stress - True Strain Curve for Large - grained Fe - 40% Al as a Function of Temperature.

Work - hardening rates of off - stoichiometric FeAl alloys (Fe - 40% Al) measured by Baker et.al [6], decreases with increasing temperature upto 700 K. At temperature ≥ 750K after an initial period of work hardening at low strain, no further work hardening occurred. At temperatures above 800K no work hardening was observed in any alloy [Fig. 2.14]. The region of rapidly decreasing yield stress with increasing temperatures roughly coincides with the temperature range where little or no work hardening was observed.

A scanning electron microscopy study has been carried out of fractured surfaces obtained from slowly cooled Fe - Al alloys pulled in tension and containing upto 23 atomic % Al by Marcinkowski et.al [7]. It has been found that alloys possessing upto about 20 at% Al fractured in a ductile manner by void nucleation and coalescence. However, alloys containing upto 25 at % Al failed in a brittle manner by a transgranular mode, while those possessing higher Al concentrations fractured intergranularly in a brittle manner. The loss of ductility and resulting brittle fracture is associated with the retardation of cross slip occasioned by the onset of long range atomic order. On the other hand, the change in brittle fracture from transgranular to intergranular is related to the decrease in slip produced APB's and/or low angle boundaries within the grain interiors. The high angle grain boundaries, with their relatively large degree of disorder, thus provide the only high energy path along which crack propagation can occur. In no case, fracture behaviour could be associated with impurity segregation at the grain boundaries.

2.5.1 Effect of Cr Addition

Chromium addition was found to have a strong beneficial effect on improving the ductility of the ordered alloy (28%Al) [Fig.2.15]. Ductility of disordered alloy, in which the environmental effect was substantially reduced, was not affected by chromium addition. The two phase alloy containing the α-solid solution and the ordered DO_3 phase showed significant improvement in ductility with Chromium addition. 0.2% yield strength, ultimate tensile strength and rupture strength are also shown to increase with Chromium addition [Fig.2.16 (a,b,c)]. This increase is more pronounced at lower temperatures.

2.5.2 Rolling Texture in Fe - Al Cr Alloy

W Mao and Z Sun [8] studied the rolling texture development in different layers of Fe - 28% Al - 2% Cr alloy. The normal rolling texture, which is similar to shear texture in FCC metals, has a texture type of BCC metals. Also similarity of shear texture in Fe - 28%Al - 5%Cr sheet to normal rolling texture in Al sheet implies that the {110} <111> slip systems are a very important plastic deformation mechanism for Fe_3Al alloy. A strong shear texture in the surface layer is produced by only 20% pass reduction, indicating that Fe_3Al alloy sheet is sensitive to shear stress. Therefore in rolling sheets of Fe_3Al alloys a shear texture would be expected which is produced in a way that some slip systems are highly activated and lead to such a rotation of some grain orientations around TD that they do not accumulate around {111} <112> and {001} <110> but around the metastable {112} <111> and {110} <001>.

Simulation of basic texture evolution and the contribution of various types of involved slip systems for rolling deformation of polycrystalline Fe - 28%Al - 5% Cr was done by means of Tayler RC models [9]. The best correspondence between simulated and experimentally detected rolling textures was achieved for simulations which were carried out using {110} <111> and {112} <111> slip systems. These simulations also rule out the possibility of considerable amounts of slip on {001} <100> or {123} <111> systems during rolling of Fe - 28% Al - 5% Cr at ambient temperatures.

2.5.3 Effect of Zr Addition along with Cr

Fe - Al Cr alloy shows further improvement in ductility with the addition of grain refiners such as zirconium and carbon. One possible reason for such improvement may be the more uniform distribution of ductile α solid solution around each of ordered phase particles. From Fig.2.16(a,b,c) it is obvious that ductility increases with Zr addition while ultimate tensile strength and rupture strength shows minor reduction in value.

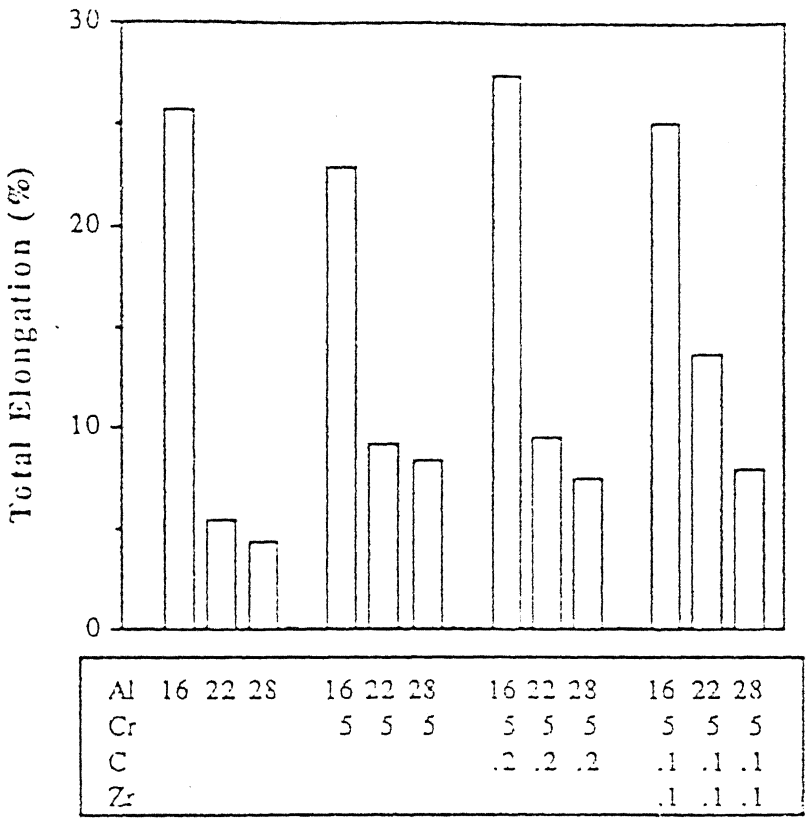

Fig. 2.15: Effect of Alloying additions to reduce the Environmental effect of Fe-Al Alloys.

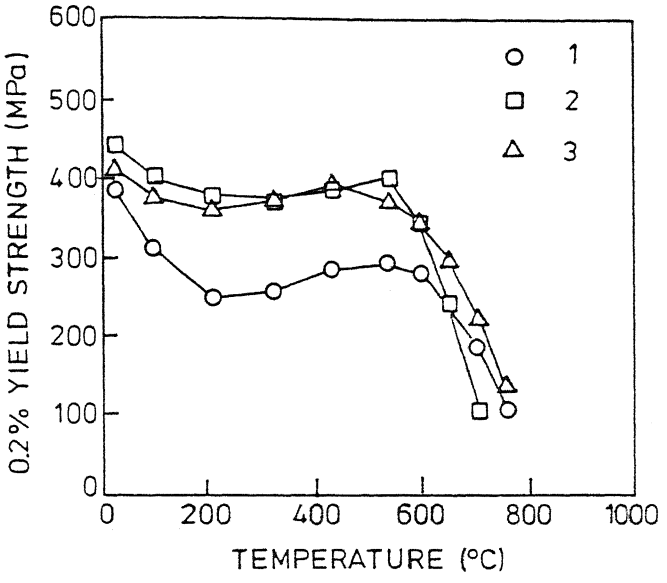
0.2% YIELD STRENGTH (MPa)
600
500
400
300
200
100
0
0
200
400
600
800
1000
TEMPERATURE (°C)
1
2
3

(a)

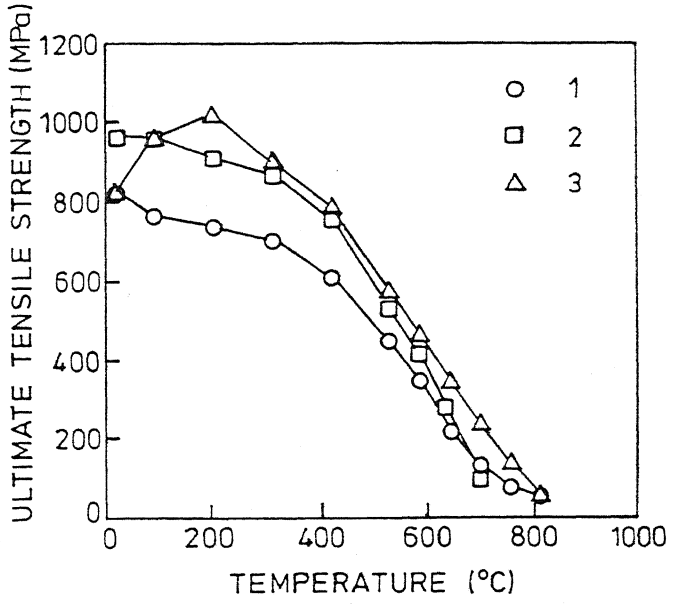
ULTIMATE TENSILE STRENGTH (MPa)
1200
1000
800
600
400
200
0
0
200
400
600
800
1000
TEMPERATURE (°C)
1
2
3

(b)

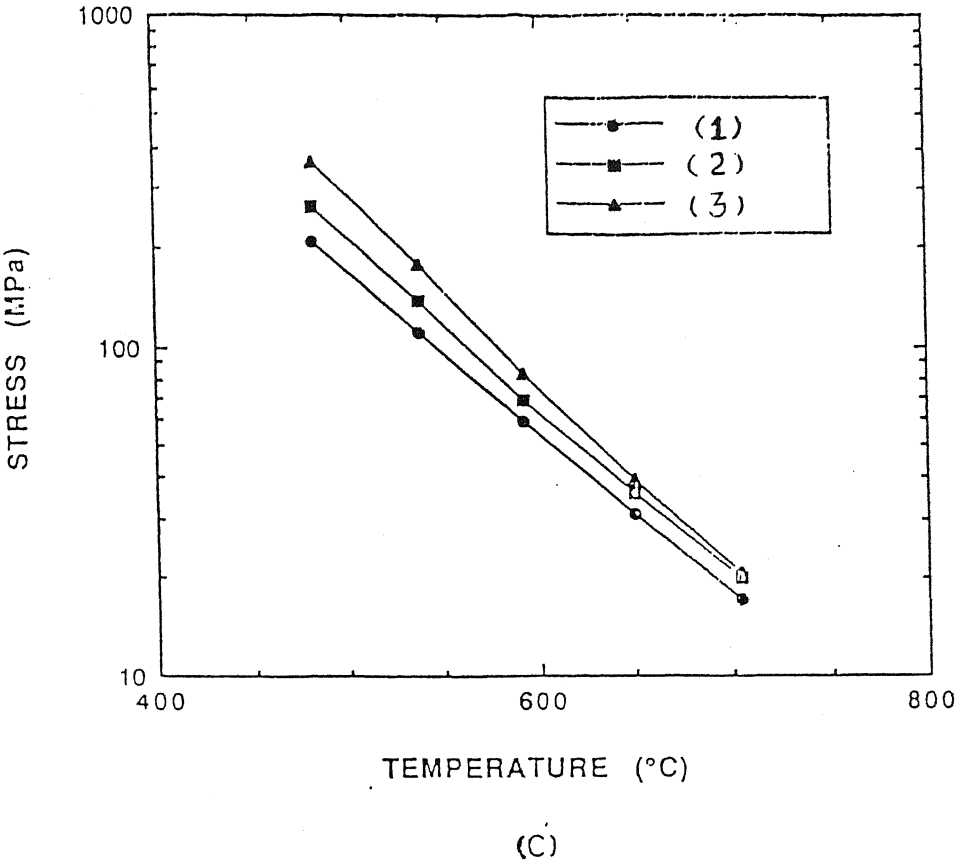

(C)

Compositions of alloys (1), (2) and (3) are given as follows:

	Alloy (atomic percent)		
	(1)	(2)	(3)
Al	28.08	28.03	28.08
Cr	2.02	5.03	5.04
B	0.04	0.04	--
Zr	--	0.08	--
Nb	--	--	0.51
C	--	--	0.20
Mo	--	--	--
Y	--	--	--
Fe	69.86	66.81	66.17

Fig. 2.16: Effect of Cr Addition on (a) 0.2% Yield Strength, (b) Ultimate Tensile Strength and (c) Rupture Strength in Fe - Al Alloy.

CHAPTER III

EXPERIMENTAL PROCEDURE

In this chapter, all experimental details stating the materials used, subsequent heat treatment given and various characterization methods used are described under the following sub topics.

3.1 MATERIALS AND INITIAL TREATMENTS

Three alloys of following composition (in at %) were taken as starting material:

(i) Fe - 28%Al

(ii) Fe - 28%Al -5%Cr.

(iii) Fe - 28%Al - 5%Cr - 5%Zr - 0.05%C

All the above alloys were received from the Oak Ridge National Laboratory, U. S. A. The alloys were produced by vacuum melting, followed by extrusion at 1100^{o}C. These were then hot rolled at 800^{o}C from 19.43mm to 8.8mm. Finally all the slabs were warm rolled at 650^{o}C from 8.8mm to 3.6 mm.

Eight samples of dimension described in Fig. 3.1 were cut from each alloy. Then these samples were reduced to half in thickness directions so that information can be obtained on all surfaces (longitudinal, transverse, rolling surface as well as mid -surface).

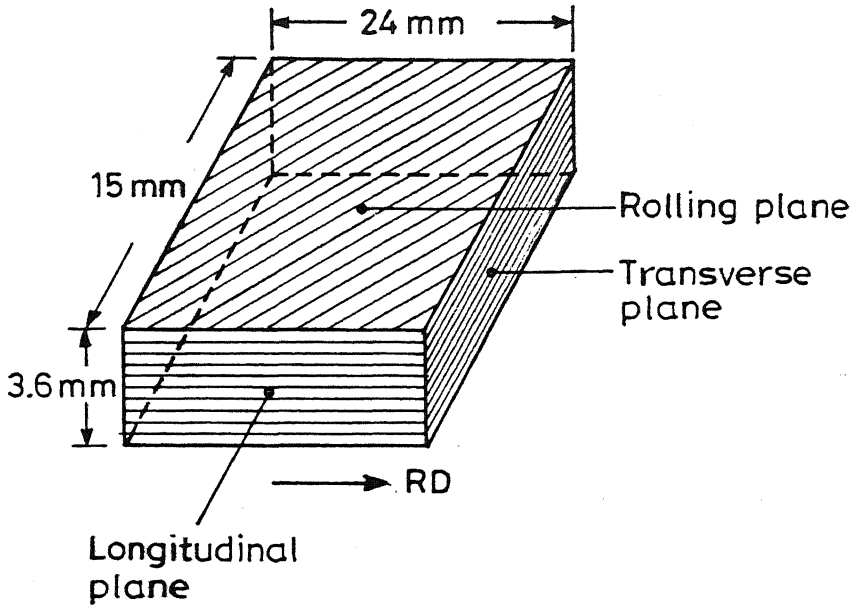

Fig. 3.1 Figure showing dimensions of specimen used and different planes viz. RP, TP, LP etc.

3.2 HEAT TREATMENT

To start with four samples of each alloy is taken and were heat treated at temperatures 400°C, 600°C, 800°C and 950°C for 1 hour followed by air cooling. After this probing heat treatment, it was decided to increase annealing time to 10 hours.

Two samples from each alloy were charged into a tube furnace kept in argon atmosphere at four different temperatures for 10 hours from atmosphere was provided so as to prevent oxidation. Four different temperatures chosen were 400°C, 600°C, 800°C and 950°C, which fall in different phase fields in the Fe - Al diagram for Fe - 28% alloys. The 400°C temperature line for Fe - 28% alloy falls in the DO_3 ordered phase field while 600°C and 800°C temperature lines fall in the $\alpha 2$ phase field and 950°C temperature line falls in the range of disordered solid solution α-Fe.

After holding the alloys at required temperature for 10 hours, one sample of each alloy at each temperature was air cooled and other was subjected to water quenching.

3.3 SPECIMEN PREPARATION

3.3.1 For X-ray Analysis

Both as received as well as heat treated samples were first ground on belt grinder and then polished on emery papers. Finally, sample were polished on a coarse polishing wheel using relatively coarse Al_2O_3 powder in water as abrasive.

3.3.2 For Optical Microscopy

Samples obtained after x-ray scanning were subjected to final fine polishing on a fine polishing wheel. Then these samples were etched using an etchant consisting of acetic acid, nitric acid and

hydrochloric acid in ratio 8:4:1 (by volume). Etching time was few seconds in each case.

3.3.3 For Scanning Electron Microscopy

Samples preparation was same as in optical microscopy, except that etching time was more (approx. 4 times than that for optical microscopy). This was done in order to bring out the relief features clearly.

3.3.4 For Differential Scanning Chalorimetry

Two samples, weighing 46.5 mg. each, were taken from each alloy. The weights of all samples taken were equal so that data obtained for each alloy can be compared with one another.

3.4 CHARACTERIZATION METHODS

As received specimens as well as heat treated ones were analysed using various characterization techniques viz. x-ray diffraction, scanning electron microscopy, optical microscopy, differential scanning chalorimetry etc. These are described under various subsections as follows:

3.4.1 X-Ray Diffraction

Samples obtained after various heat treatment were analysed through x-ray diffraction technique (for each sample x-ray scanning was done on both rolling as well as mid plane). The instrument used was Seifert ISO - Debyflex - 1001 diffractometer with Cr target. Radiation used was Crkα. Instrument was set to operate at 40kV and 30mA. The following parameters were used all throughout during the measurements:

i) Scanning speed =1.2^{o}/minute

ii) Chart speed = 12 mm/minute

iii) Counts per minute = 5 K

iv) Time constant = 10 Sec.

The various phases present in each sample were identified by matching experimental data with standard X-ray crystallography data provided in the ASTM index cards.

3.4.2 Microscopy

a) Optical Microscopy

The polished and etched samples were observed under a Leitz Metallux 3 optical microscope. Each sample was observed on all four surfaces (rolling, transverse, longitudinal and mid plane).As far as possible, magnifications were kept the same for all samples.

b) Scanning Electron Microscopy

Scanning electron microscopy (SEM) on all samples was carried out using a JEOL JSM-840A Scanning Electron Microscope. For each alloy, observations were made on both rolling plane as well as on mid plane. The instrument was operated mostly at 15kV and 60 μA. It was duly aligned each time and set for highest resolving power before observation. Most often secondary electron mode was used to see microstructures. Images were recorded using a camera attached to the instrument.Energy Dispersive Analysis of x-rays (EDAX) was done to determine chemical composition of phases present in selected samples.

3.4.3 Differential Scanning Chalorimetry

Differential Scanning Chalorimetry has been done in order to gain an insite into kinetics of transformation processes in present alloys.Specimen and a reference material were heated in

DSC at heating rate of 20 degree/min. This was kept constant for each of three alloys. The rate of heat input to specimen relative to reference is directly related to amount of transformation product in the specimen.

The DSC operation was carried out in a stanton Redcroft DSC 1500 machine. In this equipment, both the reference (annealed Pt) and the sample have same thermal environment and the thermal resistances between the samples and the environment and the reference and the environment are identical.

The specimens were loaded in the DSC cell at room temperature and equilibriated for few minutes. High purity argon gas was passed through the cell to avoid oxidation. Two specimens were used for each heat treatment and results obtained were found to be highly reproducible. Output was mCal/Sec. The net heat flow to the reference relative to sample was recorded as a function of temperature.

CHAPTER IV

RESULTS

4.1 RESULTS OF OPTICAL MICROSCOPY

Optical micrographs of all three alloys in as received condition as well as after subjecting them to various annealing treatments were taken. Micrographs were taken on all four planes, namely rolling plane (RP), mid plane (MP), transverse plane (TP) and longitudinal plane (LP). These micrographs alongwith various observations from them are described in following subtopics.

4.1.1 Fe-28% Al Alloy

Optical micrographs of as received sample on all four planes RP, MP, TP and LP are shown in Fig. 4.1 (a-d). All micrographs show grains elongated in rolling direction. TP micrographs show grains compressed due to rolling. From these micrographs, one can tell that this alloy is single phase which has later been confirmed by EDAX analysis.

Microstructures on all four planes (RP, MP, TP and LP) vary in almost similar fashion with annealing temperatures. Thus in all cases, rolling plane (RP) microstructures are presented as representative ones. Figures 4.2 (a-d) show microstructures of samples heat treated at 400^{o}C, 600^{o}C, 800^{o}C and 950^{o}C respectively for 1 hour followed by air cooling. Figs. 4.3 (a-d) show microstructures of Fe-28% Al alloys heat treated at above four temperatures for 10 hours followed by air cooling. Fig. 4.4 (a-d)

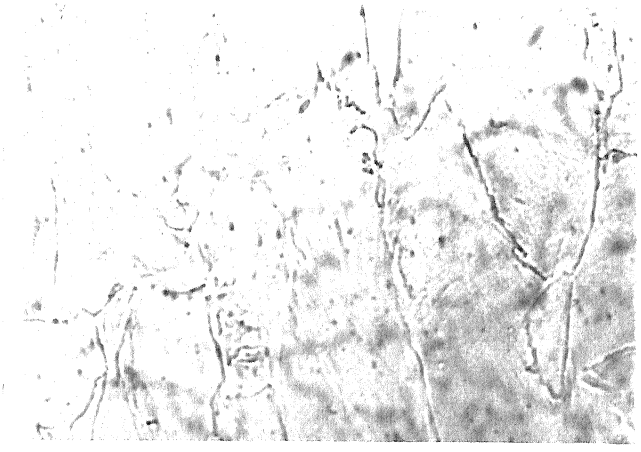

(a)

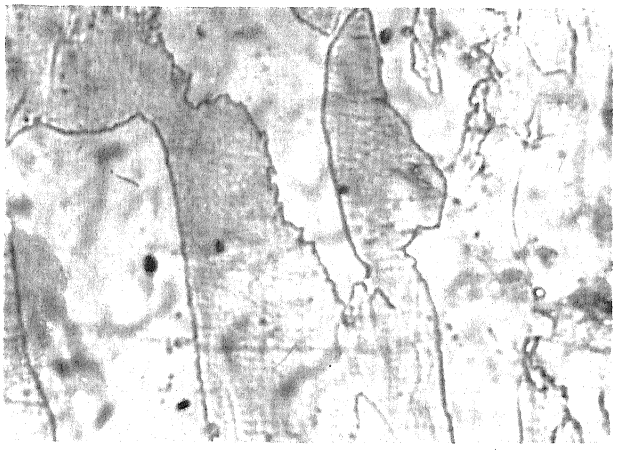

(b)

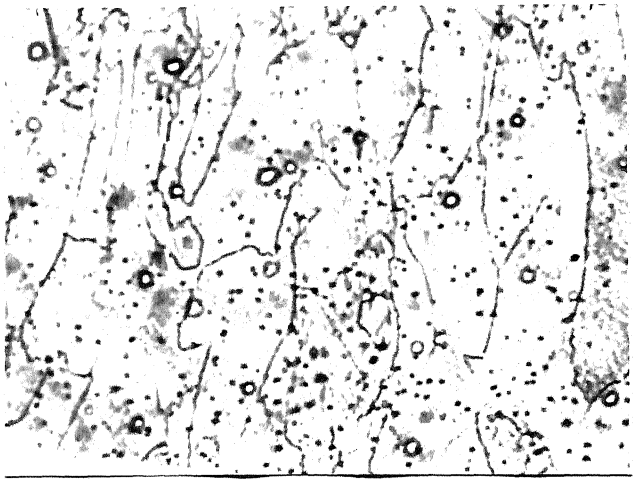

(c)

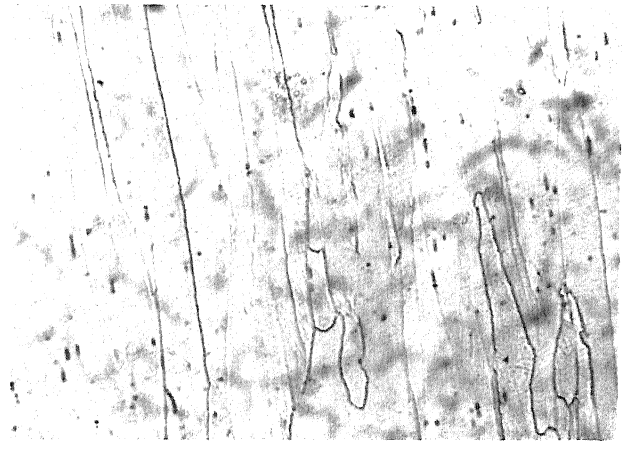

(d)

Fig. 4.1: Optical Micrographs of as received Fe-28% Al Alloy. (100×)
(a) RP, (b) MP, (c) TP and (d) LP

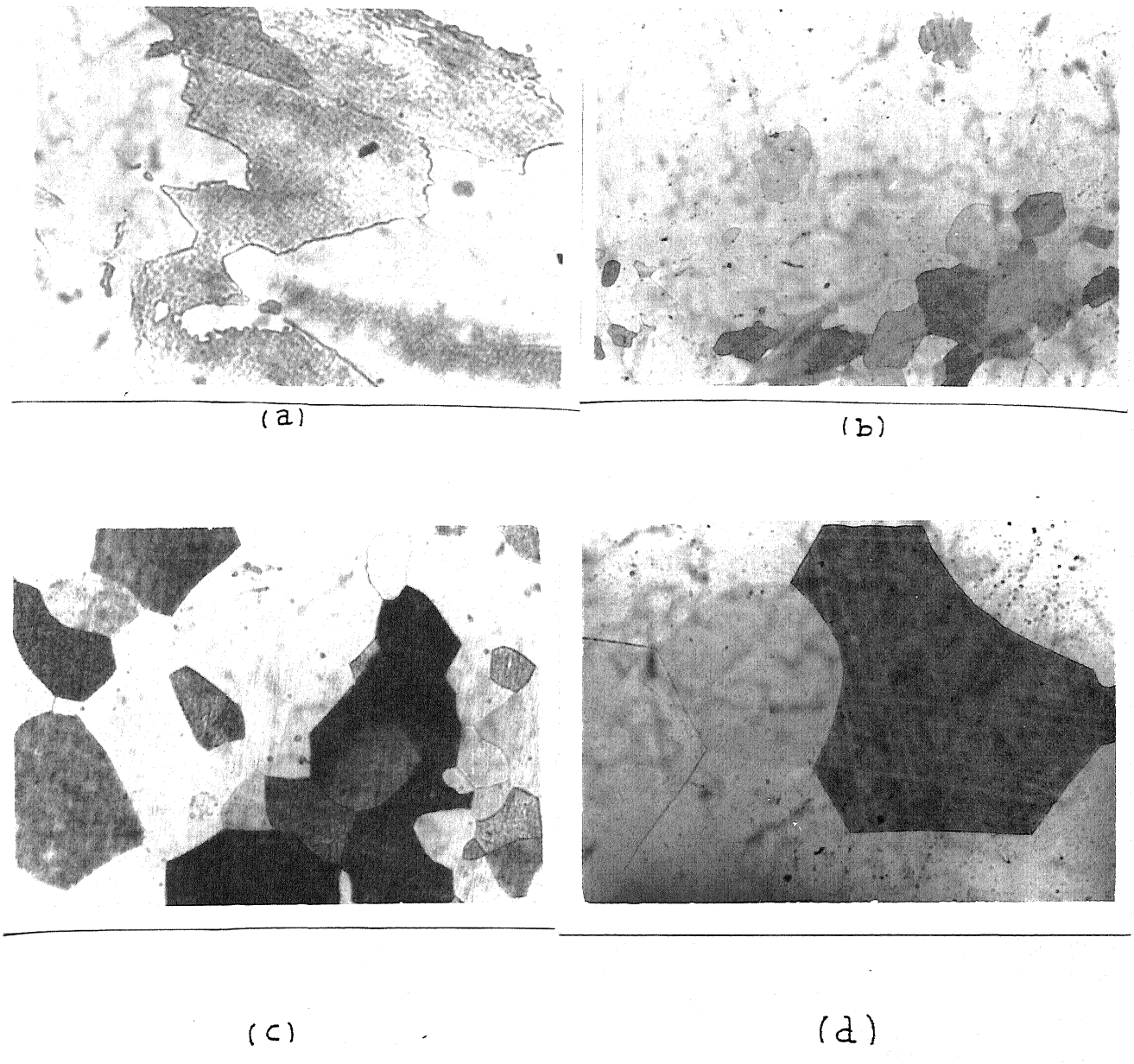

Fig. 4.2: Optical Micrographs on RP of Fe - 28% Al Alloy in heat treated condition (for 1 hour). (100×)

(a) 400°C/1h/AC (b) 600°C/1h/AC

(c) 800°C/1h/AC (d) 950°C/1h/AC

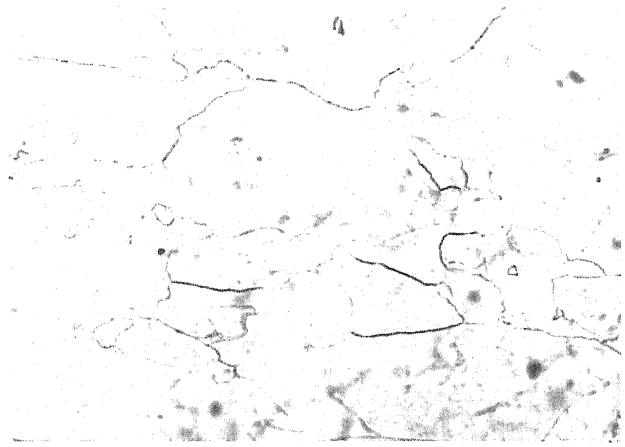

(a)

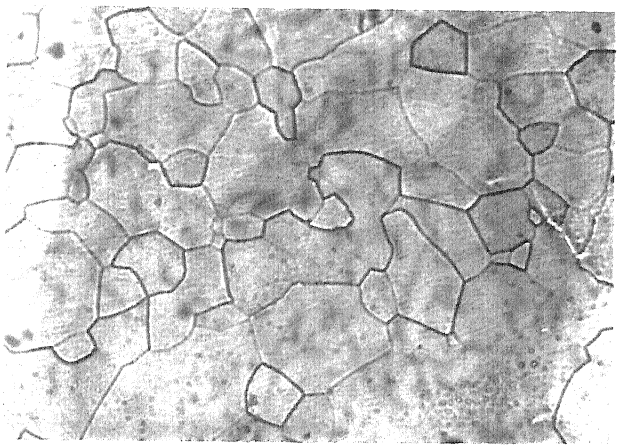

(b)

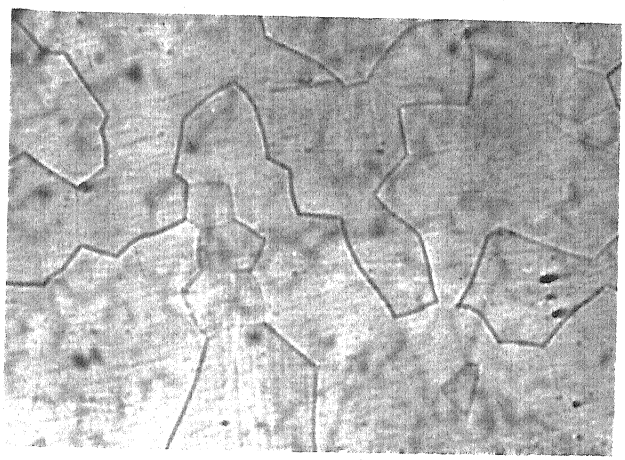

(c)

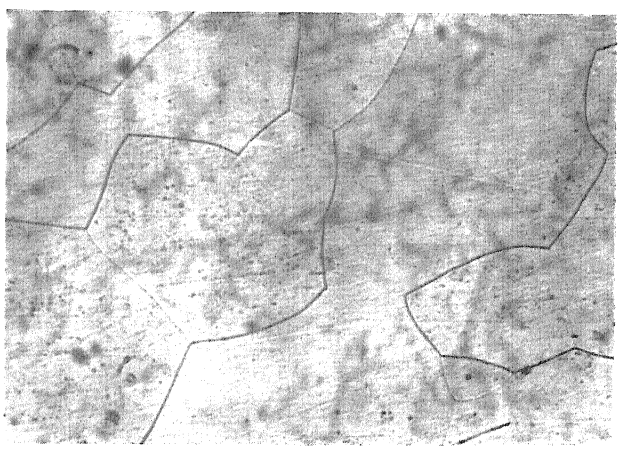

(d)

Fig. 4.3: Optical Micrographs on RP of Fe - 28% Al Alloy in heat treated condition (for 10 hours follwed by AC). (100X)

(a) 400°C/10h/AC (b) 600°C/10h/AC

(c) 800°C/10h/AC (d) 950°C/10h/AC

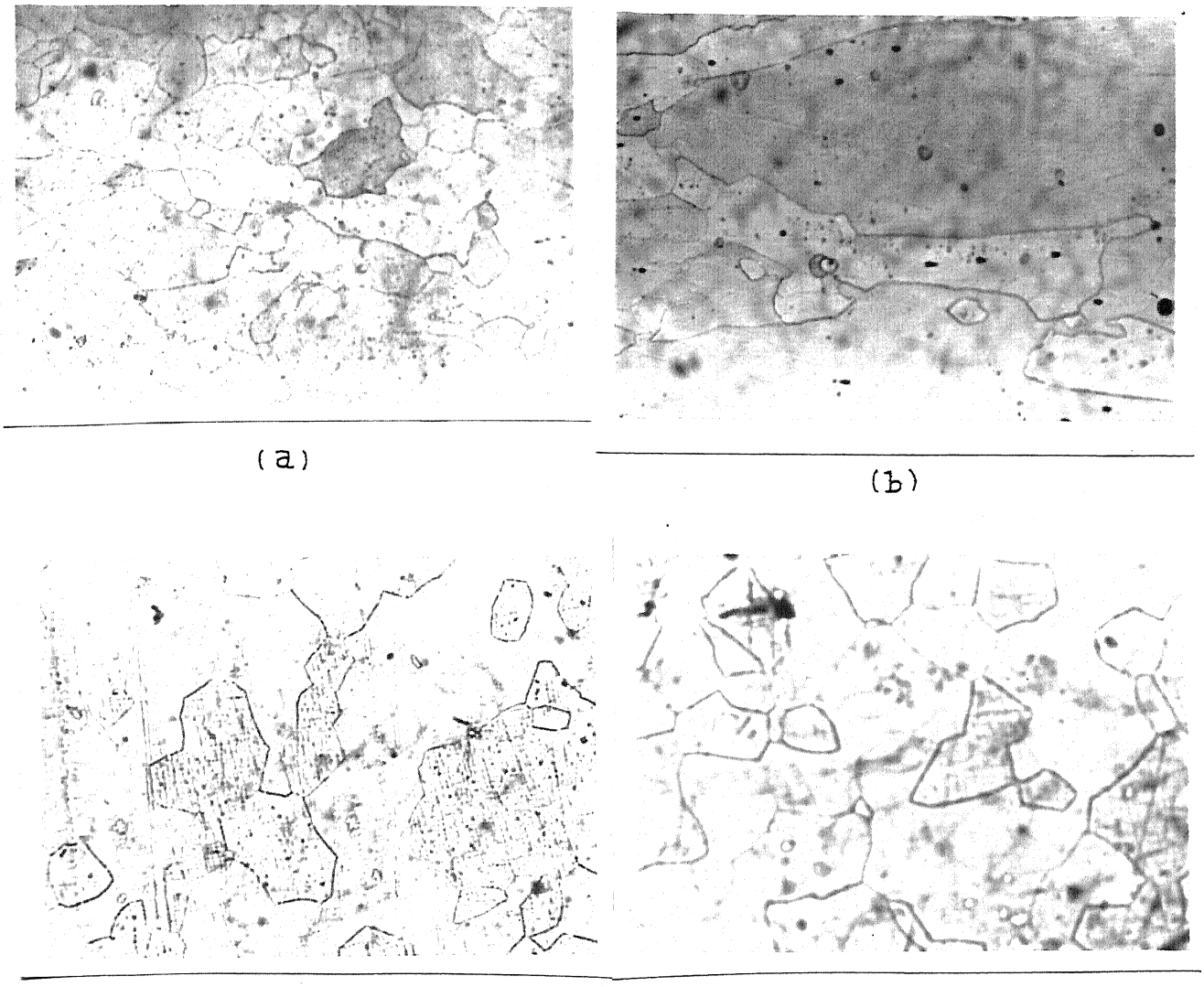

Fig. 4.4: Optical Micrographs on RP of Fe - 28% Al Alloy in heat treated condition (for 10 hours follwed by WQ). (100 X)

(a) 400°C/10h/WQ (b) 600°C/10h/WQ

(c) 800°C/10h/WQ (d) 950°C/10h/WQ

show microstructures of samples heat treated at above four temperatures for 10 hour followed by water quenching.

It is clear from all figures 4.2, 4.3 and 4.4 that recrystallization begins near about annealing temperature of 600°C and as temperature is increased, equiaxed grains (which formed as a result of recrystallization) grow further.

4.1.2 Fe-28% Al - 5% Cr Alloy

Optical micrographs of as received sample on all four planes RP, MP, TP and LP are shown in Fig. 4.5 (a-d). All micrographs show grains elongated in rolling direction. TP micrographs show grains compressed due to rolling. From optical micrographs, this alloy also appears to be single phase which was later confirmed by EDAX analysis.

Fig. 4.6 (a-d) show optical micrographs on rolling plane of samples heat treated at 400°C, 600°C, 800°C and 950°C respectively for 1 hour followed by air cooling. Fig. 4.7 (a-d) show optical micrographs of samples on RP annealed at above four temperatures for 10 hours followed by air cooling. Fig. 4.8 (a-d) show microstructures of samples on RP heat treated at above four temperatures for 10 hours followed by water quenching.

Features observed from these micrographs are almost similar as in case of Fe-28% Al alloy except that grain size is somewhat lower in case of Fe-28% Al - 5% Cr alloy. Thus, chromium addition seems to have the effect of grain refinement to a little extent.

4.1.3 Fe-28% Al - 5% Cr - 5% Zr - 0.05% C Alloy

Fig. 4.9 (a-d) show optical micrographs of as received samples taken on RP, MP, TP and LP respectively. This alloy

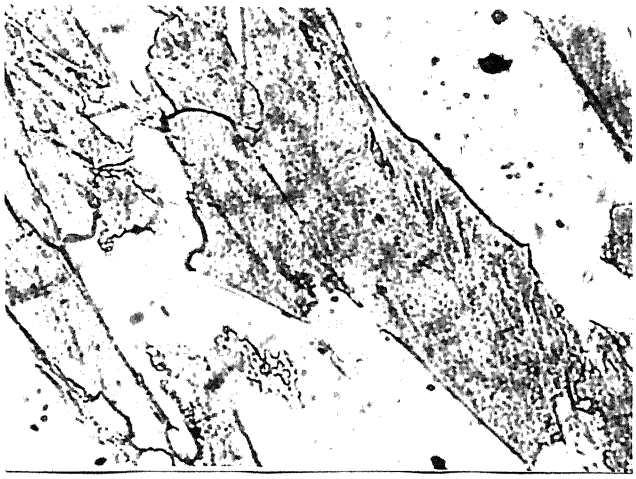

(a)

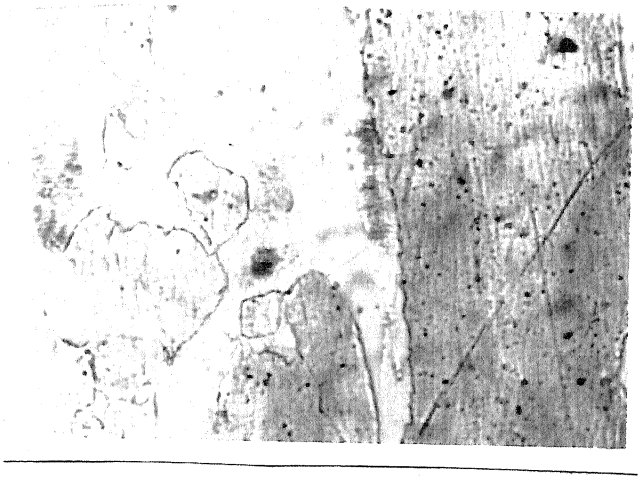

(b)

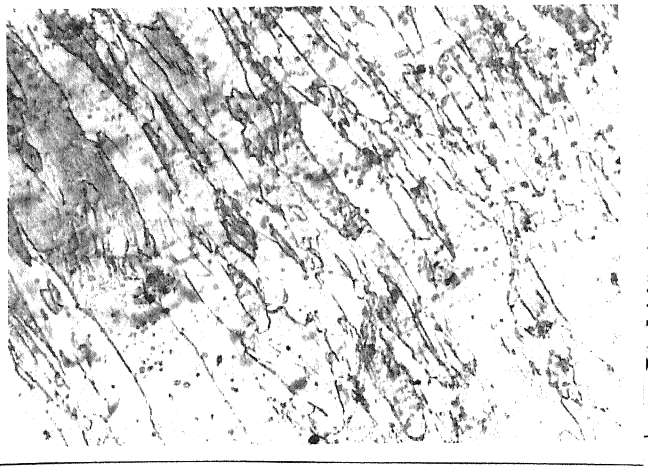

(c)

(d)

Fig. 4.5: Optical Micrographs of as received Fe-28% Al-5% Cr Alloy.(100X)
(a) RP, (b) MP, (c) TP and (d) LP

(a)

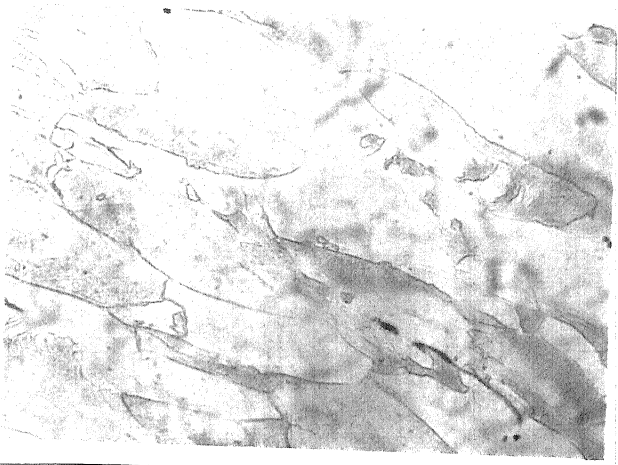

(b)

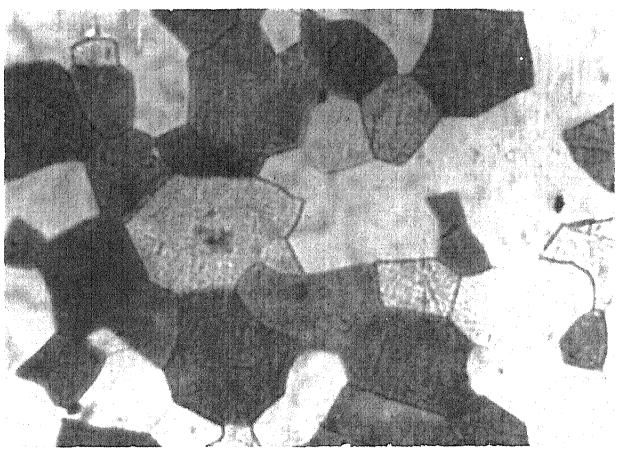

(c)

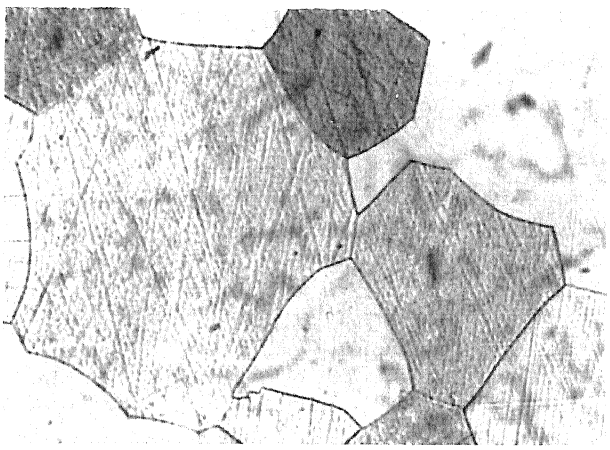

(d)

Fig. 4.6: Optical Micrographs on RP of Fe - 28% Al - 5% Cr Alloy in heat treated condition (for 1 hour). (100X)

(a) 400^{o}C/1h/AC (b) 600^{o}C/1h/AC

(c) 800^{o}C/1h/AC (d) 950^{o}C/1h/AC

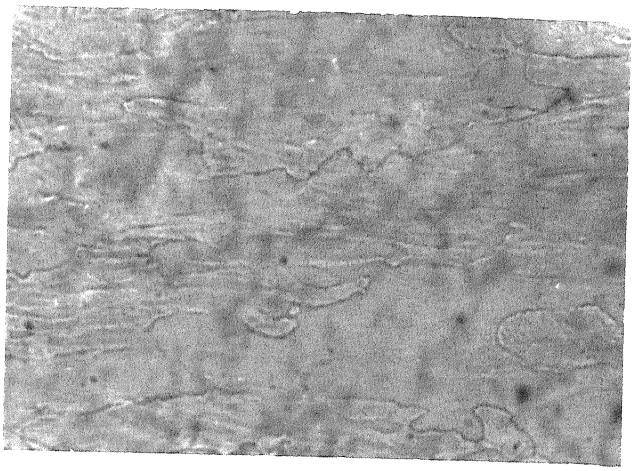

(a)

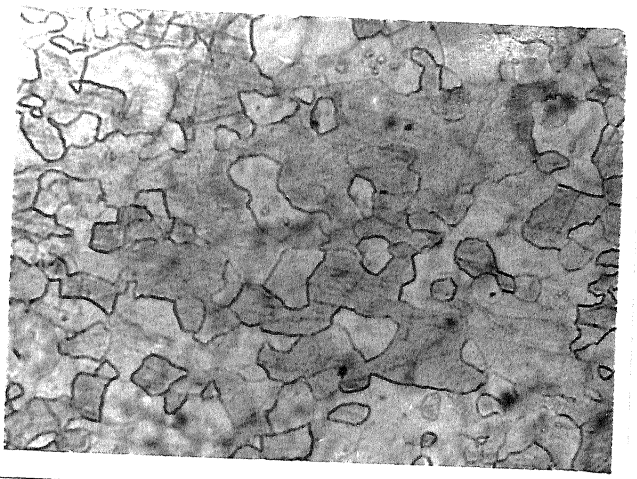

(b)

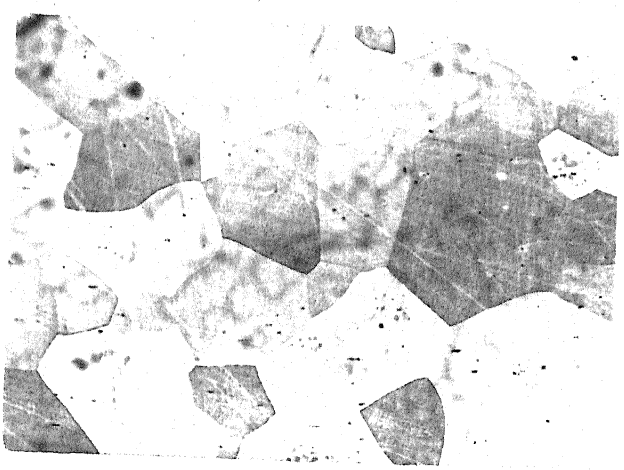

(c)

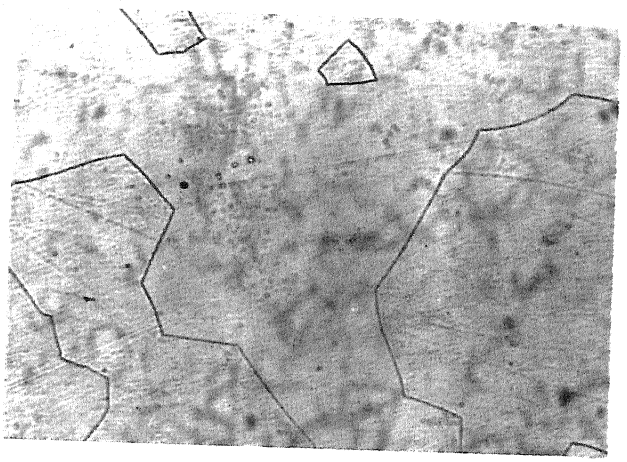

(d)

Fig. 4.7: Optical Micrographs on RP of Fe - 28% Al - 5% Cr Alloy in heat treated condition (for 10 hours follwed by AC).(100X)

(a) 400°C/10h/AC (b) 600°C/10h/AC

(c) 800°C/10h/AC (d) 950°C/10h/AC

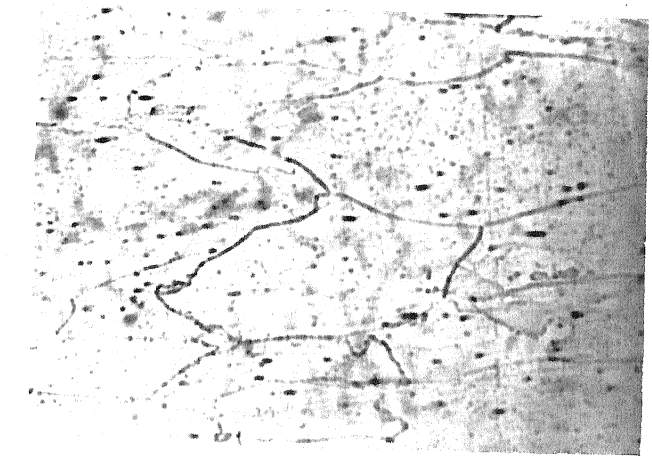

(a)

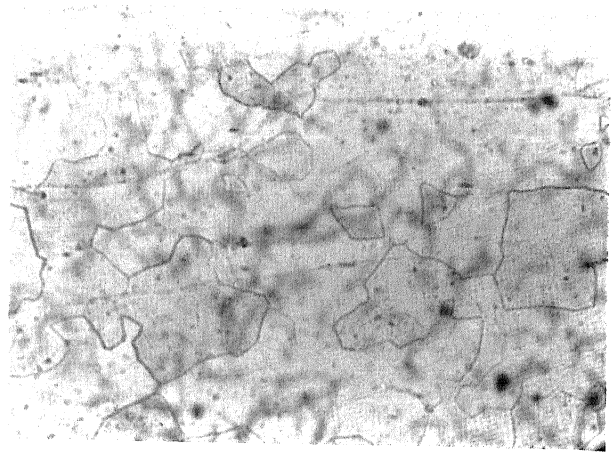

(b)

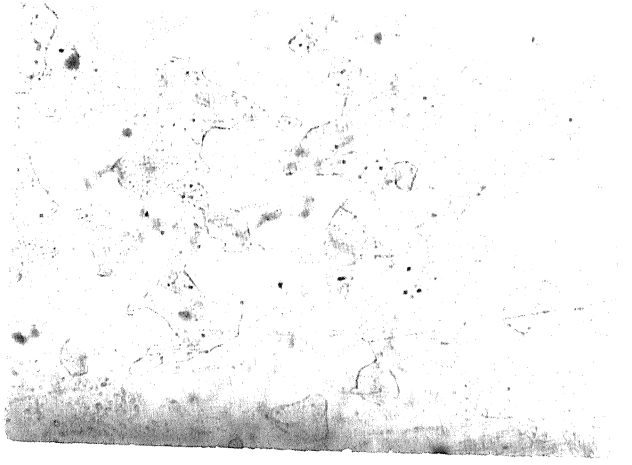

(c)

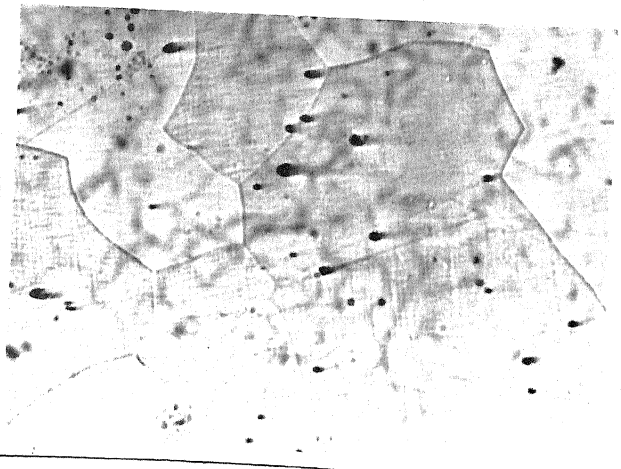

(d)

Fig. 4.8: Optical Micrographs on RP of Fe - 28% Al- 5% Cr Alloy in heat treated condition (for 10 hours follwed by WQ). (100 X)

(a) 400°C/10h/WQ (b) 600°C/10h/WQ

(c) 800°C/10h/WQ (d) 950°C/10h/WQ

appears to be two phase if we look at these micrographs. This was later confirmed by EDAX analysis (please see Sec. 4.3). Second phase got fragmented and aligned in rolling direction as a result of hot rolling done on this alloy. No preferential segregation of second phase appears to take place. Grain size, in case of this alloy, is very small as compared to other two alloys. Thus, zirconium addition along with chromium seems to have the effect of grain refinement to a great extent.

Fig. 4.10 (a-d) show optical micrographs of samples on rolling plane, heat treated at 400^{o}C, 600^{o}C, 800^{o}C and 950^{o}C for 1 hour followed by air cooling. Optical micrographs on rolling plane of samples, heat treated at above four temperatures for 10 hours followed by air cooling are presented in Fig. 4.11 (a-d). Fig. 4.12 (a-d) show optical micrographs of samples, heat treated at above four temperatures for 10 hours followed by water quenching.

From all figures, it can be observed that recrystallization in matrix phase (at few places) begins near about annealing temperature of 600^{o}C. As annealing temperature is increased, recrystallized (equiaxed) matrix grains grow. One feature that distinguishes this alloy from other two (Fe-28% Al and Fe-28% Al - 5% Cr) is that unlike other two alloys recrystallization is not uniform throughout the matrix phase in case of this alloy. This may be attributed to the presence of second phase particles which grow to some extent with annealing temperature (no recrystallization phenomenon seems to occur in case of precipitate (second) phase particles).

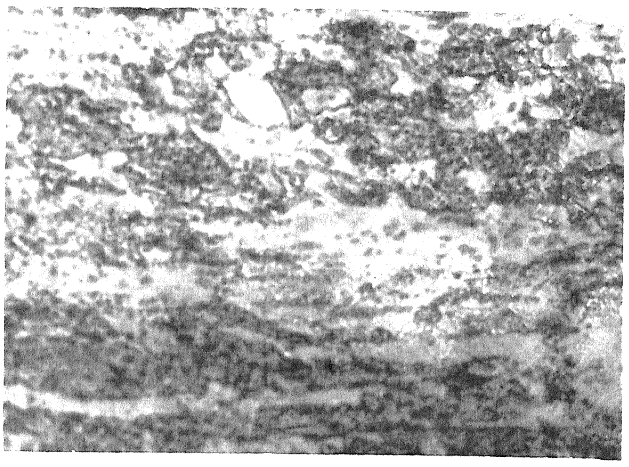

(a)

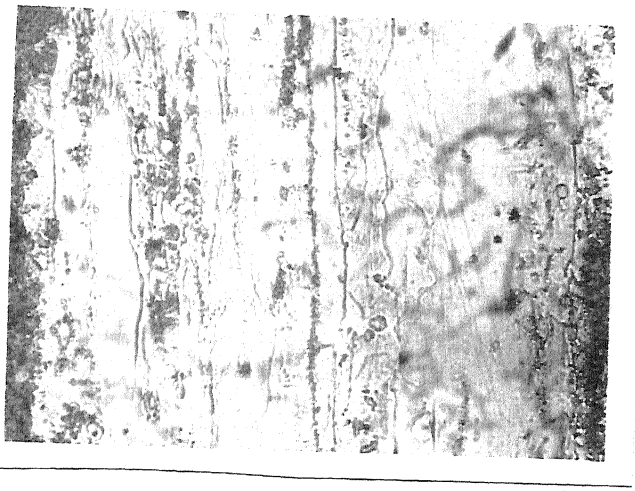

(b)

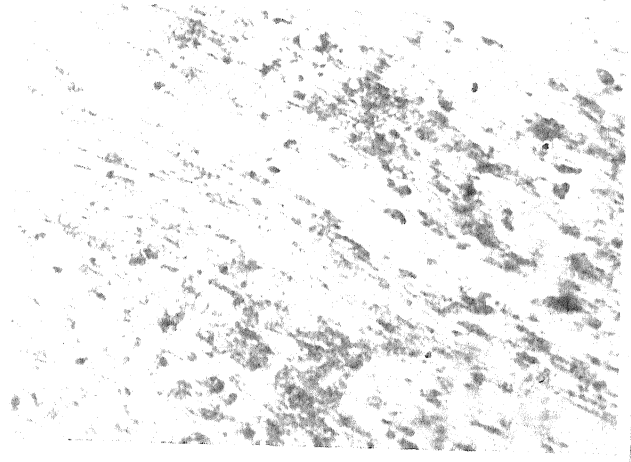

(c)

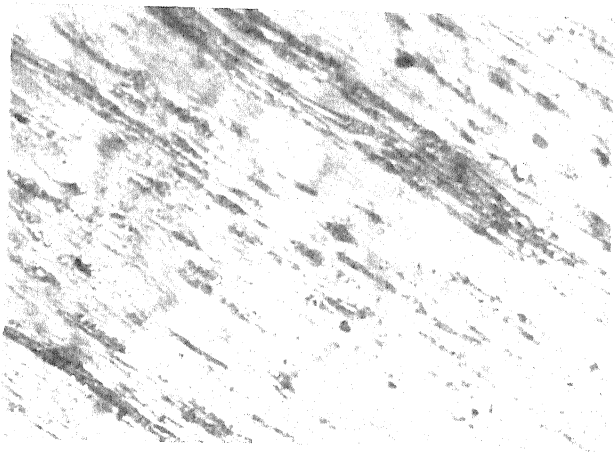

(d)

Fig. 4.9: Optical Micrographs of as received Fe-28% Al- 5% Cr - 5% Zr - 0.05% C Alloy. (200X)
(a) RP, (b) MP, (c) TP and (d) LP

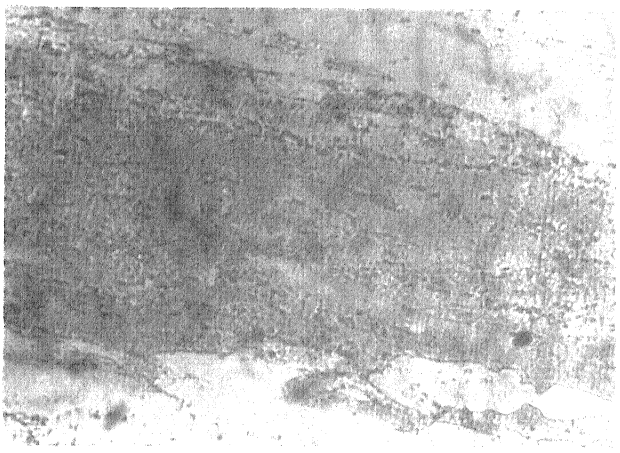

(a)

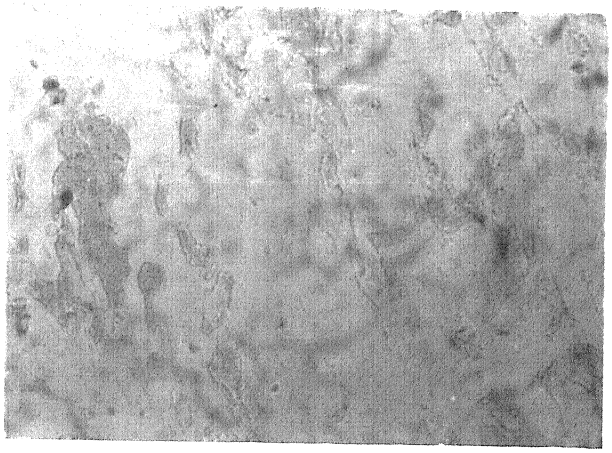

(b)

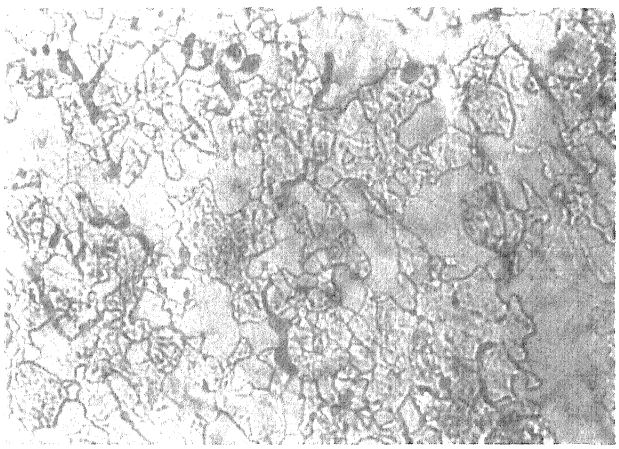

(c)

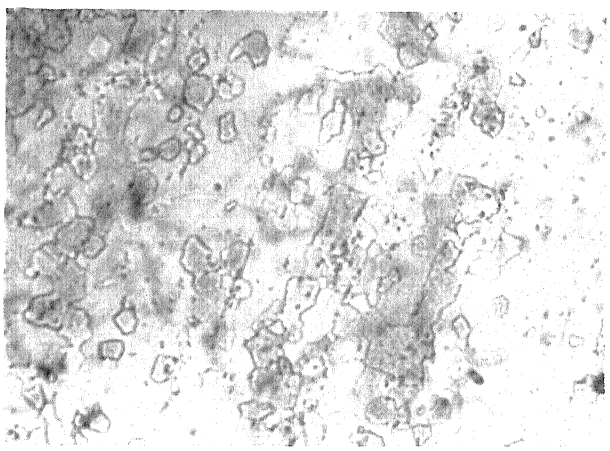

(d)

Fig. 4.10: Optical Micrographs on RP of Fe - 28% Al - 5% Cr - 5% Zr - 0.05% C Alloy in heat treated condition (for 1 hour). (200X)

(a) 400°C/1h/AC (b) 600°C/1h/AC

(c) 800°C/1h/AC (d) 950°C/1h/AC

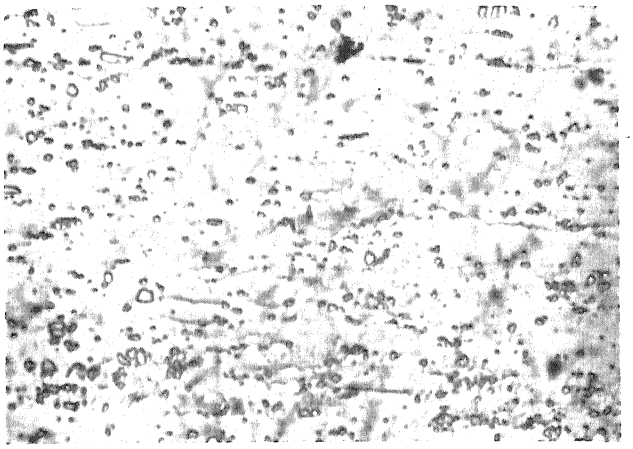

(a)

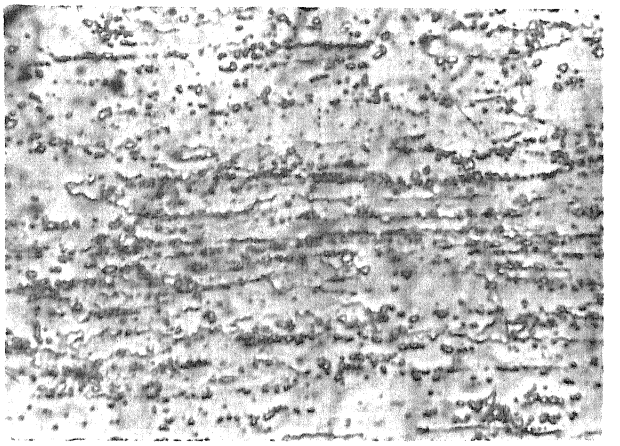

(b)

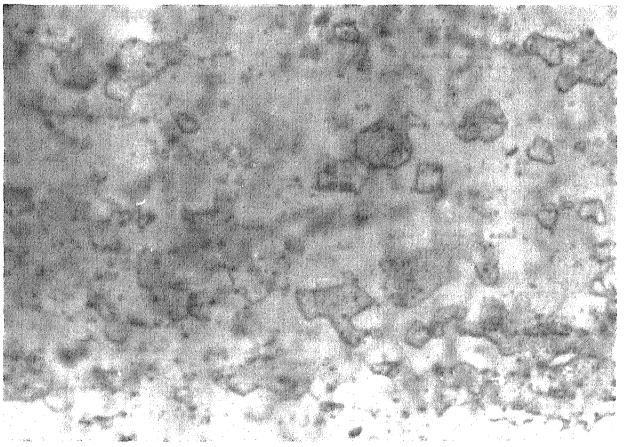

(c)

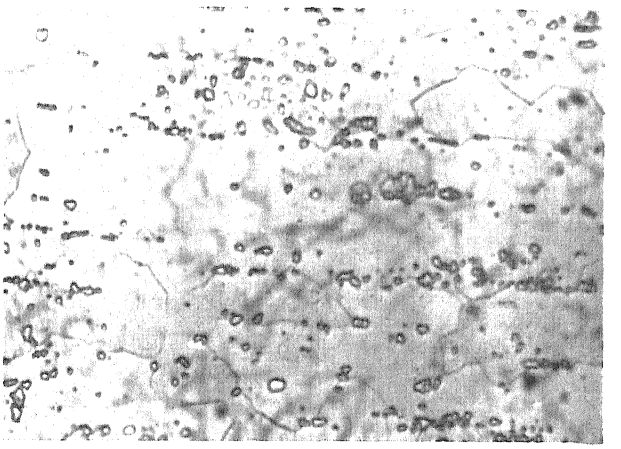

(d)

Fig. 4.11: Optical Micrographs on RP of Fe - 28% Al - 5% Cr - 5% Zr - 0.05% C Alloy in heat treated condition (for 10 hours follwed by AC). (500X)

(a) 400°C/10h/AC (b) 600°C/10h/AC

(c) 800°C/10h/AC (d) 950°C/10h/AC

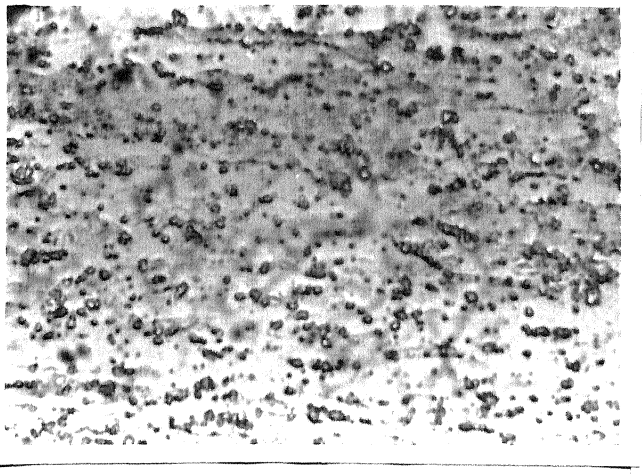

(a)

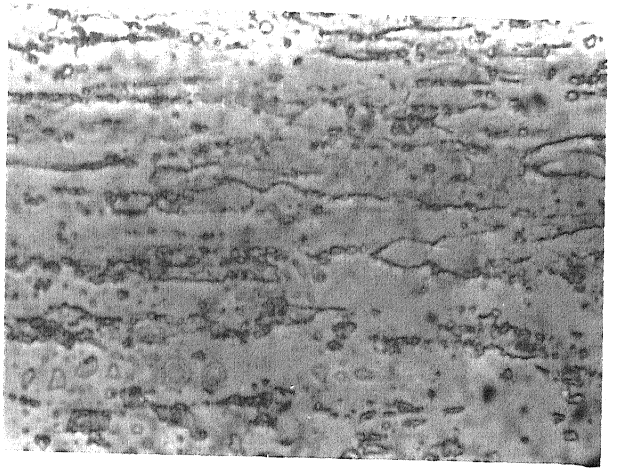

(b)

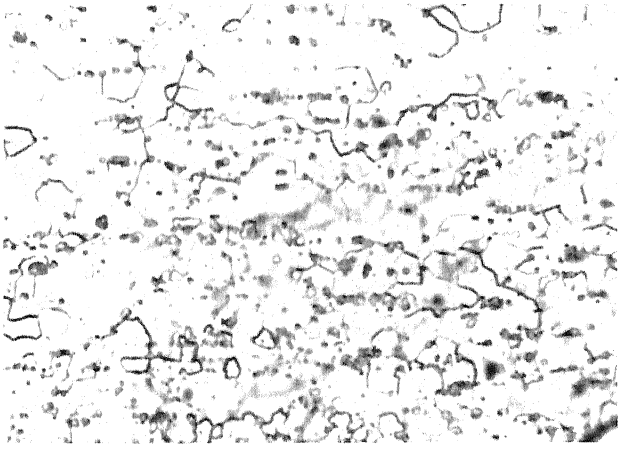

(c)

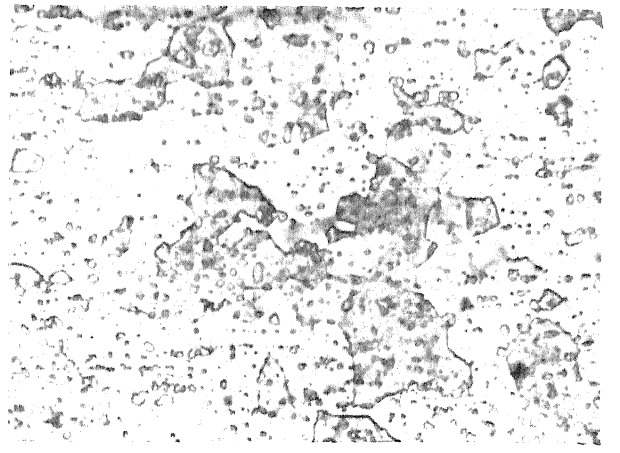

(d)

Fig. 4.12: Optical Micrographs on RP of Fe - 28% Al-5% Cr - 5% Zr - 0.05% C Alloy in heat treated condition (for 10 hours follwed by WQ). (500X)

(a) $400^{o}C/10h/WQ$ (b) $600^{o}C/10h/WQ$

(c) $800^{o}C/10h/WQ$ (d) $950^{o}C/10h/WQ$

4.2 RESULTS OF X-RAY STUDIES

X-ray diffraction patterns were taken for all three alloys in the as received condition as well as after subjecting them to various annealing treatments. Results are presented in tabular form as follows.

4.2.1 Standard X-ray Diffraction Tables for Fe_3Al, FeAl, Fe_3Zr and α-Fe

To start with standard x-ray diffraction tables for Fe_3Al, FeAl, Fe_3Zr and α-Fe are given which were used to identify peaks obtained in x-ray diffraction patterns of alloys subjected to various annealing treatments.

Table 4.1: Fe_3Al.

d (Å)	I/I_o	h k l
3.34	60	111
2.89	50	200
2.04	100	220
1.79	20	311
1.67	10	222
1.45	80	400
1.33	10	331
1.29	10	420
1.18	90	422
1.11	20	511,333
1.02	70	440

Table 4.2: FeAl.

d (Å)	I/I_o	h k l
2.899	8	100
2.048	100	110
1.6722	3	111
1.4472	14	200
1.2949	2	210
1.1820	25	211
1.0238	8	220
0.9650	1	300
0.9157	9	310
0.8358	4	222

Table 4.3: Fe_3Zr.

d (Å)	I/I_o	h k l
2.936	5	400
2.681	20	331
2.384	50	422
2.249	100	511,333
2.07	100	440
1.977	20	531
1.957	20	600,442
1.853	5	620
1.786	10	533
1.766	10	622
1.635	20	711,551
1.620	20	640
1.521	20	731,553
1.46	20	800
1.427	50	733
1.376	100	822,660
1.35	80	751,555
1.284	50	911,753
1.275	50	842
1.225	20	931
1.193	80	844
1.175	100	933,771

Table 4.4: α-Fe.

d (Å)	I/I_o	h k l
2.0268	100	110
1.4332	20	200
1.1702	30	211
1.0134	10	220
0.9064	12	310
0.8275	6	222

4.2.2 X-ray Diffraction Tables for alloys subjected to heat treatments at 400°C, 600°C, 800°C and 950°C respectively for 1 hour (only rolling plane):

a) Fe - 28%Al alloy

X-ray diffraction data for this alloy in as received condition after heat treatment at 400°C, 600°C, 800°C and 950°C respectively for 1 hour in each case (followed by air cooling) are given in following tables:

Table 4.5(a): As received sample

2θ	θ	I	I/I_{max}	d(Å)	(h k l)
46.5	23.25	14.0	1.5	2.90	(200) Fe_3Al/(100) FeAl
68.0	34.00	930.0	100.0	2.048	(220) Fe_3Al/(110) FeAl
86.5	43.25	9.0	0.96	1.67	(222) Fe_3Al/(111) FeAl
104.0	52.00	40.0	4.3	1.45	(400) Fe_3Al/(200) FeAl

Table 4.5(b): Sample heat treated at 400°C for 1 hr. followed by AC.

2θ	θ	I	I/I_{max}	d(Å)	(h k l)
32.5	16.25	12.0	3.9	4.09	---
40.0	20.00	14.00	4.5	3.35	(111) Fe_3Al
46.5	23.25	13.0	4.2	2.90	(200) Fe_3Al/(100) FeAl
68.0	34.00	308.0	100.0	2.048	(220) Fe_3Al/(110) FeAl
86.5	43.25	11.0	3.6	1.67	(222) Fe_3Al/(111) FeAl
104.0	52.00	41.0	13.3	1.45	(400) Fe_3Al/(200) FeAl

Table 4.5(c): Sample heat treated at 600°C for 1 hr. followed by AC.

2θ	θ	I	I/I_{max}	d(Å)	(h k l)
46.5	23.25	6.0	16.7	2.90	(200) Fe_3Al/(100) FeAl
68.0	34.00	36.0	100.0	2.048	(220) Fe_3Al/(110) FeAl
104.5	52.25	11.0	30.5	1.45	(400) Fe_3Al/(200) FeAl

Table 4.5(d): Sample heat treated at 800°C for 1 hr. followed by AC.

2θ	θ	I	I/I_{max}	d(Å)	(h k l)
40.0	20.00	9.00	22.0	3.35	(111) Fe_3Al
68.0	34.00	41.0	100.0	2.04	(220) Fe_3Al/(110) FeAl
82.0	41.00	6.0	14.6	1.74	(311) Fe_3Al
86.5	43.25	32.0	78.0	1.67	(222) Fe_3Al/(111) FeAl

Table 4.5(e): Sample heat treated at 950°C for 1 hr. followed by AC.

2θ	θ	I	I/I_{max}	d(Å)	(h k l)
40.5	20.25	10.00	24.0	3.35	(111) Fe_3Al
46.5	23.25	6.0	14.3	2.90	(200) Fe_3Al/(100) FeAl
86.5	43.25	7.0	16.7	1.67	(222) Fe_3Al/(111) FeAl
104.0	52.00	42.0	100.0	1.45	(400) Fe_3Al/(200) FeAl
124.0	62.00	12.0	28.6	1.297	(420) Fe_3Al/(210) FeAl

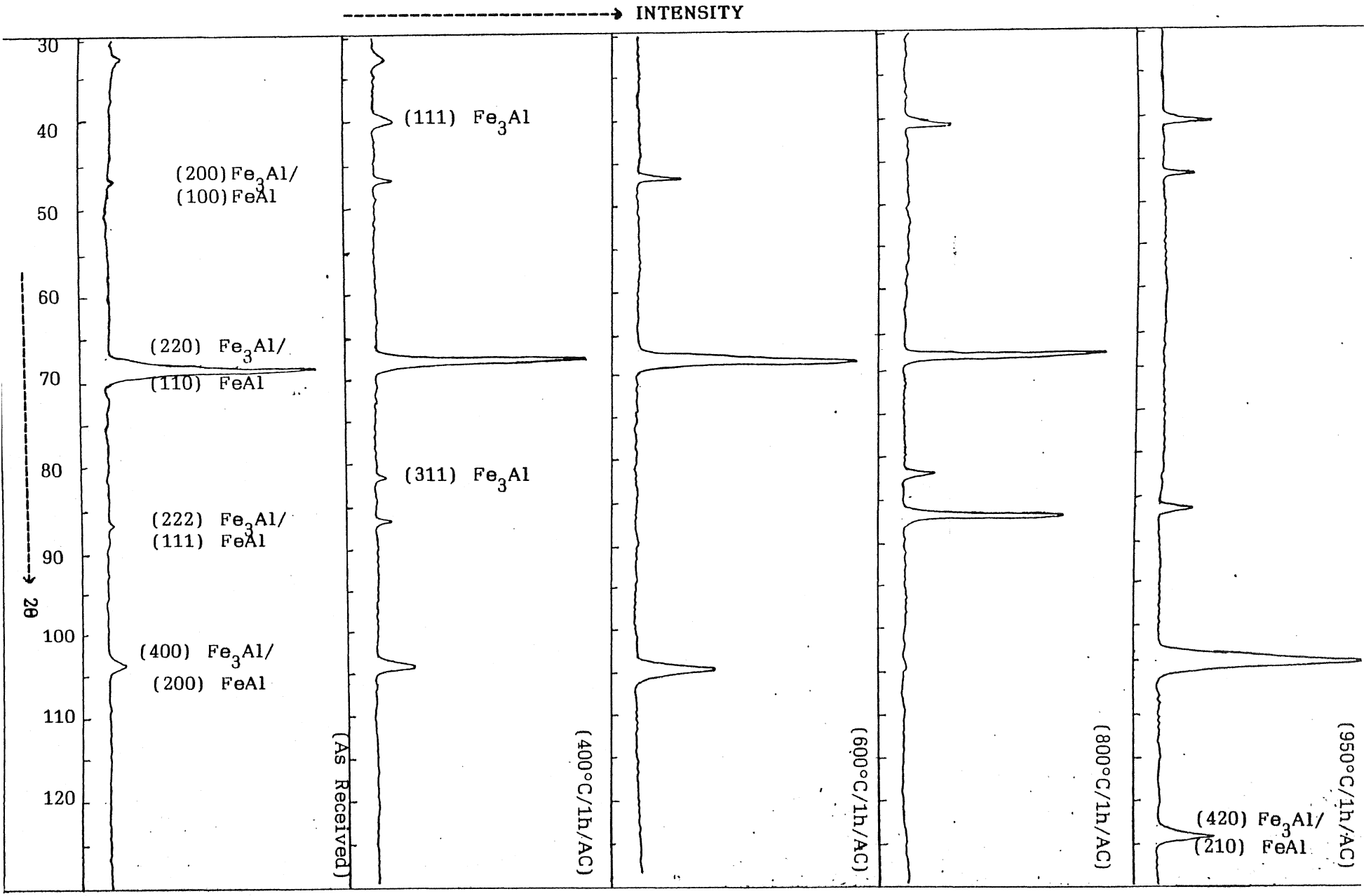
INTENSITY
2θ
30
40
50
60
70
80
90
100
110
120
(200) Fe3Al/
(100) FeAl
(220) Fe3Al/
(110) FeAl
(222) Fe3Al/
(111) FeAl
(400) Fe3Al/
(200) FeAl
(As Received)
(111) Fe3Al
(311) Fe3Al
(400°C/1h/AC)
(600°C/1h/AC)
(800°C/1h/AC)
(420) Fe3Al/
(210) FeAl
(950°C/1h/AC)

The X-ray diffraction results are also given in graphical form in Fig.4.13 for easy comprehension.

It is clear from Table 4.1 and 4.2 that diffraction peaks for Fe_3Al and FeAl are almost coincident. Hence, it is difficult to distinguish between the two only from x-ray diffraction results. EDAX (please see section 4.3) taken at various points in single phase Fe - 28%Al alloy have shown that its stoichiometric composition is Fe_3Al.

From Fig.4.13, it can be observed that the (220) peak of Fe_3Al is strongest in all cases except in case of alloy subjected to heat treatment at 950°C for 1 hour followed by air cooling. However at this stage the (400) peak of Fe_3Al, which was rather weak and even absent in 800°C treated material, becomes very strong. Material heat treated at 800°C (followed by air cooling), on the other hand, shows a strong (222) Fe_3Al peak which is practically absent in all the other samples.

From these results it is clear that there is a distinct texture effect in this material as a function of heat treatment. Although, texturally, the as received and the materials heat treated at 400°C and 600°C are quite similar showing that the (220) planes are predominantly parallel to the rolling plane, the material heat treated at 800°C shows that a substantial number of planes of the (222) type are parallel to the rolling plane; by contrast the material heat treated at 950°C has a majority of (400) planes parallel to the rolling plane.

b) Fe - 28% Al - 5% Cr Alloy

X-ray diffraction data for this alloy in the as received condition as well as after heat treatment at 400°C, 600°C, 800°C and 950°C for 1 hour (followed by air cooling) are presented in following Tables:

Table 4.6 (a) : As received sample.

2θ	θ	I	I/I_{max}	d(Å)	(h k l)
31.0	15.5	13.0	8.6	4.29	---
32.5	16.25	15.0	9.9	4.09	---
38.5	19.25	17.0	11.0	3.47	---
46.5	23.25	24.0	15.8	2.90	(200) Fe_3Al/(100) FeAl
68.0	34.00	152.0	100.0	2.048	(220) Fe_3Al/(110) FeAl
86.5	43.25	12.0	7.9	1.67	(222) Fe_3Al/(111) FeAl
104.0	52.00	112.0	73.0	1.45	(400) Fe_3Al/(200) FeAl

Table 4.6 (b) : Sample heat treated at 400°C for 1 hr. followed by AC.

2θ	θ	I	I/I_{max}	d(Å)	(h k l)
46.5	23.25	26.0	28.0	2.90	(200) Fe_3Al/(100) FeAl
68.0	34.00	93.0	100.0	2.048	(220) Fe_3Al/(110) FeAl
86.5	43.25	9.0	9.7	1.67	(222) Fe_3Al/(111) FeAl
104.5	52.25	86.0	92.5	1.45	(400) Fe_3Al/(200) FeAl

Table 4.6 (c) : Sample heat treated at 600°C for 1 hr. followed by AC.

2θ	θ	I	I/I_{max}	d(Å)	(h k l)
46.5	23.25	29.0	24.8	2.90	(200) Fe_3Al/(100) FeAl
68.0	34.00	66.0	56.5	2.048	(220) Fe_3Al/(110) FeAl
86.5	43.25	16.0	13.6	1.67	(222) Fe_3Al/(111) FeAl
104.5	52.25	117.0	100.0	1.45	(400) Fe_3Al/(200) FeAl

Table 4.6 (d) : Sample heat treated at 800°C for 1 hr. followed by AC.

2θ	θ	I	I/I_{max}	d(Å)	(h k l)
40.5	20.25	8.0	33.0	3.35	(111) Fe_3Al
46.5	23.25	24.0	100.0	2.90	(200) Fe_3Al/(100) FeAl
68.0	34.00	11.0	46.0	2.048	(220) Fe_3Al/(110) FeAl
82.0	41.00	8.0	33.0	1.74	(311) Fe_3Al
86.5	43.25	20.0	83.0	1.67	(222) Fe_3Al/(111) FeAl
104.5	52.25	13.0	54.0	1.45	(400) Fe_3Al/(200) FeAl

Table 4.6 (e) : Sample heat treated at 950°C for 1 hr. followed by AC.

2θ	θ	I	I/I_{max}	d(Å)	(h k l)
40.5	20.25	8.0	6.0	3.35	(111) Fe_3Al
46.5	23.25	134.0	100.0	2.90	(200) Fe_3Al/(100) FeAl
104.5	52.25	12.0	9.0	1.45	(400) Fe_3Al/(200) FeAl

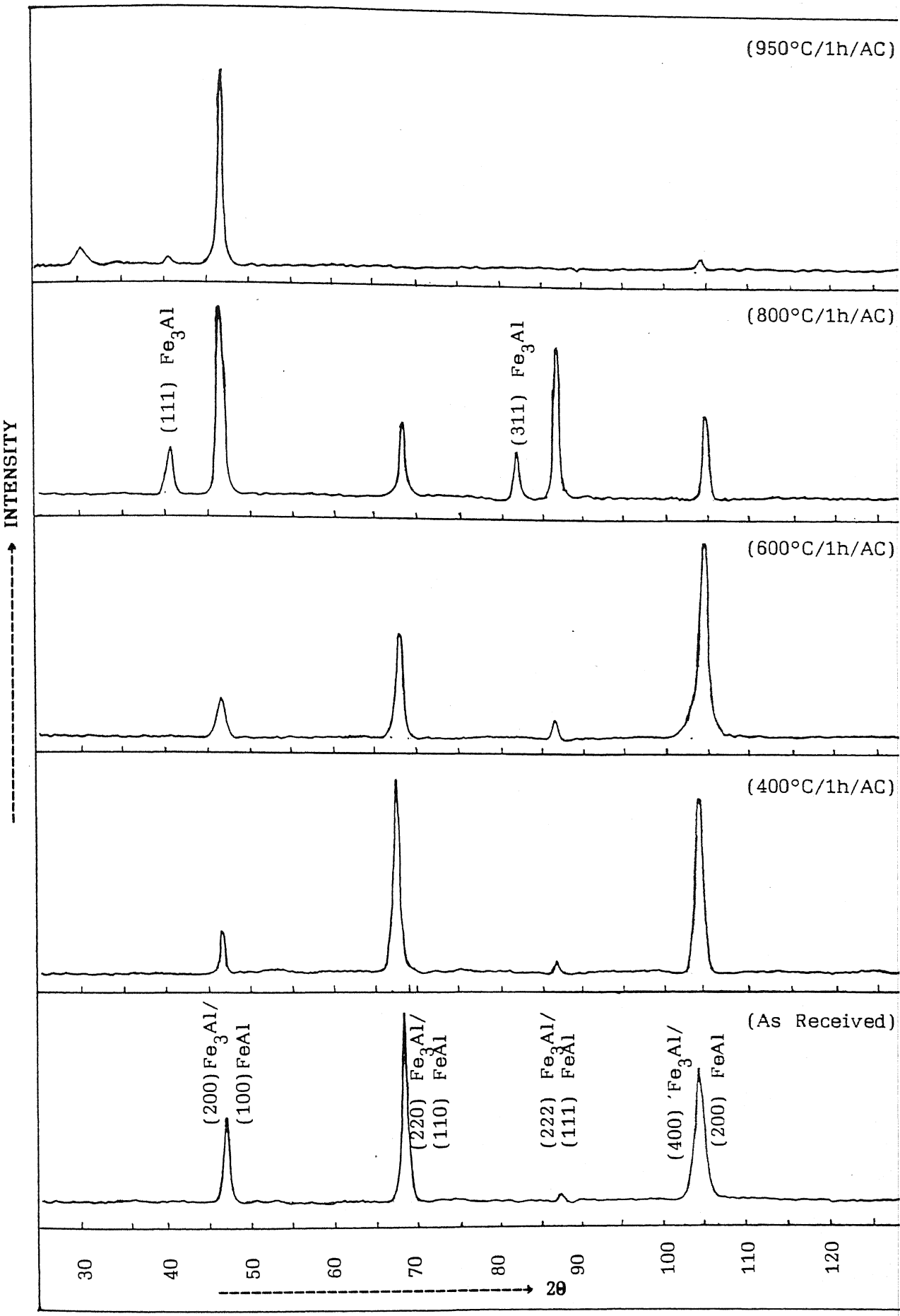

Fig. 4.14 : X-ray diffraction pattern of Fe-28% Al - 5% Cr alloy on RP

In addition to this, results are also presented in graphical form in Fig.4.14 for easy comprehension.

The (220) peak of Fe_3Al, which is strong in as received alloy, weakens as annealing temperature is raised and disappears after annealing at 950°C. This tread is similar to one obtained in case of Fe - 28%Al alloy. By contrast the (200) peak of Fe_3Al strengthens as annealing temperature is raised and becomes the strongest peak after annealing of 950°C. The (400) peak of Fe_3Al behaves in a rather similar fashion as the (220) except that the (400) Fe_3Al peak is strongest for alloy subjected to annealing schedule 600°C/1h/AC. Other significant feature of Fig.4.14 is presence of (111) and (311) peaks of Fe_3Al in alloy annealed at 800°C for 1 hour. In short, texturally there is not much difference in the as received material and materials annealed upto 600°C, whereas distinctly different textures are obtained for the 800°C and 950°C treated materials.

c) Fe - 28% Al - 5% Cr - 5% Zr - 0.05% C Alloy

Tables 4.7 (a-e) present x-ray diffraction data for this alloy in as received condition as well as after subjecting this alloy to annealing treatments at 400°C, 600°C, 800°C and 950°C for 1 hour:

Table 4.7 (a) : As received sample.

2θ	θ	I	I/I_{max}	d(Å)	(h k l)
32.5	16.25	16.0	22.0	4.09	---
38.5	19.75	18.0	24.0	3.47	---
46.5	23.25	26.0	35.0	2.90	(200) Fe_3Al/(100) FeAl
58.0	29.0	14.0	19.0	2.36	(422) Fe_3Zr
60.0	30.0	15.0	20.0	2.29	(511, 333) Fe_3Zr
68.0	34.00	74.0	100.0	2.048	(220) Fe_3Al/(110) FeAl
86.5	43.25	24.0	32.0	1.67	(222) Fe_3Al/(111) FeAl
104.0	52.00	60.0	81.0	1.45	(400) Fe_3Al/(200) FeAl/ (800) Fe_3Zr

Table 4.7 (b) : Sample heat treated at 400°C for 1 hr. followed by AC.

2θ	θ	I	I/I_{max}	d(Å)	(h k l)
46.5	23.25	20.0	33.0	2.90	(200) Fe_3Al/(100) FeAl
58.0	29.0	7.5	12.5	2.36	(422) Fe_3Zr
60.5	30.25	8.0	13.3	2.29	(511, 333) Fe_3Zr
68.0	34.00	39.0	65.0	2.048	(220) Fe_3Al/(110) FeAl
86.5	43.25	13.0	21.7	1.67	(222) Fe_3Al/(111) FeAl
95.5	47.75	7.0	11.7	1.547	(731, 553) Fe_3Zr
104.5	52.25	60.0	100.0	1.45	(400) Fe_3Al/(200) FeAl/ (800) Fe_3Zr

Table 4.7 (c) : Sample heat treated at 600°C for 1 hr. followed by AC.

2θ	θ	I	I/I_{max}	d(Å)	(h k l)
40.5	20.25	7.0	9.9	3.30	(111) Fe_3Al
46.5	23.25	7.0	9.9	2.90	(200) Fe_3Al/(100) FeAl
68.0	34.00	71.0	100.0	2.048	(220) Fe_3Al/(110) FeAl
86.5	43.25	8.0	11.26	1.67	(222) Fe_3Al/(111) FeAl
104.5	52.25	18.0	25.3	1.45	(400) Fe_3Al/(200) FeAl/ (800) Fe_3Zr
124.0	62.00	8.0	11.26	1.297	(420) Fe_3Al/(210) FeAl/ (911, 753) Fe_3Zr

Table 4.7 (d) : Sample heat treated at 800°C for 1 hr. followed by AC.

2θ	θ	I	I/I_{max}	d(Å)	(h k l)
40.5	20.25	8.0	6.5	3.30	(111) Fe_3Al
46.5	23.25	8.0	6.5	2.90	(200) Fe_3Al/(100) FeAl
68.0	34.00	123.0	100.0	2.048	(220) Fe_3Al/(110) FeAl
86.5	43.25	8.0	6.5	1.67	(222) Fe_3Al/(111) FeAl
104.5	52.25	13.0	10.5	1.45	(400) Fe_3Al/(200) FeAl/ (800) Fe_3Zr

Table 4.7 (e) : Sample heat treated at 950°C for 1 hr. followed by AC.

2θ	θ	I	I/I_{max}	d(Å)	(h k l)
46.5	23.25	9.5	11.3	2.90	(200) Fe_3Al/(100) FeAl
60.0	30.00	3.5	4.16	2.29	(511, 333) Fe_3Zr
68.0	34.00	84.0	100.0	2.048	(220) Fe_3Al/(110) FeAl
86.5	43.25	7.0	8.33	1.67	(222) Fe_3Al/(111) FeAl
104.0	52.00	66.5	79.20	1.45	(400) Fe_3Al/(200) FeAl/ (800) Fe_3Zr

These results are also presented in Fig.4.15. Following features can be easily traced from this figure.

The (220) peak of Fe_3Al is strongest in almost all cases. The (400) peak of Fe_3Al is another strong peak which is found in all the samples, those were annealed at 600°C and 800°C for 1 hour. Another feature is the presence of (422), (511) and (333) peaks of Fe_3Zr alloy in almost all cases. This result, along with EDAX, SEM and optical microscopic analysis (please see section 4.3) confirms that this is a two phase alloy. When this alloy was annealed at 800°C for 1 hour (followed by air cooling), only (220) Fe_3Al peak was present and all others practically vanish.

After subjecting all the three alloys to probing heat treatments at 400°C, 600°C, 800°C and 950°C respectively for 1 hour, it was decided to increase the annealing time to 10 hours (temperatures remaining unchanged) so that the phases present at different annealing temperatures more or less attain an

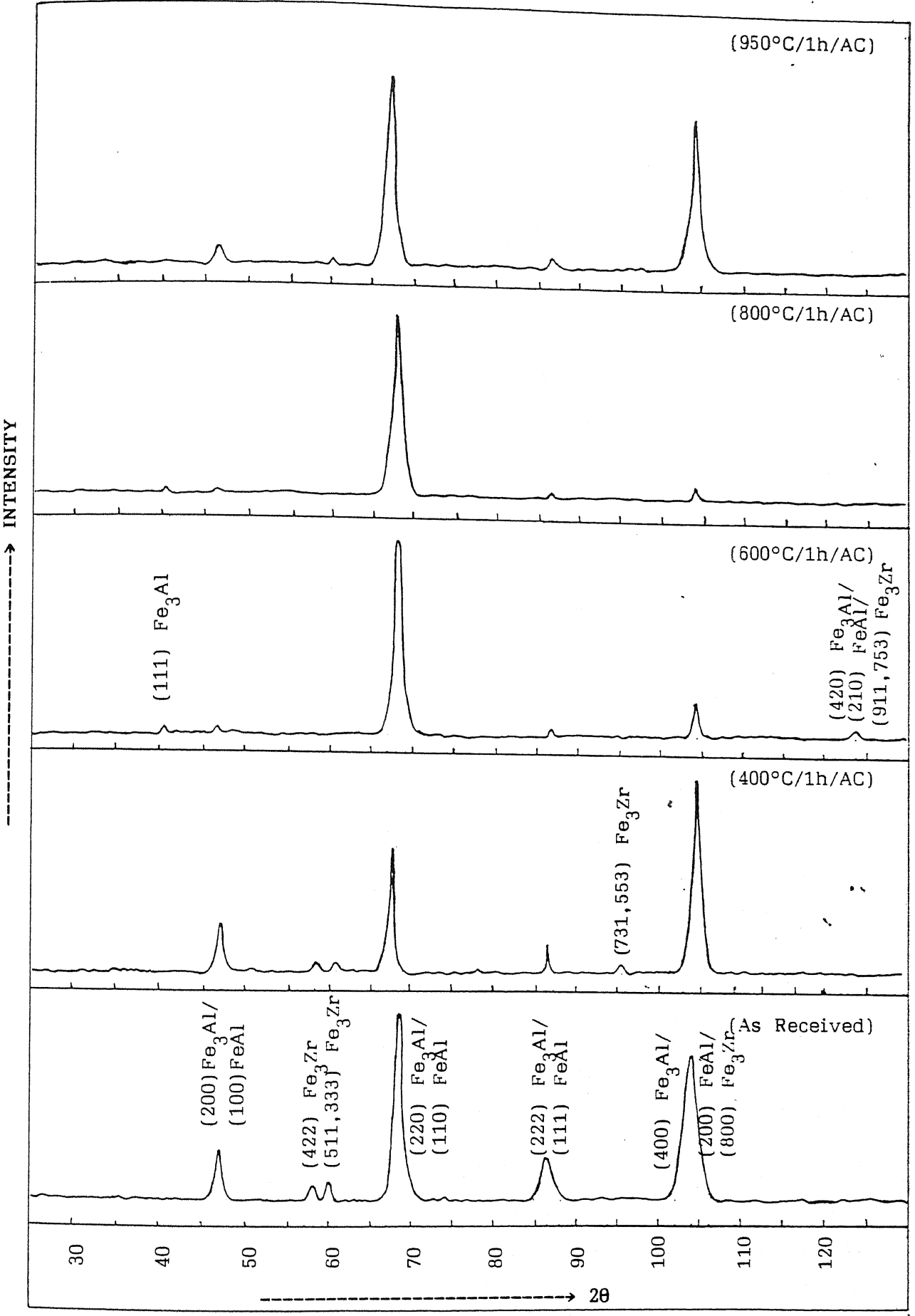

Fig. 4.15 : X-ray diffraction pattern of Fe-28% Al - 5% Cr - 5% Zr - 0.05% C alloy on RP

equilibrium stage. In addition to this, it was also decided to subject one set of samples to water quenching. In addition, diffraction patterns were taken from both the rolling plane and the mid plane of each sample. X-ray diffraction data taken for these alloys are tabulated in Section 4.2.3, 4.2.4 and 4.2.5 respectively.

4.2.3 Fe - 28%Al Alloy

4.2.3.1 Tables for X-ray Diffraction Data on Rolling plane:

Table 4.8(i): As Received Sample

2θ	θ	I	I/I_{max}	d(Å)	(h k l)
46.5	23.25	14.0	1.5	2.90	(200) Fe_3Al/(100) FeAl
68.0	34.00	930.0	100.0	2.048	(220) Fe_3Al/(110) FeAl
86.5	43.25	9.0	0.96	1.67	(222) Fe_3Al/(111) FeAl
104.0	52.00	40.0	4.3	1.45	(400) Fe_3Al/(200) FeAl

Table 4.8 (ii) (a): Sample Heat Treated at 400°C for 10 hour followed by Air Cooling.

2θ	θ	I	I/I_{max}	d(Å)	(h k l)
32.5	16.25	7.5	4.6	4.09	-
40.0	20.00	4.5	2.8	3.35	(111) Fe_3Al
46.5	23.25	8.5	5.2	2.90	(200) Fe_3Al/(100) FeAl
68.0	34.0	162.0	100.0	2.04	(220) Fe_3Al/(110) FeAl
86.5	43.25	2.5	1.5	1.67	(222) Fe_3Al/(111) FeAl
104.0	52.0	76.0	46.9	1.45	(400) Fe_3Al/(200) FeAl

Table 4.8 (ii) (b): Sample Heat Treated at 400°C for 10 hour followed by Water Quenching.

2θ	θ	I	I/I_{max}	d(Å)	(h k l)
33.0	16.5	18.5	6.5	4.05	---
40.0	20.00	11.0	4.0	3.35	(111) Fe_3Al
46.5	23.25	13.0	4.5	2.90	(200) Fe_3Al/(100) FeAl
68.0	34.00	285.0	100.0	2.04	(220) Fe_3Al/(110) FeAl
86.5	43.25	3.0	1.0	1.67	(222) Fe_3Al/(111) FeAl
104.0	52.00	69.0	24.2	1.45	(400) Fe_3Al/(200) FeAl

Table 4.8 (iii) (a): Sample Heat Treated at 600°C for 10 hour followed by Air Cooling.

2θ	θ	I	I/I_{max}	d(Å)	(h k l)
32.5	16.25	11.5	3.4	4.09	---
46.5	23.25	6.5	1.9	2.90	(200) Fe_3Al/(100) FeAl
68.0	34.00	340.0	100.0	2.048	(220) Fe_3Al/(110) FeAl
86.5	43.25	1.5	0.44	1.67	(222) Fe_3Al/(111) FeAl
104.0	52.0	41.5	12.2	1.45	(400) Fe_3Al/(200) FeAl

Table 4.8 (iii) (b): Sample Heat Treated at 600°C for 10 hour followed by Water Quenching.

2θ	θ	I	I/I_{max}	d(Å)	(h k l)
32.0	16.00	6.0	3.6	4.15	---
46.5	43.25	8.5	5.1	2.90	(200) Fe_3Al/(100) FeAl
68.0	34.00	166.0	100.0	2.04	(220) Fe_3Al/(110) FeAl
86.0	43.00	3.0	1.8	1.68	(222) Fe_3Al/(111) FeAl
104.0	52.00	92.0	55.4	1.45	(400) Fe_3Al/(200) FeAl

Table 4.8 (iv) (a): Sample Heat Treated at 800°C for 10 hour followed by Air Cooling.

2θ	θ	I	I/I_{max}	d(Å)	(h k l)
32.5	16.25	9.5	3.3	4.09	---
46.5	23.25	3.0	1.0	2.90	(200) Fe_3Al/(100) FeAl
68.0	34.00	285.0	100.0	2.048	(220) Fe_3Al/(110) FeAl
104.0	52.0	50.0	17.5	1.45	(400) Fe_3Al/(200) FeAl

Table 4.8 (iv) (b): Sample Heat Treated at 800°C for 10 hour followed by Water Quenching.

2θ	θ	I	I/I_{max}	d(Å)	(h k l)
32.5	16.25	16.5	5.8	4.09	---
46.5	43.25	9.0	3.1	2.90	(200) Fe_3Al/(100) FeAl
68.0	34.00	285.0	100.0	2.048	(220) Fe_3Al/(110) FeAl
104.0	52.00	48.0	16.8	1.45	(400) Fe_3Al/(200) FeAl

Table 4.8 (v) (a): Sample Heat Treated at 950°C for 10 hour followed by Air Cooling.

2θ	θ	I	I/I_{max}	d(Å)	(h k l)
32.5	16.25	13.0	4.6	4.09	---
40.0	20.00	7.5	2.6	3.35	(111) Fe_3Al
46.5	23.25	3.0	1.0	2.90	(200) Fe_3Al/(100) FeAl
68.0	34.00	285.0	100.0	2.048	(220) Fe_3Al/(110) FeAl
86.5	43.25	9.0	3.1	1.67	(222) Fe_3Al/(111) FeAl
104.0	52.0	16.0	5.6	1.45	(400) Fe_3Al/(200) FeAl

Table 4.8 (v) (b): Sample Heat Treated at 950°C for 10 hour followed by Water Quenching.

2θ	θ	I	I/I_{max}	d(Å)	(h k l)
32.5	16.25	18.5	13.2	4.09	---
46.5	23.05	4.0	2.85	2.90	(200) Fe_3Al/(100) FeAl
68.0	34.00	140.0	100.0	2.048	(220) Fe_3Al/(110) FeAl
104.0	52.00	18.0	13.0	1.45	(400) Fe_3Al/(200) FeAl

4.2.3.2 Tables for X-ray Diffraction Data on Mid Plane:

Table 4.9 (i): As received sample.

2θ	θ	I	I/I_{max}	d(Å)	(h k l)
31.0	15.50	18.0	8.0	4.29	---
38.0	19.0	14.0	6.25	3.52	---
40.0	20.00	15.0	6.70	3.35	(111) Fe_3Al
46.5	23.25	63.0	28.0	2.90	(200) Fe_3Al/(100) FeAl
68.0	34.00	53.0	24.0	2.048	(220) Fe_3Al/(110) FeAl
86.5	43.25	8.0	3.6	1.68	(222) Fe_3Al/(111) FeAl
104.0	52.0	224.0	100.6	1.45	(400) Fe_3Al/(200) FeAl

Table 4.9 (ii) (a): Sample heat treated at 400°C for 10 hour followed by Air Cooling.

2θ	θ	I	I/I_{max}	d(Å)	(h k l)
31.0	15.50	17.5	1.75	4.28	---
40.0	20.00	43.5	4.35	3.35	(111) F_3Al
46.5	23.05	162.0	16.20	2.90	(200) Fe_3Al/(100) FeAl
68.0	34.00	9.5	0.95	2.048	(220) Fe_3Al/(110) FeAl
82.0	41.00	1.5	0.15	1.75	(311) Fe_3Al
104.0	104.00	1000.0	100.0	1.45	(400) Fe_3Al/(200) FeAl

Table 4.9 (ii) (b): Sample heat treated at 400°C for 10 hour followed by Water Quenching.

2θ	θ	I	I/I_{max}	d(Å)	(h k l)
40.0	20.00	3.0	3.00	3.35	(111) F_3Al
46.5	23.05	16.5	16.50	2.90	(200) Fe_3Al/(100) FeAl
68.0	34.00	35.5	35.50	2.048	(220) Fe_3Al/(110) FeAl
86.5	43.25	2.5	2.5	1.67	(222) Fe_3Al/(111) FeAl
104.0	52.00	99.5	100.0	1.45	(400) Fe_3Al/(200) FeAl

Table 4.9 (iii) (a): Sample heat treated at 600°C for 10 hour followed by Air Cooling.

2θ	θ	I	I/I_{max}	d(Å)	(h k l)
33.0	16.50	13.5	7.5	4.29	---
46.5	23.05	14.5	8.10	2.90	(200) Fe_3Al/(100) FeAl
68.0	34.00	178.0	100.00	2.048	(220) Fe_3Al/(110) FeAl
86.5	43.25	1.0	0.56	1.67	(222) Fe_3Al/(111) FeAl
104.5	52.25	56.0	31.4	1.45	(400) Fe_3Al/(200) FeAl

Table 4.9 (iii) (b): Sample heat treated at 400°C for 10 hour followed by Water Quenching.

2θ	θ	I	I/I_{max}	d(Å)	(h k l)
38.0	19.00	17.0	3.60	3.52	---
46.5	23.25	45.5	9.70	2.90	(200) Fe_3Al/(100) FeAl
68.0	34.00	77.0	16.40	2.048	(220) Fe_3Al/(110) FeAl
86.5	43.25	7.0	1.5	1.67	(222) Fe_3Al/(111) FeAl
104.0	52.25	470.0	100.0	1.45	(400) Fe_3Al/(200) FeAl

Table 4.9 (iv) (a): Sample heat treated at 800°C for 10 hour followed by Air Cooling.

2θ	θ	I	I/I_{max}	d(Å)	(h k l)
32.5	16.25	15.5	2.30	4.09	---
40.0	20.00	45.0	6.80	3.35	(111) Fe_3Al
46.5	23.25	11.5	1.70	2.90	(200) Fe_3Al/(100) FeAl
68.0	34.00	660.0	100.00	2.048	(220) Fe_3Al/(110) FeAl
82.0	41.00	14.5	2.2	1.75	(311) Fe_3Al
86.5	43.25	4.0	0.61	1.67	(222) Fe_3Al/(111) FeAl
104.5	52.00	34.5	5.2	1.45	(400) Fe_3Al/(200) FeAl

Table 4.9 (iv) (b): Sample heat treated at 800°C for 10 hour followed by Water Quenching.

2θ	θ	I	I/I_{max}	d(Å)	(h k l)
32.5	16.25	16.5	8.30	4.09	---
38.5	19.25	9.5	4.80	3.52	---
46.0	23.00	9.5	4.80	2.90	(200) Fe_3Al/(100) FeAl
68.0	34.00	198.0	100.00	2.048	(220) Fe_3Al/(110) FeAl
104.0	52.00	86.5	43.70	1.45	(400) Fe_3Al/(200) FeAl

Table 4.9 (v) (a): Sample heat treated at 950°C for 10 hour followed by Air Cooling.

2θ	θ	I	I/I_{max}	d(Å)	(h k l)
46.5	23.05	5.0	8.50	2.90	(200) Fe_3Al/(100) FeAl
68.0	34.00	58.5	100.00	2.048	(220) Fe_3Al/(110) FeAl
82.0	41.00	49.5	84.60	1.75	(311) Fe_3Al
103.5	52.00	7.5	12.8	1.45	(400) Fe_3Al/(200) FeAl

Table 4.9 (v) (b): Sample heat treated at 950°C for 10 hour followed by Water Quenching.

2θ	θ	I	I/I_{max}	d(Å)	(h k l)
46.5	23.25	11.0	8.00	2.90	(200) Fe_3Al/(100) FeAl
68.0	34.00	138.0	100.00	2.048	(220) Fe_3Al/(110) FeAl
103.5	51.75	25.5	18.5	1.45	(400) Fe_3Al/(200) FeAl

The x-ray diffraction results are also given in a graphical form in Fig.4.16, 4.17, 4.18 and 4.19 for easy comprehension.

4.2.3(a) Effect of heat treatment on diffraction patterns of each sample:

From Fig.4.16 and 4.17, it is obvious that there is no significant effect of heat treatment on rolling plane x-ray diffraction patterns of Fe - 28%Al alloy in both air cooled as well as water quenched conditions. In both cases the (220) peak of Fe_3Al is the strongest at all temperatures as well as in as

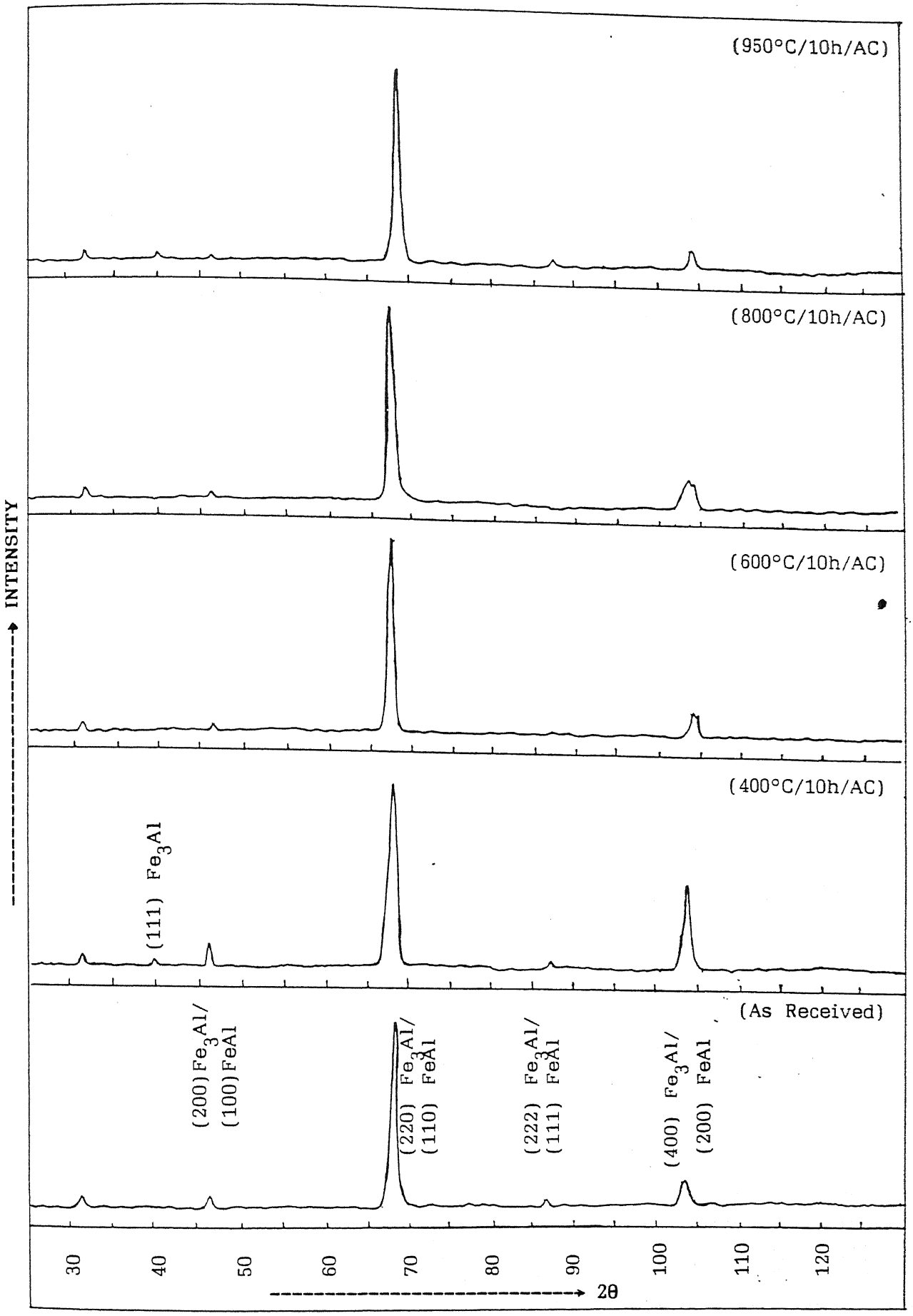

Fig. 4.16 : X-ray diffraction pattern of Fe-28% Al alloy on RP

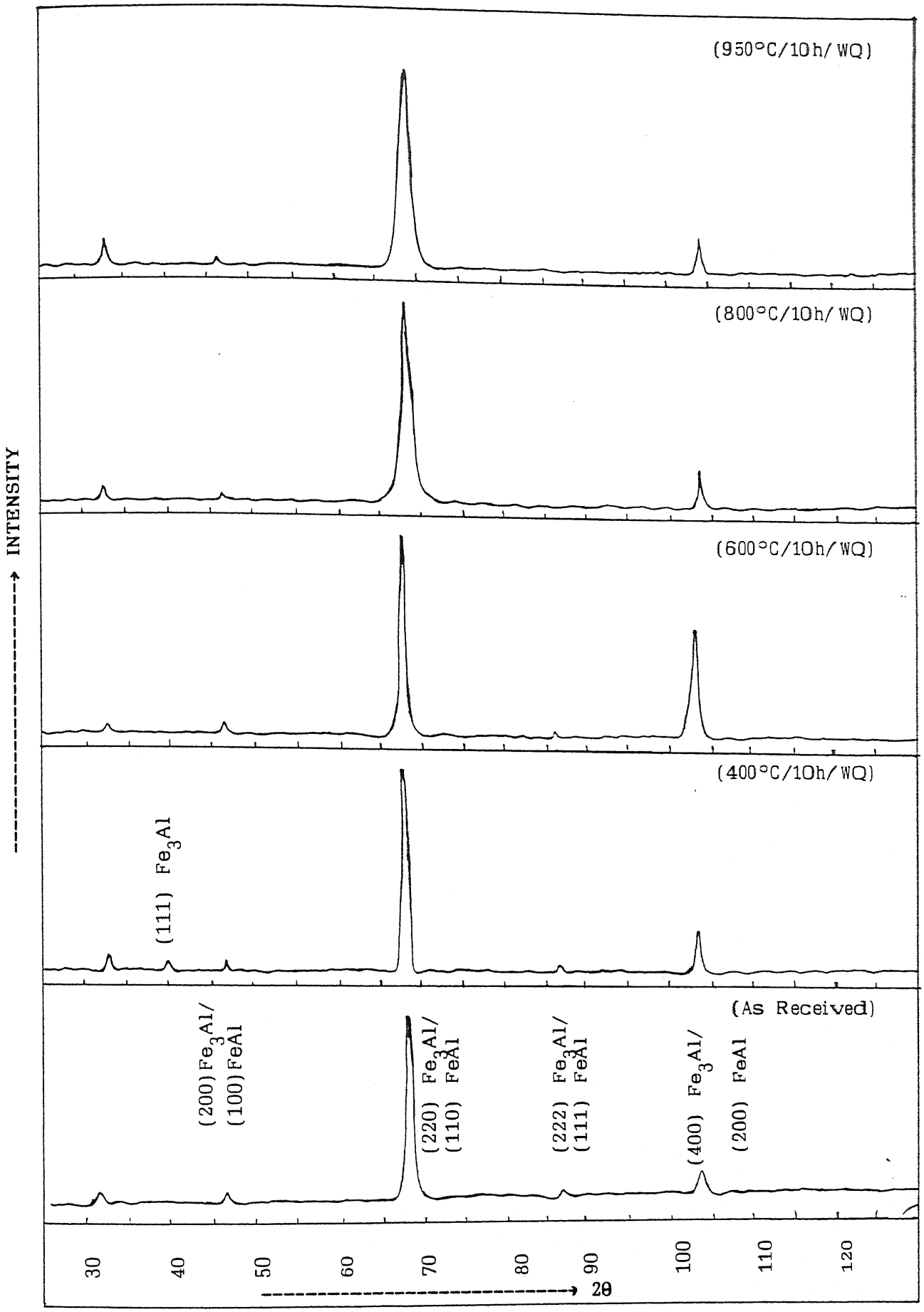

Fig. 4.17 : X-ray diffraction pattern of Fe-28% Al alloy on RP

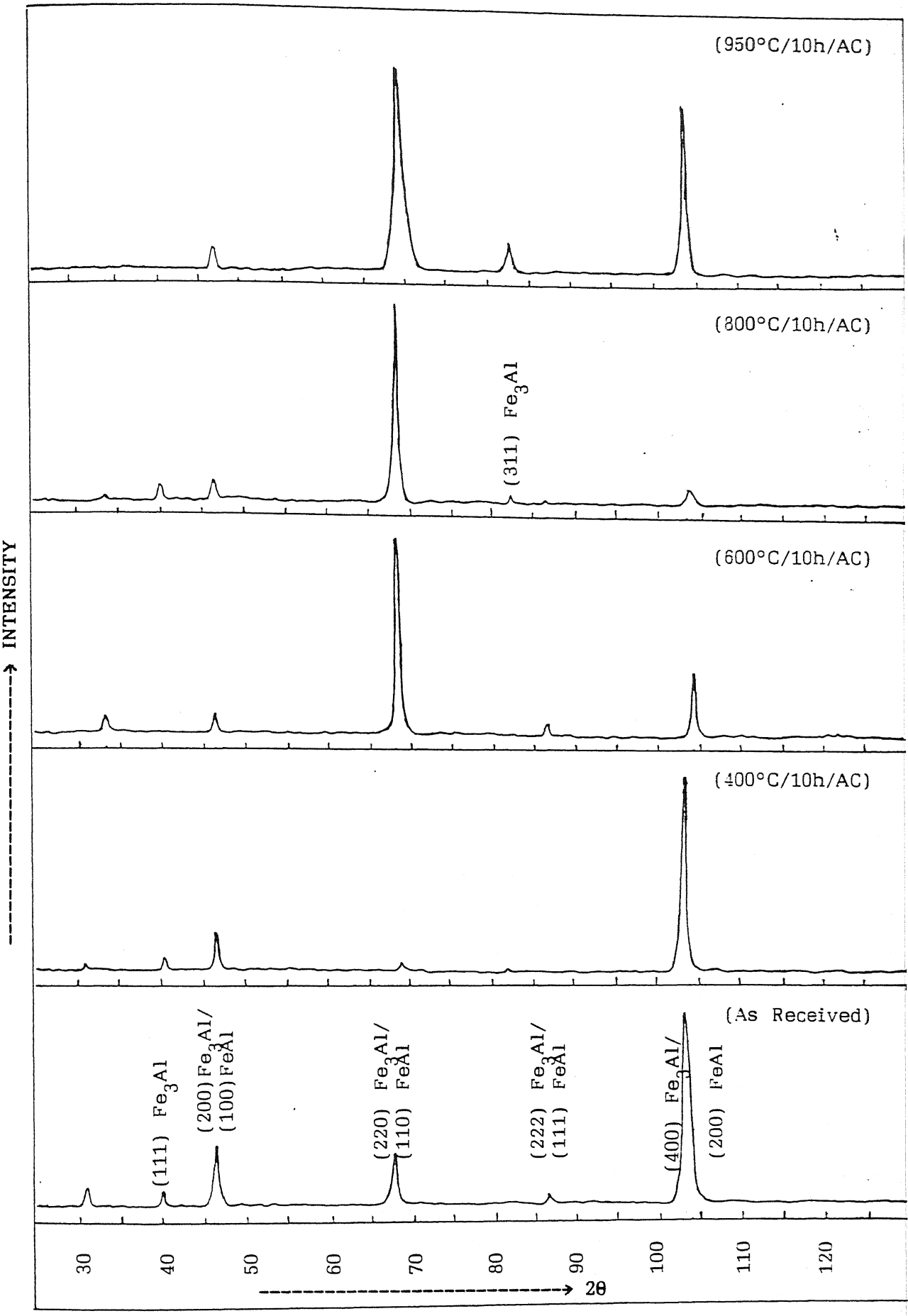

Fig. 4.18 : X-ray diffraction pattern of Fe-28% Alalloy on MP

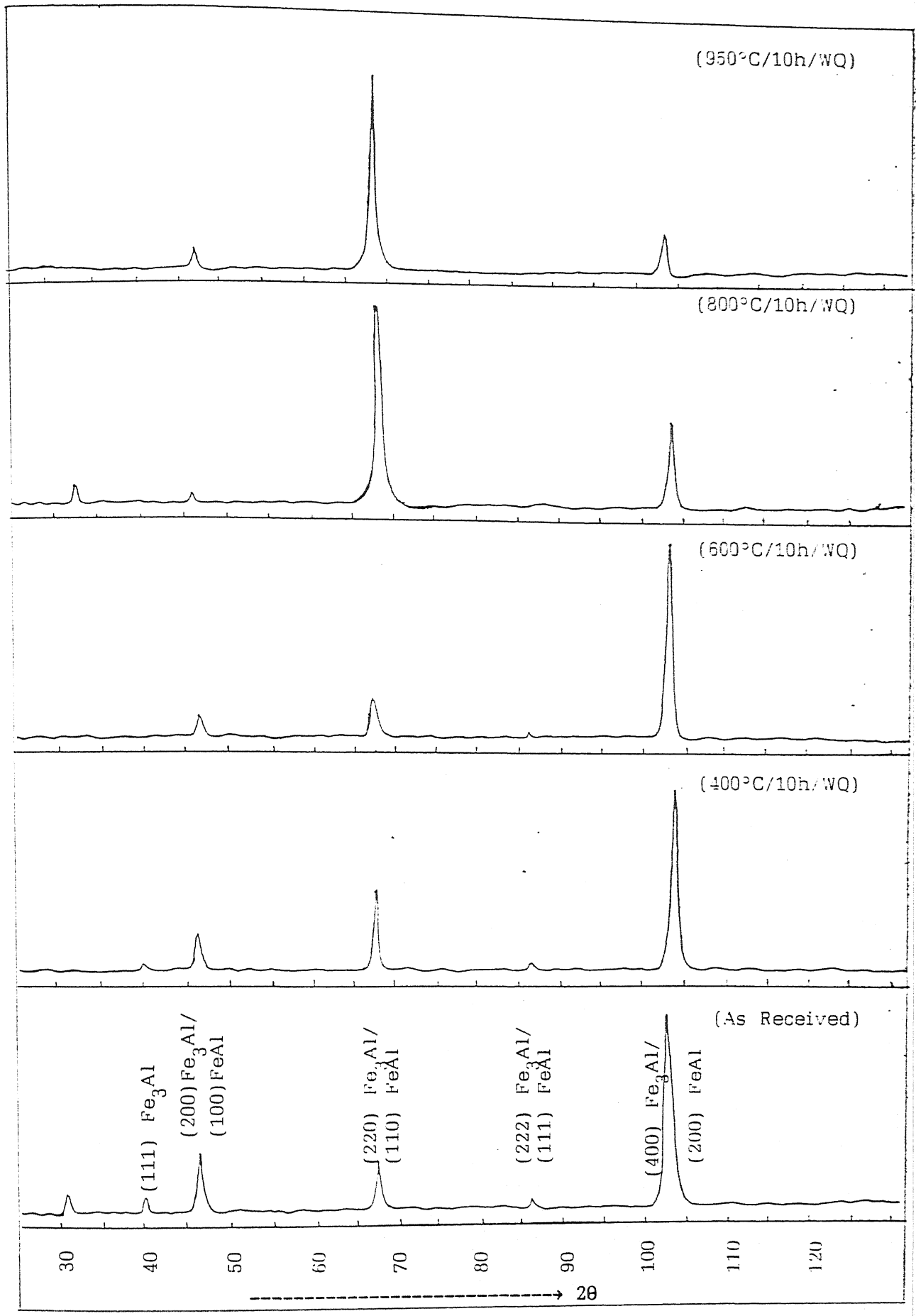

Fig. 4.19 : X-ray diffraction pattern of Fe-28% Al alloy on MP

received condition. In case of the sample subjected to heat treatment schedule 600°C/10h/WQ (600°C is the temperature, slightly below which, recrystallization begins), (400) peak of Fe_3Al is also significant. In case of mid plane x-ray diffraction patterns of the alloy, in both air cooled and water quenched condition, (220) peak of Fe_3Al strengthens as annealing temperature is raised [Fig.4.18 and 4.19]. In case of air cooled alloy [Fig.4.18], (400) peak of Fe_3Al is strongest at lower temperatures (as received condition and in heat treated condition at 400°C/10h/Al). As annealing temperature is raised to 600°C and 800°C, intensity of this peak becomes very low and finally at 950°C, this peak again becomes a prominent peak.In case of water quenched alloy [Fig.4.19], (400) Fe_3Al peak is strongest till annealing temperature is raised to 600°C. As temperature is further raised, this peak weakens. In addition to this, (222) peak of Fe_3Al which was very weak at initial temperatures disappears as temperature is raised above 600°C.

4.2.3(b) Differences between X-ray diffraction patterns of various samples:

i) Air cooled (AC) alloys on rolling plane (RP) and on mid plane (MP) [Fig.4.16 and 4.18]:

In case of diffraction patterns on rolling plane [Fig.4.16], (220) peak of Fe_3Al is strongest in all cases. In contrast to this, (400) peak of Fe_3Al is generally the strongest in case of diffraction patterns on mid plane [Fig.4.18]. Diffraction patterns of both cases are very similar for alloys which were given annealing treatments of 600°C/10h and 800°C/10h.

ii) Water quenched (WQ) alloys on rolling plane (RP) and on mid plane (MP): [Fig.4.17 and 4.19]

In case of x-ray diffraction patterns on rolling plane [4.17], (220) peak of Fe_3Al is the strongest in all cases. In contrast to this, in case of diffraction patterns on mid plane [Fig.4.19], (400) peak of Fe_3Al is the strongest peak till annealing temperature of 600°C. As annealing temperature is raised to 800°C and 950°C, (220) peak becomes strongest and diffraction patterns in both cases become very similar.

iii) Rolling plane X-ray diffraction patterns for air cooled samples and water quenched samples: [Fig.4.16 and 4.17]

Diffraction patterns of samples in both the condition are exactly similar, except for samples heat treated at 600°C for 10 hour in which case (400) peak of Fe_3Al is stronger in the water quenched sample and is also somewhat shifted towards lower value of 2θ.

iv) Mid plane X-ray diffraction patterns for air cooled samples and water quenched samples : [Fig.18 and 4.19]

The diffraction patterns of samples in the two conditions are quite similar in as received sample and in sample heat treated at 400°C and 800°C for 10 hour. At annealing temperature of 600°C, the two patterns show sharp contrast. In case of air cooled alloy (220) Fe_3Al peak is strongest while (400) Fe_3Al peak is strongest in the other case. In case of alloy heat treated at 950°C for 10 hour (followed by water quenching) only the (220) peak of Fe_3Al is prominent while in case of air cooled alloy (400) peak of Fe_3Al is also significant. In case of air cooled alloys, low intensity

peaks [(220) Fe_3Al, (111) Fe_3Al, (311) Fe_3Al etc.] are more in number as compared to water quenched alloys.

4.2.4 Fe - 28% Al - 5% Cr Alloy

X-ray diffraction patterns for this alloy, too, were taken on both rolling plane as well as on mid plane.

4.2.4.1 Tables for X-ray Diffraction patterns on Rolling Plane:

Table 4.10 (i) : As received sample.

2θ	θ	I	I/I_{max}	d(Å)	(h k l)
31.0	15.5	13.0	8.6	4.29	---
32.5	16.25	15.0	9.9	4.09	---
38.5	19.25	17.0	11.0	3.47	---
46.5	23.25	24.0	15.8	2.90	(200) Fe_3Al/(100) FeAl
68.0	34.00	152.0	100.0	2.048	(220) Fe_3Al/(110) FeAl
86.5	43.25	12.0	7.9	1.67	(222) Fe_3Al/(111) FeAl
104.0	52.00	112.0	73.0	1.45	(400) Fe_3Al/(200) FeAl

Table 4.10 (ii) (a): Sample heat treated at 400°C for 10 hour followed by Air Cooling.

2θ	θ	I	I/I_{max}	d(Å)	(h k l)
39.5	19.75	9.5	5.9	3.35	(111) Fe_3Al
46.5	43.25	13.0	8.00	2.90	(200) Fe_3Al/(100) FeAl
68.0	34.00	162.0	100.00	2.048	(220) Fe_3Al/(110) FeAl
86.5	43.25	5.5	3.46	1.67	(222) Fe_3Al/(111) FeAl
104.5	52.00	116.0	71.6	1.45	(400) Fe_3Al/(200) FeAl

Table 4.10 (ii) (b): Sample heat treated at 400°C for 10 hour followed by Water Quenching.

2θ	θ	I	I/I_{max}	d(Å)	(h k l)
40.0	20.00	26.5	23.50	3.35	(111) Fe_3Al
46.5	23.25	22.0	19.50	2.90	(200) Fe_3Al/(100) FeAl
68.0	34.00	66.5	59.00	2.048	(220) Fe_3Al/(110) FeAl
82.0	41.00	5.5	5.0	1.75	(311) Fe_3Al
86.0	43.00	14.0	12.4	1.68	(222) Fe_3Al/(111) FeAl
104.0	52.00	113.0	100.0	1.45	(400) Fe_3Al/(200) FeAl

Table 4.10 (iii) (a): Sample heat treated at 600°C for 10 hour followed by Air Cooling.

2θ	θ	I	I/I_{max}	d(Å)	(h k l)
33.0	16.50	5.5	3.30	4.09	---
39.5	19.75	9.0	5.40	3.38	(111) Fe_3Al
46.5	23.25	11.5	7.00	2.90	(200) Fe_3Al/(100) FeAl
68.0	34.00	165.0	100.00	2.048	(220) Fe_3Al/(110) FeAl
86.5	43.25	1.2	7.20	1.67	(222) Fe_3Al/(111) FeAl
104.5	52.25	82.0	49.7	1.45	(400) Fe_3Al/(200) FeAl

Table 4.10 (iii) (b): Sample heat treated at 600°C for 10 hour followed by Water Quenching.

2θ	θ	I	I/I_{max}	d(Å)	(h k l)
32.5	16.25	7.5	3.00	4.09	---
46.5	23.25	12.5	5.00	2.90	(200) Fe_3Al/(100) FeAl
68.0	34.00	246.0	100.00	2.048	(220) Fe_3Al/(110) FeAl
86.5	43.25	6.0	2.43	1.67	(222) Fe_3Al/(111) FeAl
104.0	52.00	90.0	36.6	1.45	(400) Fe_3Al/(200) FeAl

Table 4.10 (iv) (a): Sample heat treated at 800°C for 10 hour followed by Air Cooling.

2θ	θ	I	I/I_{max}	d(Å)	(h k l)
46.5	23.25	15.5	11.70	2.90	(200) Fe_3Al/(100) FeAl
68.0	34.00	132.0	100.00	2.048	(220) Fe_3Al/(110) FeAl
86.5	43.25	8.5	6.40	1.67	(222) Fe_3Al/(111) FeAl
104.0	52.00	90.5	68.6	1.45	(400) Fe_3Al/(200) FeAl

Table 4.10 (iv) (b): Sample heat treated at 800°C for 10 hour followed by Water Quenching.

2θ	θ	I	I/I_{max}	d(Å)	(h k l)
32.5	16.25	11.0	9.50	4.09	---
46.5	23.25	9.0	7.80	2.90	(200) Fe_3Al/(100) FeAl
68.0	34.00	115.0	100.00	2.048	(220) Fe_3Al/(110) FeAl
86.5	43.25	3.5	3.0	1.67	(222) Fe_3Al/(111) FeAl
104.0	52.00	22.0	19.1	1.45	(400) Fe_3Al/(200) FeAl

Table 4.10 (v) (a): Sample heat treated at 950°C for 10 hour followed by Air Cooling.

2θ	θ	I	I/I_{max}	d(Å)	(h k l)
32.5	16.25	6.5	6.9	4.09	---
40.0	20.00	4.5	4.8	3.35	(111) Fe_3Al
46.5	23.05	4.5	4.8	2.90	(200) Fe_3Al/(100) FeAl
68.0	34.00	94.0	100.00	2.048	(220) Fe_3Al/(110) FeAl
86.5	43.25	5.5	5.90	1.67	(222) Fe_3Al/(111) FeAl
104.5	52.25	73.5	78.2	1.45	(400) Fe_3Al/(200) FeAl

Table 4.10 (v) (b): Sample heat treated at 950°C for 10 hour followed by Water Quenching.

2θ	θ	I	I/I_{max}	d(Å)	(h k l)
32.5	16.25	12.0	10.50	4.09	---
46.5	23.25	10.0	8.80	2.90	(200) Fe_3Al/(100) FeAl
68.0	34.00	114.0	100.00	2.048	(220) Fe_3Al/(110) FeAl
86.5	43.25	4.5	4.0	1.67	(222) Fe_3Al/(111) FeAl
104.0	52.00	21.5	19.0	1.45	(400) Fe_3Al/(200) FeAl

4.2.4.2 Tables for X-ray Diffraction patterns on Mid Plane.

Table 4.11 (i): As received sample.

2θ	θ	I	I/I_{max}	d(Å)	(h k l)
31.0	15.50	14.0	11.2	4.29	---
32.5	16.25	20.0	16.0	4.09	---
38.0	19.0	14.0	11.2	3.47	---
46.5	23.25	27.0	21.6	2.90	(200) Fe_3Al/(100) FeAl
68.0	34.00	125.0	100.00	2.048	(220) Fe_3Al/(110) FeAl
104.5	52.25	81.0	64.8	1.45	(400) Fe_3Al/(200) FeAl

Table 4.11 (ii) (a): Sample heat treated at 400°C for 10 hour followed by Air Cooling.

2θ	θ	I	I/I_{max}	d(Å)	(h k l)
32.5	16.25	12.0	10.0	4.09	---
46.5	23.25	18.5	15.0	2.90	(200) Fe_3Al/(100) FeAl
68.0	34.00	57.0	46.0	2.048	(220) Fe_3Al/(110) FeAl
104.0	52.00	124.0	100.0	1.45	(400) Fe_3Al/(200) FeAl

Table 4.11 (ii) (b): Sample heat treated at 400°C for 10 hour followed by Water Quenching.

2θ	θ	I	I/I_{max}	d(Å)	(h k l)
31.0	15.50	19.5	12.20	4.28	---
40.0	20.00	17.0	10.5	3.35	(111) Fe_3Al
46.5	23.25	100.0	62.5	2.90	(200) Fe_3Al/(100) FeAl
68.0	34.00	63.5	40.0	2.048	(220) Fe_3Al/(110) FeAl
104.5	52.25	160.0	100.0	1.45	(400) Fe_3Al/(200) FeAl

Table 4.11 (iii) (a): Sample heat treated at 600°C for 10 hour followed by Air Cooling.

2θ	θ	I	I/I_{max}	d(Å)	(h k l)
46.5	23.25	28.5	21.6	2.90	(200) Fe_3Al/(100) FeAl
68.0	34.00	98.0	74.2	2.048	(220) Fe_3Al/(110) FeAl
104.5	52.25	132.0	100.0	1.45	(400) Fe_3Al/(200) FeAl

Table 4.11 (iii) (b): Sample heat treated at 600°C for 10 hour followed by Water Quenching.

2θ	θ	I	I/I_{max}	d(Å)	(h k l)
33.0	16.50	7.5	3.00	4.09	---
46.5	23.25	10.0	3.90	2.90	(200) Fe_3Al/(100) FeAl
68.0	34.00	256.0	100.00	2.048	(220) Fe_3Al/(110) FeAl
104.0	52.00	62.0	24.2	1.45	(400) Fe_3Al/(200) FeAl

Table 4.11 (iv) (a): Sample heat treated at 800°C for 10 hour followed by Air Cooling.

2θ	θ	I	I/I_{max}	d(Å)	(h k l)
46.5	23.25	13.0	29.2	2.90	(200) Fe_3Al/(100) FeAl
68.0	34.00	34.5	77.5	2.048	(220) Fe_3Al/(110) FeAl
104.5	52.25	44.5	100.0	1.45	(400) Fe_3Al/(200) FeAl

Table 4.11 (iv) (b): Sample heat treated at 800°C for 10 hour followed by Water Quenching.

2θ	θ	I	I/I_{max}	d(Å)	(h k l)
32.5	16.25	27.0	10.00	4.09	---
46.5	23.25	7.0	2.6	2.90	(200) Fe_3Al/(100) FeAl
68.0	34.00	270.0	100.00	2.048	(220) Fe_3Al/(110) FeAl
104.0	52.00	24.0	8.9	1.45	(400) Fe_3Al/(200) FeAl

Table 4.11 (v) (a): Sample heat treated at 950°C for 10 hour followed by Air Cooling.

2θ	θ	I	I/I_{max}	d(Å)	(h k l)
32.5	16.25	3.5	3.3	4.09	---
46.5	23.25	3.0	2.8	2.90	(200) Fe_3Al/(100) FeAl
68.0	34.00	106.0	100.0	2.048	(220) Fe_3Al/(110) FeAl
86.5	43.25	4.5	4.2	1.67	(311) Fe_3Al
104.5	52.25	47.5	45.0	1.45	(400) Fe_3Al/(200) FeAl

Table 4.11 (v) (b): Sample heat treated at 950°C for 10 hour followed by Water Quenching.

2θ	θ	I	I/I_{max}	d(Å)	(h k l)
32.5	16.25	11.5	8.60	4.09	---
46.0	23.00	6.5	4.90	2.90	(200) Fe_3Al/(100) FeAl
68.0	34.00	134.0	100.00	2.048	(220) Fe_3Al/(110) FeAl
104.0	52.00	18.5	14.0	1.45	(400) Fe_3Al/(200) FeAl

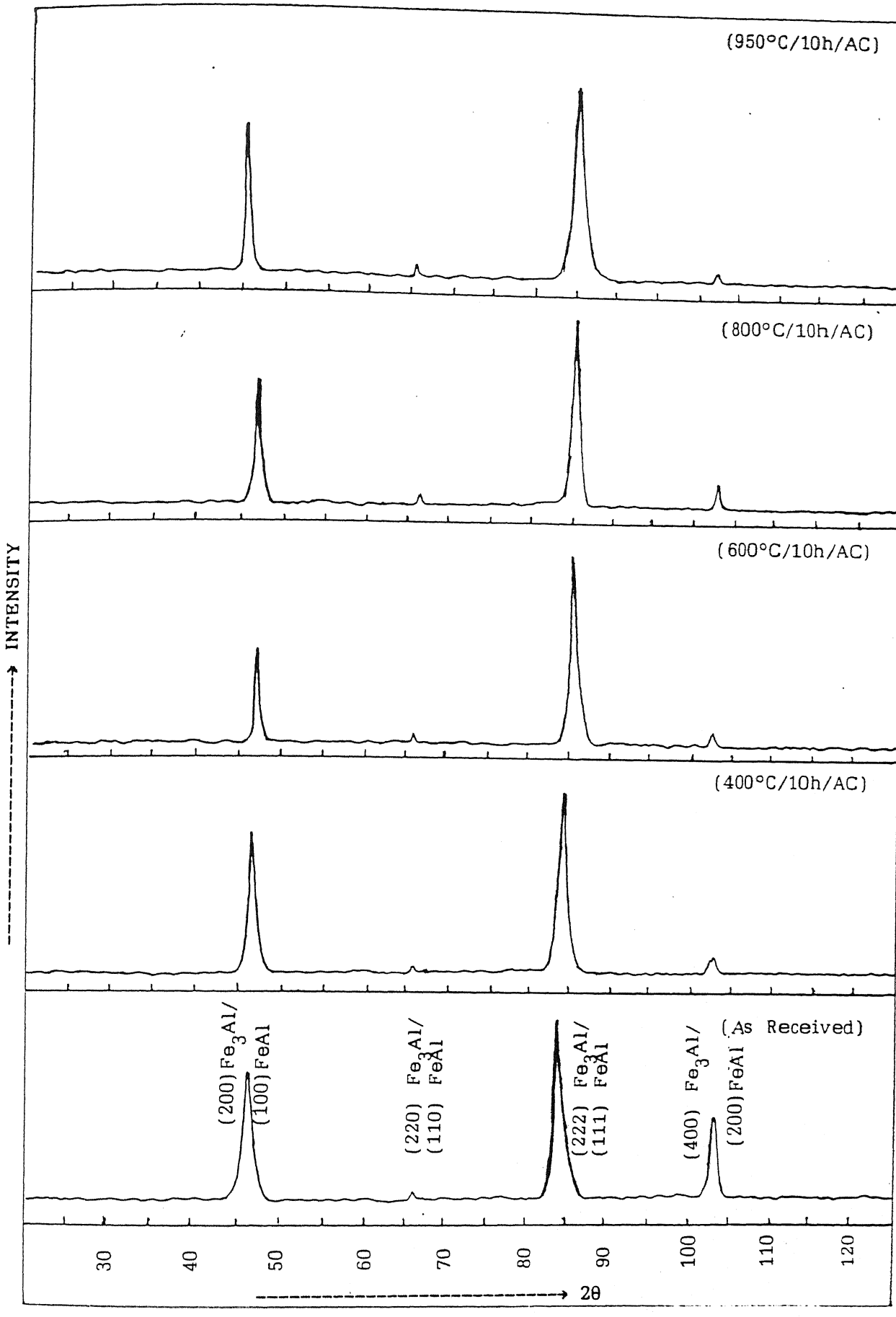

Fig. 4.20 : X-ray diffraction pattern of Fe-28% Al - 5% Cr alloy on RP

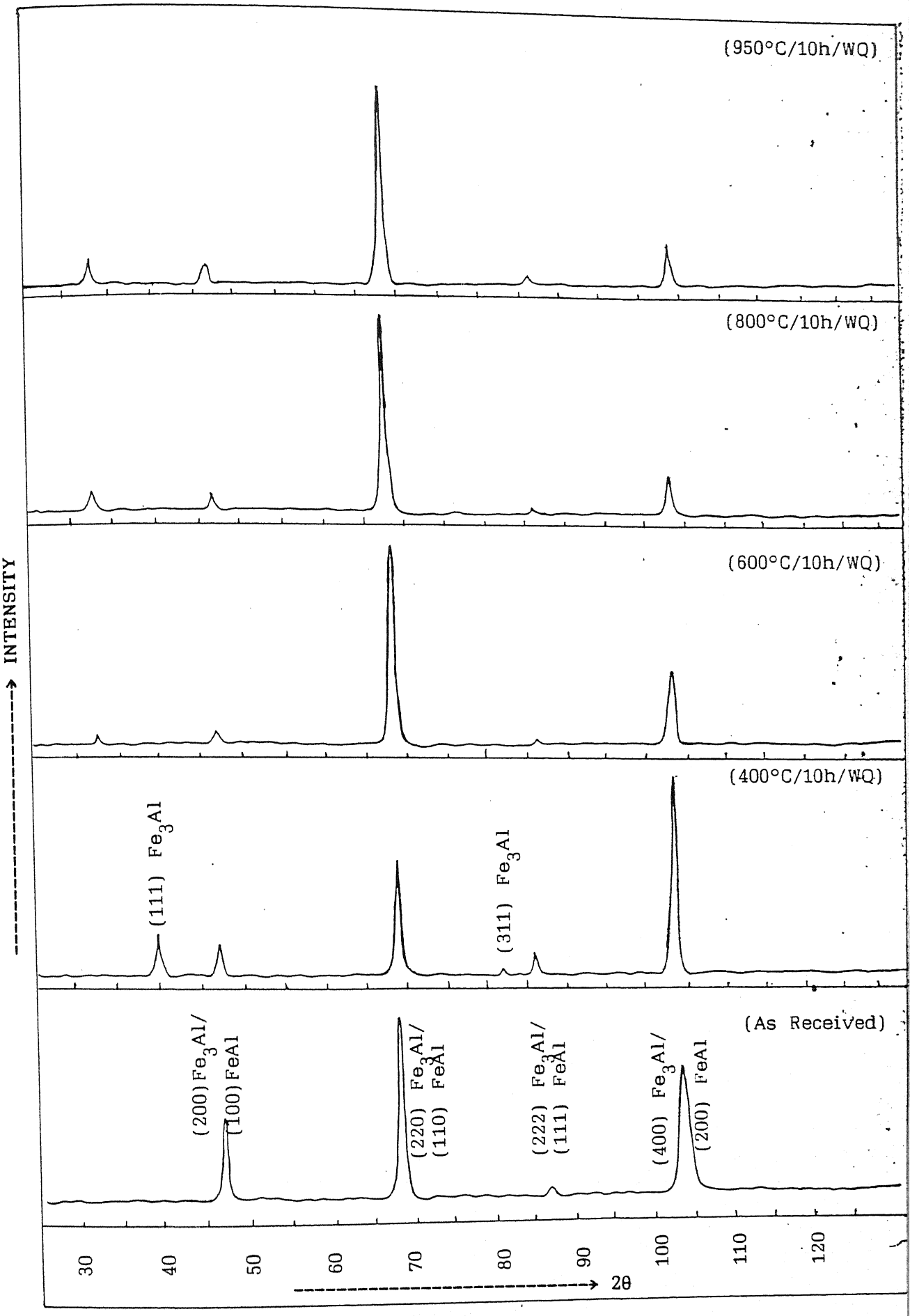

Fig. 4.21 : X-ray diffraction pattern of Fe-28% Al- 5% Cr alloy on RP

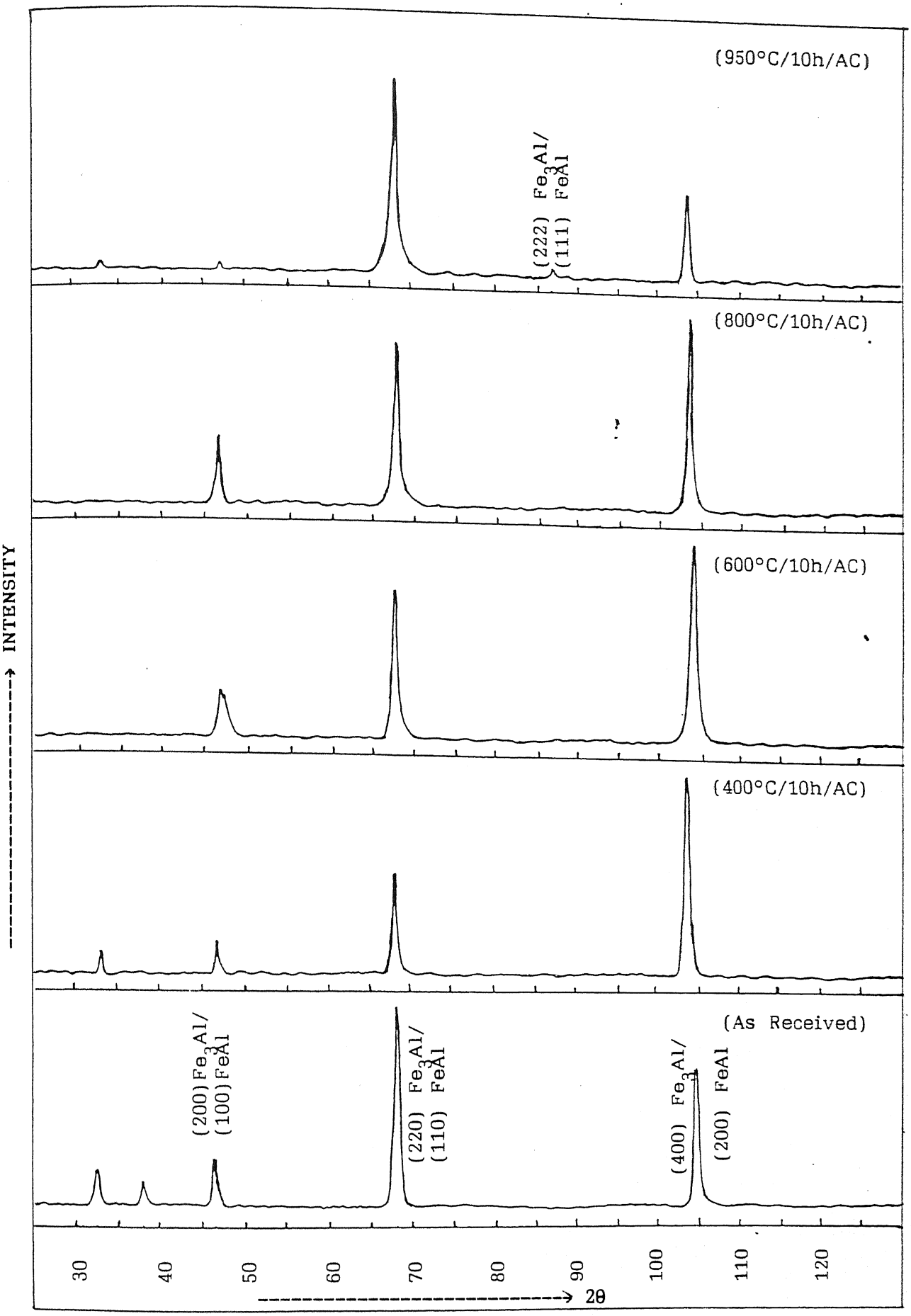

Fig. 4.22 : X-ray diffraction pattern of Fe-28% Al - 5% Cr alloy on MP

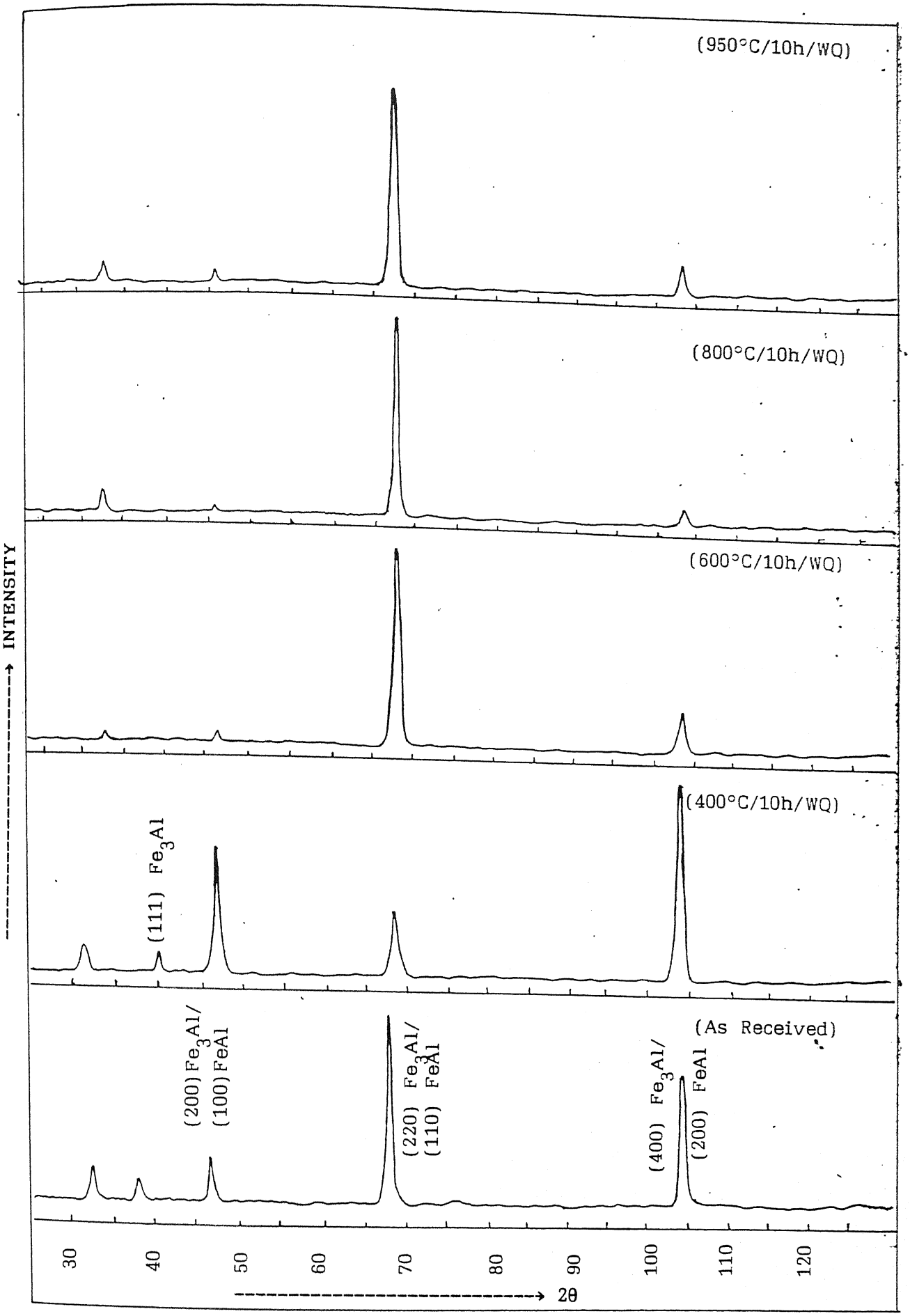

Fig. 4.23 : X-ray diffraction pattern of Fe-28% Al - 5% Cr alloy on MR

In addition to these tables, X-ray diffraction patterns are also presented in a graphical form in Fig.4.20, 4.21, 4.22 and 4.23 for easy comprehension.

4.2.4.(a) Effect of heat treatment on diffraction patterns ofeach sample:

In case of rolling plane x-ray diffraction patterns of both water quenched and air cooled alloys [Fig.4.21 and 4.20], (220) Fe_3Al peak is strongest and (400) Fe_3Al peak is another strong peak in all cases. (200) peak of Fe_3Al weakens as the alloy is annealed. In case of sample subjected to annealing treatment 400°C/10h/WQ, (400) peak of Fe_3Al is stronger than (220) Fe_3Al peak on RP.

Now considering mid plane x-ray diffraction patterns in case of air cooled alloys, we find that (220) peak of Fe_3Al is strongest in as received condition and in case of alloy annealed at 950°C for 10 hour. At all other annealing temperatures (400) peak of Fe_3Al is strongest. In all cases, one of (220) and (400) peak of Fe_3Al is strongest and other is next in strength. (220) peak of Fe_3Al, which was significant in all cases, becomes negligibly weak for alloy annealed at 950°C. At 950°C, only two peaks (220) and (400) Fe_3Al are present practically.

In case of mid plane x-ray diffraction patterns of water quenched alloys [Fig.4.23], (220) peak of Fe_3Al is strongest in all cases except for alloy annealed at 400°C for 10 hour. For this alloy, (400) Fe_3Al peak is strongest and (200) Fe_3Al peak is next strong peak which is a very unusual observation. Diffraction patterns of alloys annealed at 800°C and 950°C are quite similar.

In both cases, only (220) peak of Fe_3Al is significant.

4.2.4(b) Differences between X-ray diffraction patterns of various samples:

i) Air cooled alloys on rolling plane and on mid plane: [Fig.4.20 and 4.22]

In as received alloy, diffraction patterns in both cases are similar, except that (200) Fe_3Al peak is stronger on rolling plane pattern as compared to mid plane patterns. As annealing temperature is raised till 800°C, diffraction patterns in two cases are quite different. In case of rolling plane x-ray diffraction patterns, (220) Fe_3Al peak is strongest while in case of mid plane x-ray diffraction patterns, (400) Fe_3Al peak is strongest. As annealing temperature is raised to 950°C, their diffraction patterns become similar to respective as received cases. The (200) Fe_3Al peak strengthens as annealing temperature is raised in case of mid plane x-ray diffraction patterns while the same peak weakens with annealing temperature in case of rolling plane x-ray diffraction patterns.

ii) Water quenched alloys on rolling plane and on mid plane [Fig.4.21 and 4.23]

Diffraction patterns in both cases are quite similar where (220) peak of Fe_3Al is strongest in all cases except for alloys annealed at 400°C for 10 hour. Difference in two cases is observed for alloys annealed at 400°C for 10 hour where (400) peak of Fe_3Al is strongest peak is both cases,but second highest peak in case of mid plane x-ray diffraction pattern is (200) Fe_3Al and in case of rolling plane x-ray diffraction pattern, it is (220) Fe_3Al. In

addition to this (222) peak of Fe_3Al which is present in all cases in rolling plane x-ray diffraction patterns (although in very insignificant amount), is absent in all cases in mid plane x-ray diffraction patterns.

iii) Rolling plane X-ray diffraction patterns for air cooled samples and water quenched samples: [Figs.4.20 and 4.21]

The X-ray diffraction patterns in both cases are quite similar except that (400) Fe_3Al peak is stronger in air cooled samples as compared to water quenched ones. For alloys heat treated at 400^{o}C for 10 hour, a sharp contrast is observed in two cases. In case of water quenched alloy, (400) Fe_3Al and (220) Fe_3Al peaks are highest and second highest peaks and reverse is true for air cooled alloy. In addition to this, (111) and (311) peaks of Fe_3Al are also present in water quenched alloy.

iv) Mid plane X-ray diffraction patterns for air cooled samples and water quenched samples: [Fig.4.22 and 4.23]

X-ray diffraction patterns in both cases are quite similar in as received alloy and in case of alloy annealed at 400^{o}C for 10 hour, except that (200) peak of Fe_3Al is quite strong in case of water quenched alloys. As annealing temperature is raised till 800^{o}C, (220) Fe_3Al peak strengthens to a great extent in case of water quenched alloys while (400) Fe_3Al peak weakens substantially. On the other hand, (400) Fe_3Al peak strengthens in case of air cooled alloys but (220) peak of Fe_3Al is also a prominent peak in this case.

4.2.5 Fe - 28% Al - 5% Cr - 5% Zr - 0.05% C Alloy

For this alloy also, diffraction patterns were taken on both rolling plane as well on mid plane.

4.2.5.1 Tables for X-ray Diffraction patterns on Rolling Plane:

Table 4.12 (i) : As received sample.

2θ	θ	I	I/I_{max}	d(Å)	(h k l)
31.0	15.50	15.0	20.0	4.29	---
32.5	16.25	16.0	22.0	4.09	---
39.5	19.75	18.0	24.0	3.37	(111) Fe_3Al
46.5	23.25	26.0	35.0	2.90	(200) Fe_3Al/(100) FeAl
58.0	25.0	14.0	19.0	2.36	(422) Fe_3Zr
60.0	30.0	15.0	20.0	2.29	(511, 333) Fe_3Zr
68.0	34.00	74.0	100.0	2.048	(220) Fe_3Al/(110) FeAl
86.5	43.25	24.0	32.0	1.67	(222) Fe_3Al/(111) FeAl
104.0	52.00	60.0	81.0	1.45	(400) Fe_3Al/(200) FeAl/ (800) Fe_3Zr

Table 4.12 (ii) (a): Sample heat treated at 400°C for 10 hour followed by Air Cooling.

2θ	θ	I	I/I_{max}	d(Å)	(h k l)
40.5	20.25	8.5	5.8	3.31	(111) Fe_3Al
46.5	23.25	7.0	4.8	2.90	(200) Fe_3Al/(100) FeAl
60.0	30.00	25.0	3.4	2.29	(511,333) Fe_3Zr
68.0	34.00	146.0	100.0	2.048	(220) Fe_3Al/(110) FeAl
86.5	43.25	12.5	8.56	1.67	(222) Fe_3Al/(111) FeAl
104.5	52.00	63.5	43.5	1.45	(400) Fe_3Al/(200) FeAl/ (800) Fe_3Zr

Table 4.12 (ii) (b): Sample heat treated at 400°C for 10 hour followed by Water Quenching.

2θ	θ	I	I/I_{max}	d(Å)	(h k l)
33.0	16.50	10.0	9.50	4.09	---
40.0	20.0	32.5	30.5	3.35	(111) Fe_3Al
46.5	23.25	11.0	10.40	2.90	(200) Fe_3Al/(100) FeAl
58.5	29.25	3.0	3.0	2.35	(422) Fe_3Zr
60.0	30.00	4.5	4.2	2.29	(511,333) Fe_3Zr
68.0	34.00	106.0	100.00	2.048	(220) Fe_3Al/(110) FeAl
86.5	43.25	5.0	8.5	1.68	(222) Fe_3Al/(111) FeAl
104.5	52.25	59.0	55.7	1.45	(400) Fe_3Al/(200) FeAl/ (800) Fe_3Zr)

Table 4.12 (iii) (a): Sample heat treated at 600°C for 10 hour followed by Air Cooling.

2θ	θ	I	I/I_{max}	d(Å)	(h k l)
46.0	23.00	9.0	8.5	2.90	(200) Fe_3Al/(100) FeAl
58.5	29.25	2.0	1.9	2.36	(422) Fe_3Zr
60.0	30.00	3.0	2.8	2.29	(511,333) Fe_3Zr
68.0	34.00	106.0	100.0	2.048	(220) Fe_3Al/(110) FeAl
86.5	43.25	14.0	13.2	1.67	(222) Fe_3Al/(111) FeAl
104.0	52.00	83.0	78.3	1.45	(400) Fe_3Al/(200) FeAl/ (800) Fe_3Zr

Table 4.12 (iii) (b): Sample heat treated at 600°C for 10 hour followed by Water Quenching.

2θ	θ	I	I/I_{max}	d(Å)	(h k l)
46.5	23.25	13.0	14.80	2.90	(200) Fe_3Al/(100) FeAl
60.0	30.00	9.0	10.2	2.29	(511,333) Fe_3Zr
68.0	34.00	88.0	100.00	2.048	(220) Fe_3Al/(110) FeAl
86.5	43.25	18.5	21.00	1.67	(222) Fe_3Al/(111) FeAl
104.0	52.00	67.5	76.7	1.45	(400) Fe_3Al/(200) FeAl/ (800) Fe_3Zr

Table 4.12 (iv) (a): Sample heat treated at 800°C for 10 hour followed by Air Cooling.

2θ	θ	I	I/I_{max}	d(Å)	(h k l)
46.5	23.25	2.0	2.0	2.90	(200) Fe_3Al/(100) FeAl
60.0	30.0	3.0	3.1	2.29	(511, 333) Fe_3Zr
68.0	34.00	96.0	100.0	2.048	(220) Fe_3Al/(110) FeAl
86.5	43.25	8.0	8.33	1.67	(222) Fe_3Al/(111) FeAl
104.0	52.00	50.0	52.0	1.45	(400) Fe_3Al/(200) FeAl/ (800) Fe_3Zr

Table 4.12 (iv) (b): Sample heat treated at 800°C for 10 hour followed by Water Quenching.

2θ	θ	I	I/I_{max}	d(Å)	(h k l)
46.5	23.25	5.5	4.20	2.90	(200) Fe_3Al/(100) FeAl
60.0	30.00	6.5	5.0	2.29	(511,333) Fe_3Zr
68.0	34.00	130.0	100.00	2.048	(220) Fe_3Al/(110) FeAl
86.5	43.25	6.5	5.00	1.67	(222) Fe_3Al/(111) FeAl
104.0	52.00	39.0	30.0	1.45	(400) Fe_3Al/(200) FeAl/ (800) Fe_3Zr

Table 4.12 (v) (a): Sample heat treated at 950°C for 10 hour followed by Air Cooling.

2θ	θ	I	I/I_{max}	d(Å)	(h k l)
32.0	16.00	8.0	8.0	4.09	---
46.5	23.25	6.0	6.0	2.90	(200) Fe_3Al/(100) FeAl
60.0	30.00	5.0	5.0	2.29	(511,333) Fe_3Zr
68.0	34.00	99.5	100.0	2.048	(220) Fe_3Al/(110) FeAl
86.5	43.25	7.5	7.5	1.67	(222) Fe_3Al/(111) FeAl
104.0	52.00	53.0	53.0	1.45	(400) Fe_3Al/(200) FeAl/ (800) Fe_3Zr

Table 4.12 (v) (b): Sample heat treated at 950°C for 10 hour followed by Water Quenching.

2θ	θ	I	I/I_{max}	d(Å)	(h k l)
46.5	23.25	8.5	8.70	2.90	(200) Fe_3Al/(100) FeAl
60.0	30.00	6.0	6.10	2.29	(511,333) Fe_3Zr
68.0	34.00	98.0	100.00	2.048	(220) Fe_3Al/(110) FeAl
86.5	43.25	8.0	8.20	1.67	(222) Fe_3Al/(111) FeAl
104.0	52.00	49.0	50.0	1.45	(400) Fe_3Al/(200) FeAl/ (800) Fe_3Zr

4.2.5.2 Tables for X-ray diffraction patterns on mid plane:

Table 4.13 (i): As received sample.

2θ	θ	I	I/I_{max}	d(Å)	(h k l)
28.0	14.00	13.0	10.30	4.73	---
31.0	15.50	17.0	13.50	4.29	---
43.5	21.75	14	11.00	3.09	---
46.5	23.25	69.0	55.00	2.90	(200) Fe_3Al/(100) FeAl
58.5	29.25	15.0	11.90	2.36	(422) Fe_3Zr
60.0	30.00	15.0	11.90	2.29	(511,333) Fe_3Zr
66.0	33.00	13.5	10.70	2.10	(440) Fe_3Zr
68.0	34.00	19.0	15.10	2.048	(220) Fe_3Al/(110) FeAl
86.5	43.25	12.5	9.5	1.67	(222) Fe_3Al/(111) FeAl
95.5	47.75	11.0	8.7	1.547	(731, 553) Fe_3Zr
104.5	52.25	126.0	100.0	1.45	(400) Fe_3Al/(200) FeAl/ (800) Fe_3Zr

Table 4.13 (ii) (a): Sample heat treated at 400°C for 10 hour followed by Air Cooling.

2θ	θ	I	I/I_{max}	d(Å)	(h k l)
40.5	20.25	18.5	12.17	3.30	(111) Fe_3Al
46.5	23.25	39.5	26.0	2.90	(200) Fe_3Al/(100) FeAl
68.0	34.00	19.5	12.8	2.048	(220) Fe_3Al/(110) FeAl
86.5	43.25	9.0	6.0	1.67	(222) Fe_3Al/(111) FeAl
104.5	52.25	152.0	100.0	1.45	(400) Fe_3Al/(200) FeAl/ (800) Fe_3Zr

Table 4.13 (ii) (b): Sample heat treated at 400°C for 10 hour followed by Water Quenching.

2θ	θ	I	I/I_{max}	d(Å)	(h k l)
31.0	15.50	13.5	5.10	4.28	---
40.0	20.00	31.5	12.00	3.35	(111) Fe_3Al
46.5	23.25	60.0	22.60	2.90	(200) Fe_3Al/(100) FeAl
58.0	29.00	4.0	1.50	2.36	(422) Fe_3Zr
60.0	30.0	3.0	1.0	2.29	(511,333) Fe_3Zr
68.0	34.00	41.0	15.50	2.048	(220) Fe_3Al/(110) FeAl
86.5	43.25	5.5	2.1	1.67	(222) Fe_3Al/(111) FeAl
104.5	52.25	265.0	100.0	1.45	(400) Fe_3Al/(200) FeAl/ (800) Fe_3Zr

Table 4.13 (iii) (a): Sample heat treated at 600°C for 10 hour followed by Air Cooling.

2θ	θ	I	I/I_{max}	d(Å)	(h k l)
46.5	23.25	15.5	10.6	2.90	(200) Fe_3Al/(100) FeAl
60.0	30.00	2.0	1.37	2.29	(511,333) Fe_3Zr
68.0	34.00	25.5	17.5	2.048	(220) Fe_3Al/(110) FeAl
104.5	52.25	146.0	100.0	1.45	(400) Fe_3Al/(200) FeAl/ (800) Fe_3Zr

Table 4.13 (iii) (b): Sample heat treated at 600°C for 10 hour followed by Water Quenching.

2θ	θ	I	I/I_{max}	d(Å)	(h k l)
40.0	20.00	24.0	12.60	3.35	(111) Fe_3Al
46.5	23.25	56.5	29.70	2.90	(200) Fe_3Al/(100) FeAl
60.0	30.00	5.5	2.90	2.29	(511,333) Fe_3Zr
68.0	34.00	11.5	6.00	2.048	(220) Fe_3Al/(110) FeAl
86.5	43.25	20.0	10.5	1.67	(222) Fe_3Al/(111) FeAl
104.0	52.00	190.0	100.0	1.45	(400) Fe_3Al/(200) FeAl/ (800) Fe_3Zr

Table 4.13 (iv) (a): Sample heat treated at 800°C for 10 hour followed by Air Cooling.

2θ	θ	I	I/I_{max}	d(Å)	(h k l)
40.0	20.0	18.0	10.2	3.35	(111) Fe_3Al
46.5	23.25	34.5	20.0	2.90	(200) Fe_3Al/(100) FeAl
58.0	29.00	4.0	2.3	2.36	(422) Fe_3Zr
60.0	30.00	1.5	0.85	2.29	(511,333) Fe_3Zr
68.0	34.00	22.5	12.8	2.048	(220) Fe_3Al/(110) FeAl
86.5	43.25	11.0	6.25	1.67	(222) Fe_3Al/(111) FeAl
104.5	52.25	176.0	100.0	1.45	(400) Fe_3Al/(200) FeAl/ (800) Fe_3Zr

Table 4.13 (iv) (b): Sample heat treated at 800°C for 10 hour followed by Water Quenching.

2θ	θ	I	I/I_{max}	d(Å)	(h k l)
46.5	23.25	27.0	24.10	2.90	(200) Fe_3Al/(100) FeAl
60.0	30.00	5.0	4.5	2.29	(511,333) Fe_3Zr
68.0	34.00	16.5	14.70	2.048	(220) Fe_3Al/(110) FeAl
86.5	43.25	7.5	6.7	1.67	(222) Fe_3Al/(111) FeAl
104.0	52.00	112.0	100.0	1.45	(400) Fe_3Al/(200) FeAl/ (800) Fe_3Zr

Table 4.13 (v) (a): Sample heat treated at 950°C for 10 hour followed by Air Cooling.

2θ	θ	I	I/I_{max}	d(Å)	(h k l)
46.5	23.25	9.0	12.76	2.90	(200) Fe_3Al/(100) FeAl
60.0	30.00	1.0	1.4	2.29	(511,333) Fe_3Zr
68.0	34.00	37.0	52.5	2.048	(220) Fe_3Al/(110) FeAl
86.0	43.00	1.0	1.4	1.67	(222) Fe_3Al/(111) FeAl
104.5	52.25	70.5	100.0	1.45	(400) Fe_3Al/(200) FeAl/ (800) Fe_3Zr

Table 4.13 (v) (b): Sample heat treated at 950°C for 10 hour followed by Water Quenching.

2θ	θ	I	I/I_{max}	d(Å)	(h k l)
46.5	23.25	27.5	20.80	2.90	(200) Fe_3Al/(100) FeAl
60.0	30.00	3.5	2.65	2.29	(511,333) Fe_3Zr
68.0	34.00	93.0	70.50	2.048	(220) Fe_3Al/(110) FeAl
86.5	43.25	3.0	2.3	1.67	(222) Fe_3Al/(111) FeAl
104.0	52.00	132.0	100.0	1.45	(400) Fe_3Al/(200) FeAl/ (800) Fe_3Zr

X-ray diffraction results are also given in a graphical form in Fig. 4.24, 4.25, 4.26 and 4.27 for easy comprehension.

4.2.5(a) Effect of heat treatment on diffraction patterns of each sample:

In case of rolling plane x-ray diffraction pattern of both air cooled and water quenched alloys [Fig.4.24 and 4.25] annealing treatments do not seem to have any significant effect. In all cases, (220) peak of Fe_3Al is strongest and (400) Fe_3Al peak is next strong peak.

In case of mid plane x-ray diffraction patterns, (400) Fe_3Al peak is strongest in all cases. (220) peak of Fe_3Al strengthens as annealing temperature is raised. (200) Fe_3Al peak weakens with increasing annealing temperature in case of air cooled samples while reverse is the case for water quenched ones.

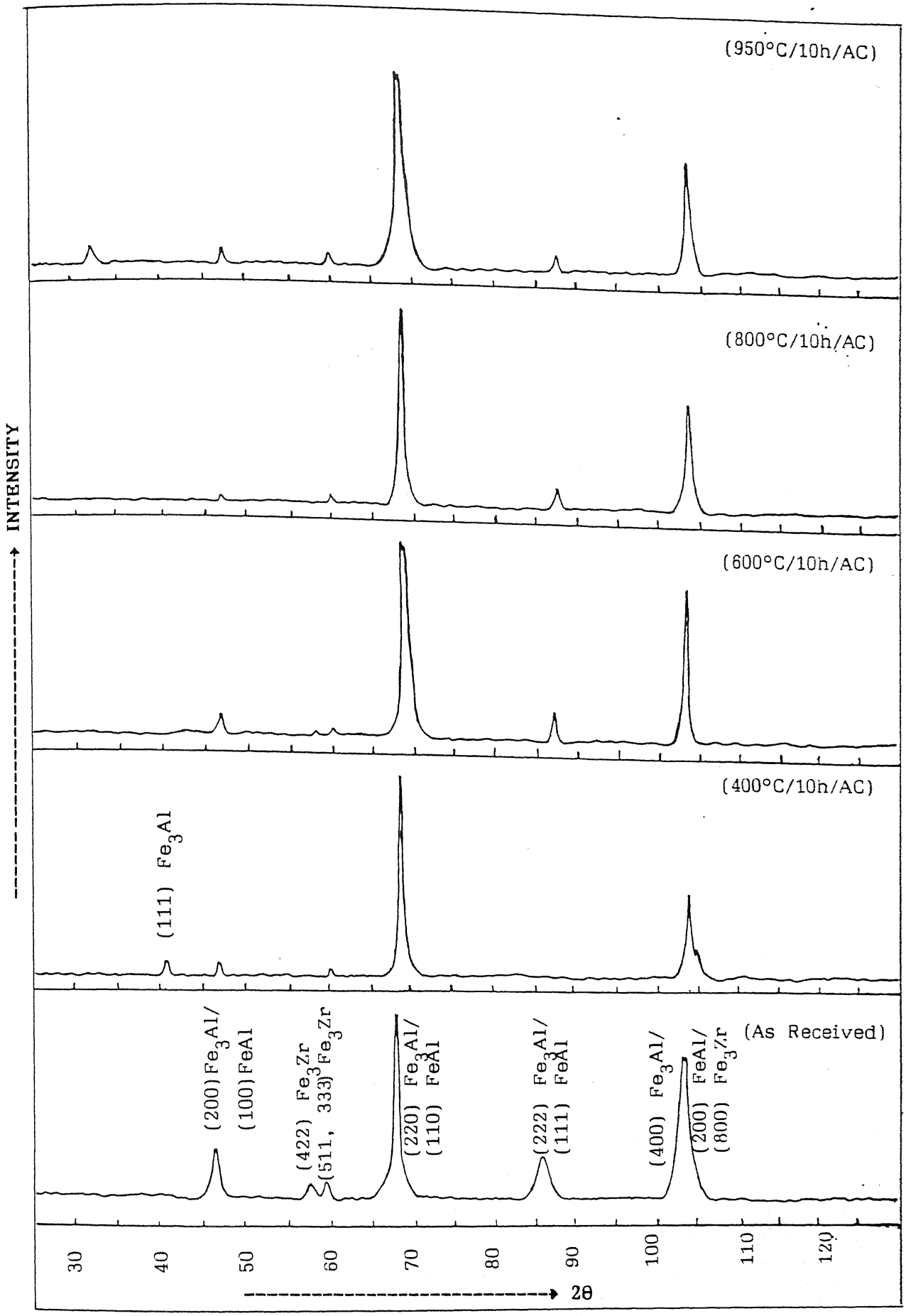

Fig. 4.24 : X-ray diffraction pattern of Fe-28% Al - 5% Cr - 5% Zr - 0.05% C alloy on RP

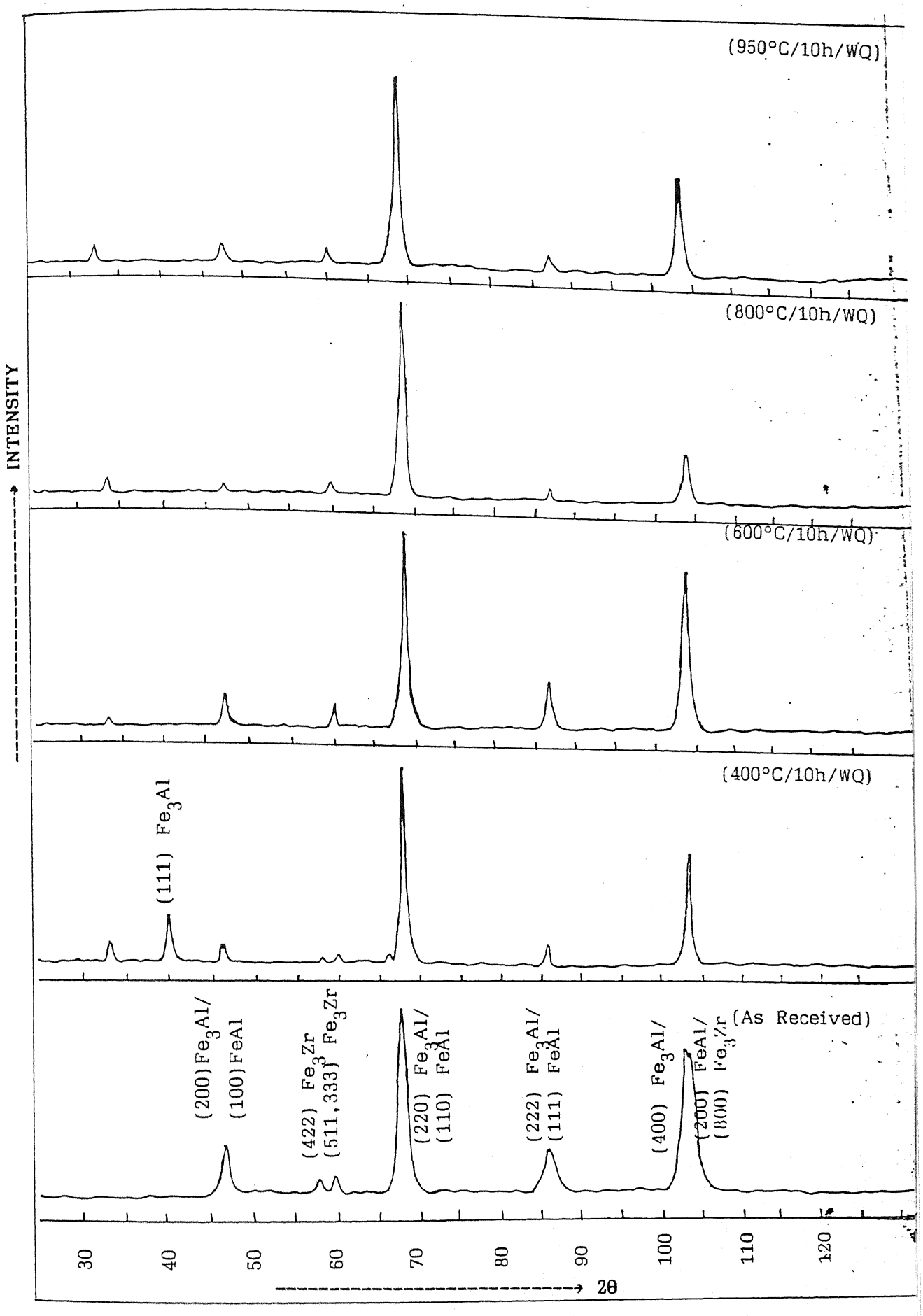

Fig. 4.25 : X-ray diffraction pattern of Fe-28% Al - 5% Cr - 5% Zr

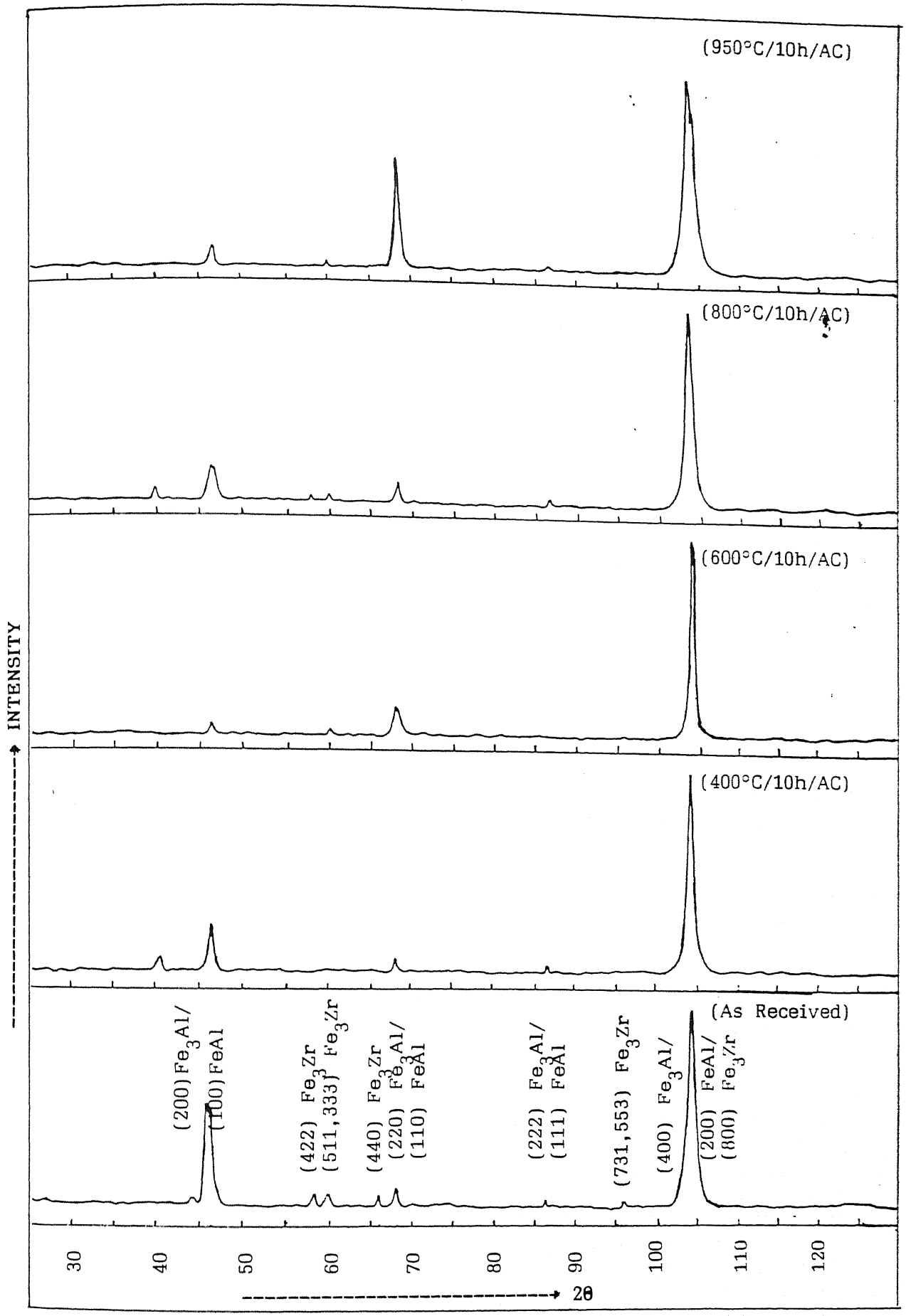

Fig. 4.26 : X-ray diffraction pattern of Fe-28% Al - 5% Cr - 5% Zr - 0.05% C alloy on MP

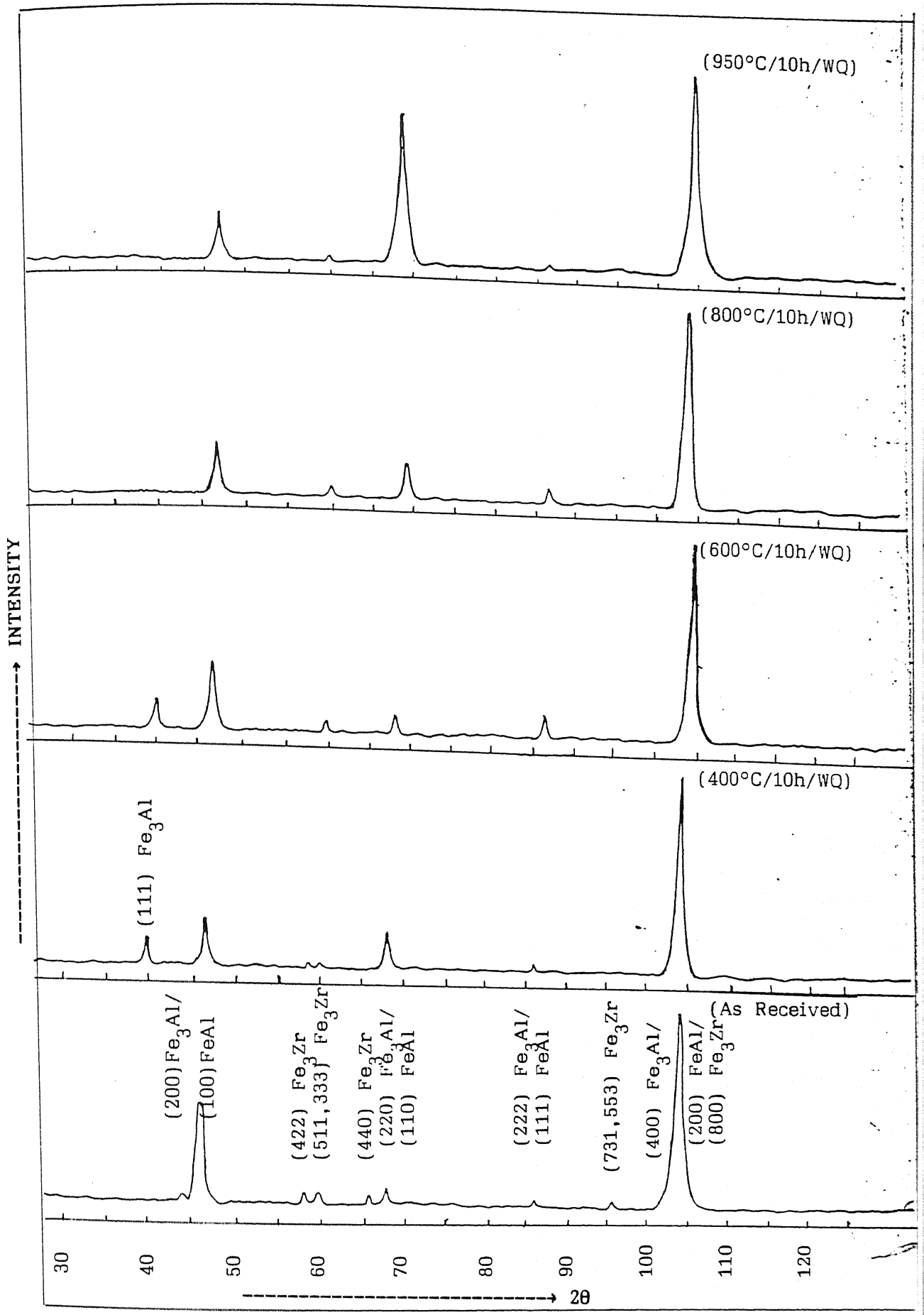

Fig. 4.27 : X-ray diffraction pattern of Fe-28% Al - 5% Cr - 5% Zr

Other peaks present in all cases (although they are very weak in nature) are (222) peak of Fe_3Al, (422), (511) and (333) peaks of Fe_3Zr etc.

4.2.5(b) Differences between X-ray diffraction patterns of various samples:

i) Air cooled alloys on rolling plane and on mid plane: [Fig.4.24 and 4.26].

In case of rolling plane x-ray diffraction patterns, (220) peak of Fe_3Al is strongest while (400) Fe_3Al peak is another prominent peak in all cases. On the other hand, (400) Fe_3Al peak is strongest in mid plane x-ray diffraction patterns and is the only strong peak in case of alloys annealed at 400^oC, 600^oC and 800^oC for 10 hours. In the as received alloy (200) Fe_3Al peak and in 950^oC/10h/AC alloy (220) Fe_3Al peak are other prominent peaks. As annealing temperature is raised, (200) peak of Fe_3Al and (422), (511), (333) peaks of Fe_3Al weaken.

ii) Water quenched alloy are rolling plane and on mid plane: [Fig.4.25 and 4.27]

In rolling plane x-ray diffraction patterns, (220) peak of Fe_3Al is strongest while (400) peak of Fe_3Al is another prominent peak which weakens slightly as annealing temperature is increased. In contrast to above, (400) Fe_3Al peak is strongest in mid plane x-ray diffraction patterns and (220) Fe_3Al peak, which was insignificant at low annealing temperatures, strengthens as annealing temperature is increased in both cases.

iii) Rolling plane X-ray diffraction patterns for air cooled samples and water quenched samples: [Fig.4.24 and 4.25]

X-ray diffraction patterns for two cases are almost exactly similar except for few low intensity peaks [(222) peak of Fe_3Al in case of alloy annealed at 400°C for 10 hour].

iv) Mid plane X-ray diffraction patterns for air cooled samples and water quenched samples: [Fig.4.26 and 4.27]

X-ray diffraction patterns for the two cases are very similar.

4.3 RESULTS OF SEM AND EDAX ANALYSIS

Scanning electron micrographs of the alloys are shown in Fig.4.28(a,b). From SEM micrographs as well as from their EDAX analysis, it is clear that Fe - 28%Al and Fe - 28%Al - 5%Cr alloys are single phase while Fe - 28%Al - 5%Cr - 5%Zr - 0.05%C alloy is a double phase alloy. EDAX analysis was done at various spots in Fe - 28%Al and Fe - 28%Al - 5%Cr alloys and composition was found to correspond very well with numerical composition of these alloys. There is no preferential precipitation of second phase. Sometimes it is spread all over grain interior and sometimes along grain boundaries in case of third alloy. From scanning electron micrograph [Fig.4.29], it can be observed that second phase got fragmented and aligned in rolling direction during the process of hot and /or warm rolling.

Scanning electron micrographs on both rolling plane and mid plane of Fe - 28% Al - 5% Cr - 5% Zr - 0.05% C alloy subjected to various annealing treatments (400°C/10h/WQ, 600°C/10h/WQ, 800°C/10h/WQ and 950°C/10h/WQ) are shown in Fig.4.30 and Fig.4.31

(a) Fe-28% Al-5% Cr

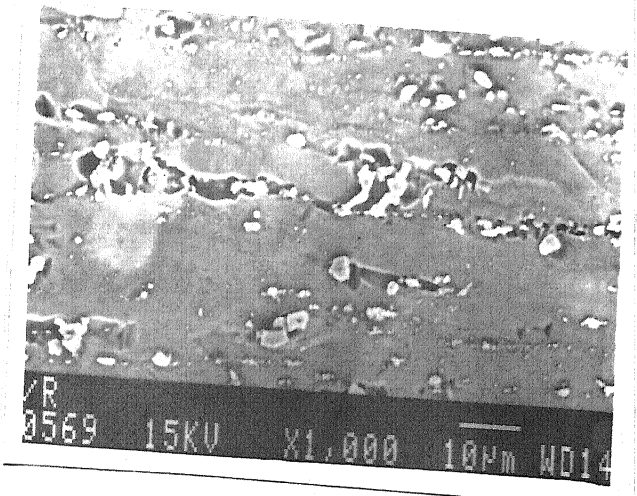

(b) Fe-28% Al-5% Cr-5% Zr-0.05%C

Fig. 4.28: Scanning Electron Micrographs of Alloys in as received condition.

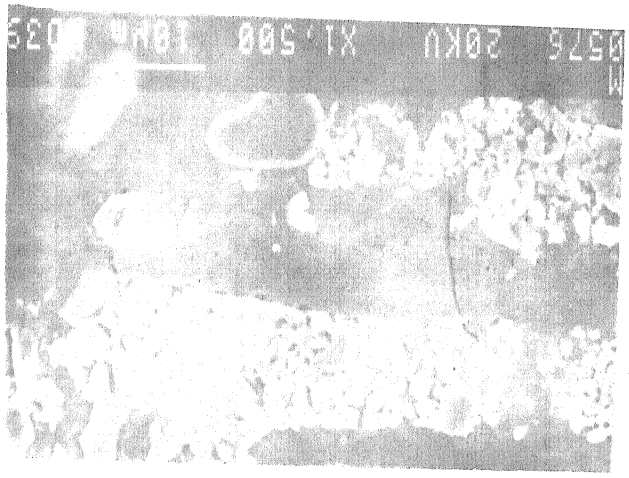

Fig. 4.29: Scanning electron micrograph showing alignment second phase particles of Fe - 28% Al -5% Cr - 5% Zr - 0.05% C alloy.

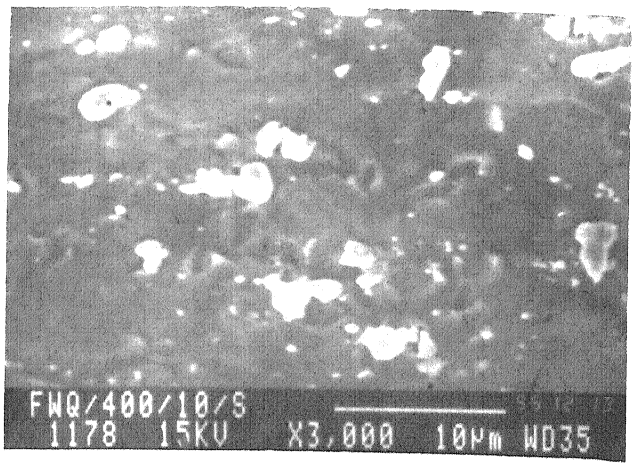

(a)

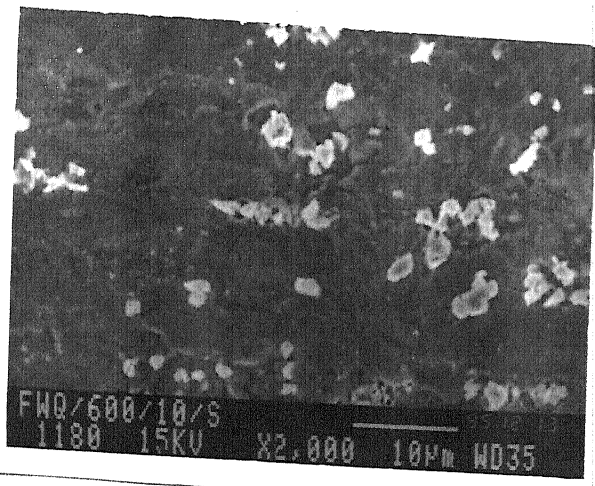

(b)

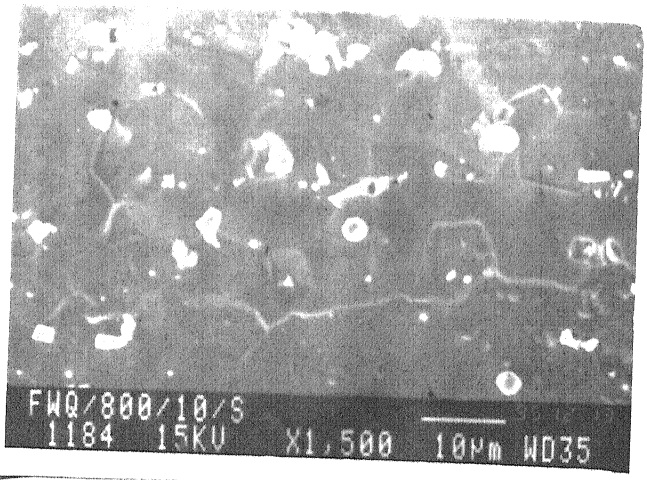

(c)

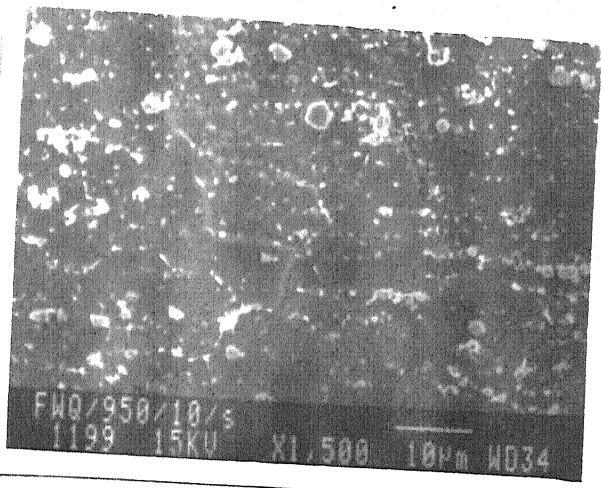

(d)

Fig. 4.30: Scanning electron micrographs of annealed Fe - 23% Al - 5% Cr - 5% Zr - 0.05% C alloy samples taken on rolling plane.

(a) 400°C/10h/WQ (b) 600°C/10h/WQ

(c) 800°C/10h/WQ (d) 950°C/10h/WQ

(a)

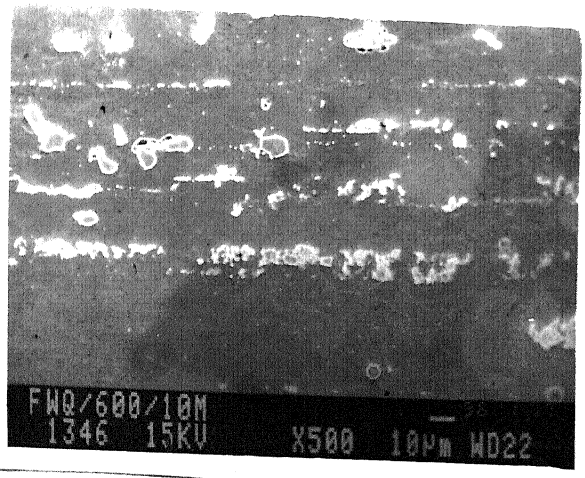

(b)

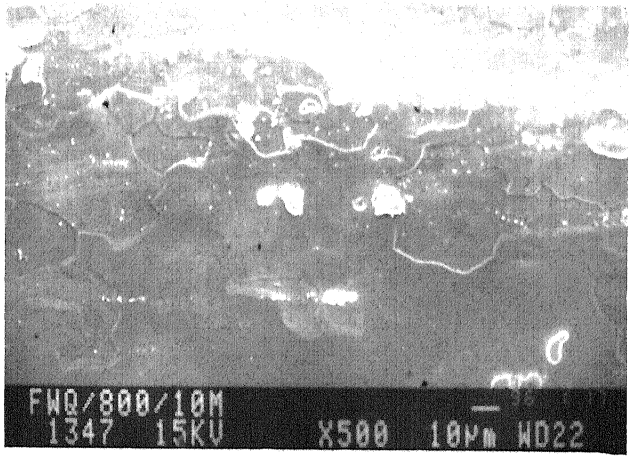

(c)

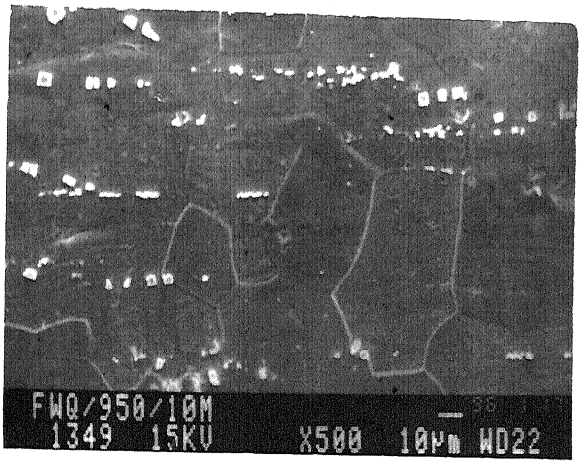

(d)

Fig.4.31: Scanning electron micrographs of annealed Fe - 28% Al - 5% Cr - 5% Zr - 0.05% C alloy samples taken on mid plane.

(a) 400^{o}C/10h/WQ (b) 600^{o}C/10h/WQ

(c) 800^{o}C/10h/WQ (d) 950^{o}C/10h/WQ

Table 4.14 Atomic percentages of various elements in matrix phase in Fe-28% Al - 5% Zr - 0.05% C alloy subjected to various annealing treatments

Element		As Received	400°c/10h		600°C/10h		800°C/10h		950°C/10h	
			AC	WQ	AC	WQ	AC	WQ	AC	WQ
Al	RP	36.71	14.80	15.64	14.75	15.91	9.32	14.17	13.82	15.21
	MP	17.32	14.57	15.38	14.25	16.34	14.48	14.79	14.79	15.25
Cr	RP	4.70	5.68	5.69	5.75	5.43	5.93	5.68	5.70	5.69
	MP	5.43	5.75	5.73	5.67	5.39	5.71	4.43	5.23	5.83
Mn	RP	0.00	0.44	0.21	0.29	0.47	0.60	0.25	0.25	0.15
	MP	0.21	0.31	0.32	0.33	0.25	0.30	0.36	0.25	0.43
Fe	RP	58.28	79.02	78.42	79.57	78.19	84.15	79.91	80.23	78.95
	MP	76.91	79.37	78.49	79.75	78.02	79.51	80.21	79.73	78.46
Zr	RP	0.31	0.06	0.04	0.00	0.00	0.00	0.00	0.00	0.00
	MP	0.13	0.00	0.08	0.00	0.00	0.00	0.21	0.00	0.03

Table 4.15 Atomic percentages of various elements in precipitate phase in Fe-28% Al - 5% Zr - 0.05% C alloy subjected to various annealing treatments

Element		As Received	400°c/10h		600°C/10h		800°C/10h		950°C/10h	
			AC	WQ	AC	WQ	AC	WQ	AC	WQ
Al	RP	28.71	15.02	16.67	19.56	19.61	19.67	15.77	15.16	18.66
	MP	20.12	15.04	12.02	12.55	14.69	13.59	12.25	14.12	11.39
Cr	RP	2.12	3.86	2.63	5.00	3.44	3.5	1.98	3.69	2.98
	MP	2.63	2.59	3.13	3.79	2.69	2.14	3.43	2.03	4.39
Mn	RP	0.00	0.22	0.27	0.22	0.20	0.00	0.08	0.34	0.25
	MP	0.21	0.26	0.23	0.65	0.28	0.12	0.40	0.24	0.27
Fe	RP	39.27	68.34	61.86	72.36	63.12	63.77	61.67	67.49	60.64
	MP	52.21	62.47	63.24	69.06	62.94	50.35	65.24	65.53	64.24
Zr	RP	29.89	12.55	18.57	2.76	13.63	12.98	20.5	13.32	17.47
	MP	24.83	19.84	21.38	13.95	19.40	33.38	18.68	18.08	19.79

respectively. Scanning electron micrographs of air cooled samples are very similar to these of WQ ones. As annealing temperature is raised, recrystallization seems to begin at 600°C followed by growth of recrystallized grains (equiaxed) as annealing temperature is increased. Annealing at various temperature does not seem to effect precipitate phase particles much except that they grow to some extent with annealing temperature.

EDAX analysis was done, on both matrix as well precipitate phases, for Fe - 28%Al - 5%Cr - 5%Zr - 0.05%C alloy subjected to various annealing treatments. Results are presented in following Table 4.14 and 4.15.

From Table 4.14, it can be observed that average matrix composition (at%) of all Fe - 28%Al - 5%Cr - 5%Zr - 0.05%C alloys (subjected to various annealing treatments) is as follows:

Al = 13 - 15%

Cr = 5 - 6%

Mn = 0.25 - 0.35%

Fe = 78 - 80%

Zr = 0.10%

Not much variation was observed in matrix phase composition as annealing temperature is increased, only exception being composition of as received alloy taken on rolling plane which showed abnormally high percentage of Al.

From Table 4.15 average composition (at%) of precipitate phase comes out to be:

Al = 11 - 21%

Cr = 2 - 5%

Mn = 0.0 - 0.3%

Fe = 60 - 70%

Zr = 15 = 25%

Composition of precipitate phase was observed to vary as annealing temperature is changed. In general, Al and Fe percentage were higher on rolling plane as compared to mid plane in all cases with one or two exceptions while Zr percentage was higher on mid plane. Zr percentage was very high in case of 800°C/10h/AC/MP alloy and as received/RP alloy while in case of 600°C/10h/AC/RP, it was exceptionally low (2.76%). A large variation in composition was observed in as received alloy and alloys in annealed condition e.g. Al and Zr content tended to decrease while that of Fe was observed to increase substantially.

4.4 RESULTS OF D.S.C. ANALYSIS

The D. S. C. patterns from the three alloys are shown in Fig.4.32(a), (b) and (c). Fig.4.32(a) shows that there is wide exothermic hump ranging from room temperature to around 600°C. Recrystallization in this alloy was found to start at around 550°C. Therefore this hump can be associated with the pre-recrystallization stage. The endothermic peak at around 600°C may be associated with the phase transformation from DO_3 to B2 in this alloy about this temperature. The rising curve beyond 600°C going upto 1100°C can be associated with recrystallization.

The D. S. C. patterns for the alloys Fe - 28% Al - 5% Cr and Fe - 28% Al - 5% Cr - 5% Zr - 0.05% C are rather similar in shape and these are quite different from that of the binary Fe -28% Al alloy. In both of them a low intensity exothermic hump is followed

by an exothermic peak, then a small endothermic depression to be followed again by an exothermic hump (in case of Fe - 28%Al - 5%Cr) and an exothermic peak (in case of the Fe - 28%Al - 5%Cr - 5%Zr - 0.05%C).

The positions of the elevations and depressions vis-a-vis the temperatures again indicate that here also clear out indication of recovery, then a transformation from DO_3 to B2 and finally the recrystallization of the alloys are discernible.

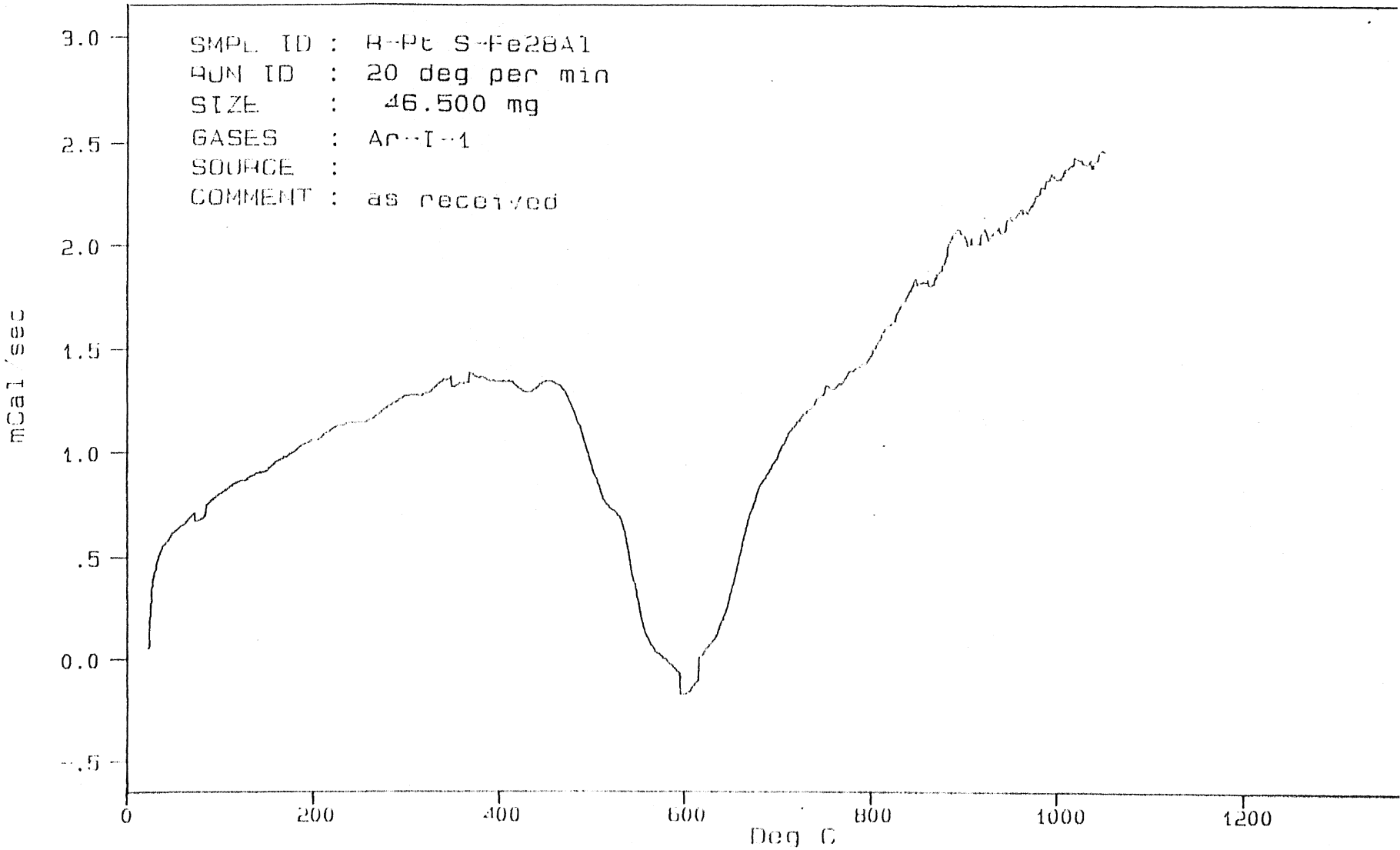

Fig.4.32(a): DSC plot for Fe-28% Al alloy in as received condition.

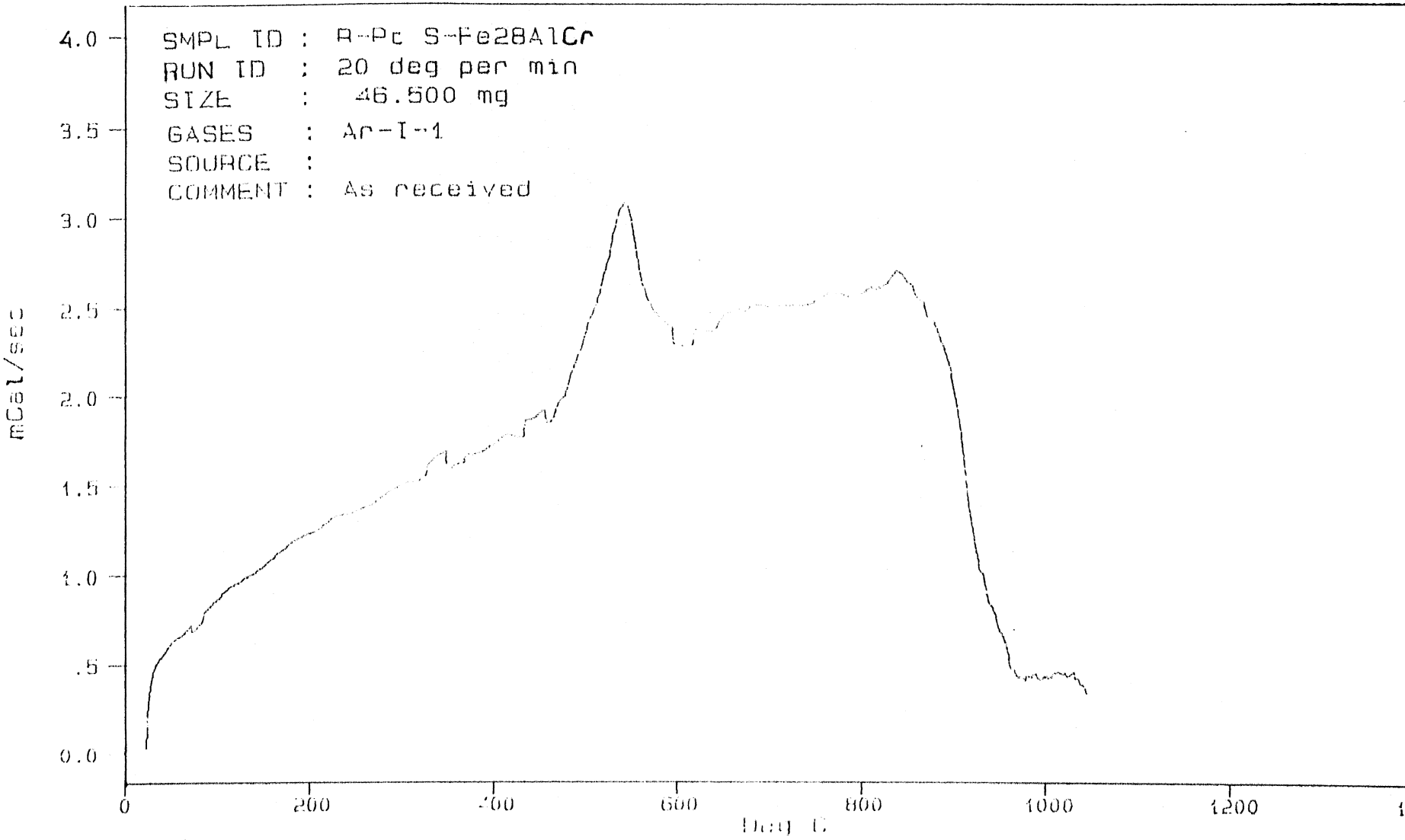

Fig.4.32(b): DSC plot for Fe-28% Al-5% Cr alloy in as received condition.

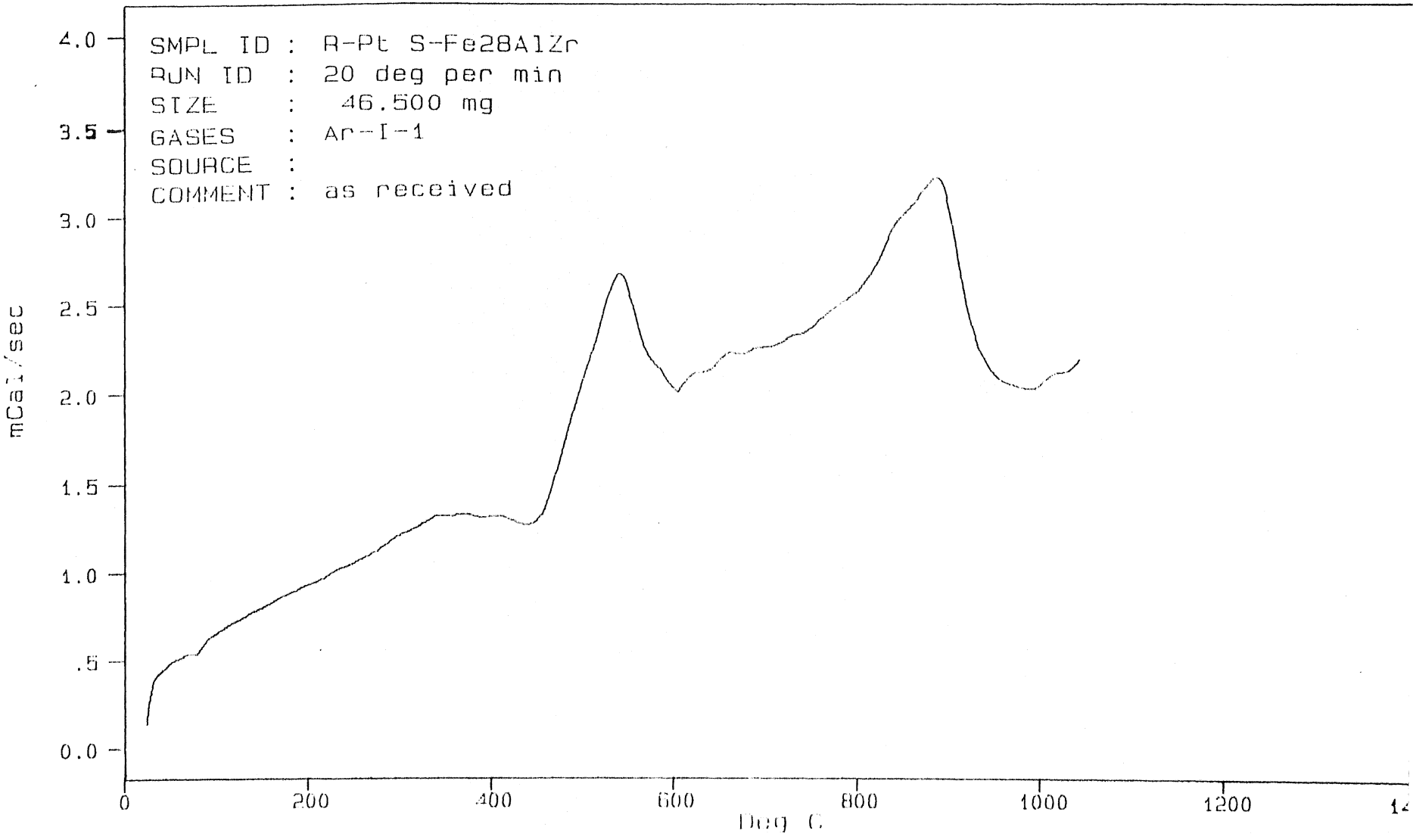

Fig.4.32(c): DSC plot for Fe-28% Al-5% Cr-5% Zr-0.05% C alloy in as received condition.

CHAPTER V

DISCUSSION

SEM, EDAX and optical microscopic analysis have shown that Fe - 28% Al and Fe -28% Al - 5% Cr alloys are single phase while Fe - 28% Al - 5% Cr - 5% Zr - 0.05% C is a double phase alloy. These results are in good agreement with those predicted by Fe - Al and Fe - Al - Cr phase diagram [Fig.2.2 and 2.4]. For both cases, given composition of alloys lies in Fe_3Al ordered phase field at room temperature. On the other hand the Zr containing alloy is evidently made up of two phases-ordered Fe_3Al and another phase which can be represented as Fe_3Zr (as per the results of this investigation).

Grain size in case of third alloy Fe - 28%Al - 5%Cr - 5%Zr - 0.05%C is very small as compared to other two alloys. Thus addition of Zr along with Cr has a strong grain refining effect. This is a well established result. Addition of Zr leads to precipitation of second phase of which, Zr is a major constituent. Presumably, these are second phase particles which lead to the grain refining effect. All the three alloys were annealed at $400^{o}C$, $600^{o}C$, $800^{o}C$ and $950^{o}C$ for 10 hours. As stated in earlier chapter, recrystallization (in matrix phase in case two phase alloy) begins at temperature slightly below $600^{o}C$. From Fe - Al phase diagram, we observe that $DO_3 \longrightarrow B2$ transformation temperature for Fe - 28% Al alloy is $550^{o}C$. Thus, recrystallization seems to begin at $DO_3 \longrightarrow B2$ transformation temperature of Fe - Al phase

diagram in case of all three alloys.

As we go across thickness direction of two phase alloy specimen, it has been found that precipitate phase composition varies while that of matrix phase remains more or less uniform Zr percentage (atomic %) in precipitate phase increases as we go from outer to interior region while Al and Fe % decrease. As a result of annealing, Al and Zr contents of precipitate phase tend to decrease while Fe content was observed to increase. This effect has to be looked into in more detail. This may also indicate that Zr may not have achieved the equilibrium partitioning between the two phases.

In case of the Fe - 28% Al alloy it appears that there is a significant structural anisotropy along the thickness direction. At the rolling surface, majority of (220) plane of Fe_3Al are parallel to rolling plane while at mid plane (central region) majority of (400) planes are parallel to rolling plane. With annealing treatment for 10 hours (followed by air cooling), the material homogenises texturally at annealing temperatures of 600^{o}C and 800^{o}C [in both cases majority of (220) planes are parallel to rolling plane throughout thickness direction). At these temperatures the material lies in the B2 (or $\alpha 2$) ordered phase field in the Fe - Al phase diagram for the Fe - 28% Al alloy. As annealing temperature is raised further (950^{o}C), textural anisotropy reappears. At this temperature the material no longer remains in the B2 (or $\alpha 2$) ordered phase field, but goes to the α Fe phase field. Thus proper annealing treatment is found to provide a means to change the crystallographic texture patterns in this material.

When annealing treatment is followed by water quenching textural patterns across thickness direction becomes similar as annealing temperature is raised to 800°C and above. This may also be explained in a similar manner.

In case of Fe - 28% Al - 5% Cr alloy specimen, in the as received condition, majority of both (220) and (400) planes are parallel to rolling plane throughout the thickness direction [although (220) Fe_3Al peak strength is slightly more than that of (400) Fe_3Al]. There is therefore hardly any anisotropy along the thickness direction. As this specimen is annealed followed by air cooling, there is no change in the texture pattern. In all cases, majority of both (220) and (400) planes are parallel to rolling plane. Slight difference in texture patterns across thickness direction can be supposed to exist in the sense that (220) peak strength is more on rolling plane while (400) peak strength is more on mid plane.Only when the material is annealed to 950°C, texture patterns becomes almost identical along thickness direction.

The scenario is altogether different, when annealed specimen were cooled by water quenching. In this case, material remains texturally isotropic throughout the thickness direction at all annealing treatments. In other words similar x-ray diffraction patterns on the RP as well as on the MP. Both (220) and (400) peaks are strong till the annealing temperature is 600°C. Beyond 600°C (i.e. $\alpha 2$ phase field onwards in Fe - Al phase diagram) the textural pattern of the material changes significantly (most of (220) planes become parallel to rolling plane).

In case of the Fe - 28% Al - 5% Cr - 5% Zr - 0.05% C alloy specimen also, texture patterns differ across thickness direction in the as received condition. On rolling surface, most of the (220) planes are parallel to rolling plane while in the interior most of the (400) planes are parallel to rolling plane. The material appears to be highly textured at the mid plane. When the material is annealed (followed by AC), interior (mid plane) of specimen shows strong tendency to remain highly textured (with most of (400) planes parallel to rolling plane). Only when annealing temperature is raised to 950°C, quite a few (220) planes also come in position parallel to rolling plane. In other words, texture intensity decreases. On the other hand, annealing seems to produce no effect on texture of rolling plane. At all temperatures, most of (220) planes and quite a few (400) planes become parallel to rolling plane. Thus, difference in texture patterns across the thickness direction persists in all cases when annealing treatment is followed by air cooling. Similar trends are observed when annealing treatment is followed by water quenching.

From the above discussion it is quite clear that structural anisotropy across the thickness direction persists in all the three alloys right from the hot rolling stage. Annealing treatments do not appear to remove this anisotropy but seem to change the nature of this anisotropy. Out of the three alloys the Fe - 28% Al - 5% Cr alloy (in as received as well as annealed and air cooled condition) shows the least anisotropy in the thickness direction. In fact the x-ray diffraction patterns taken from both the rolling planes and the mid planes of these samples are to some extent similar to those given in the ASTM files for perfectly

random condition of the alloy. Since these materials are envisaged as new structural materials in future it would be necessary to have as little through thickness anisotropy in them as possible. Although the heat treatments carried out in this investigation have been found to change the texture pattern quite significantly, these do not appear to be effective in producing an isotropic material, structure-wise. Thus further work is necessary in this direction. It is also highly imperative that future work in this direction should also involve detailed texture study using both the pole figure as well as the ODF method. Unfortunately, hardly any such data exists at the present moment.

CHAPTER VI

CONCLUSIONS

1] Fe - 28% Al and Fe -28% Al - 5% Cr are single phase while Fe - 28% Al - 5% Cr -5% Zr - 0.05% C is a dual phase alloy at room temperature. Zirconium added along with chromium to Fe - 28% Al alloy leads to precipitation of the Fe_3Zr phase.

2] Zirconium addition to Fe - 28% Al alloy has a strong grain refining effect.

3] Recrystallization in case of all alloys begins at around 550°C which is the $DO_3 \longrightarrow B2$ transformation temperature in case of binary Fe - 28% Al alloys.

4] Zr content of second phase on the Fe - 28% Al - 5% Cr - 5% Zr - 0.05% C alloy does not seem to achieve the equilibrium partitioning between the two phases during the annealing treatment given.

5] In case of Fe - 28% Al alloy, annealing treatments (600°C/10h/AC, 800°C/10h/AC, 800°C/10h/WQ, 950°C/10h/WQ) seem to make this material strongly textured and thus anisotropic. These texture patterns are also similar across the thickness direction.

6] Fe - 28% Al - 5% Cr alloy is least anisotropic along the thickness direction among all the three alloys in the as received condition. Proper annealing treatments (400°C/10h/AC, 600°C/10h/Ac, 800°C/10h/AC, 950°C/10h/AC) make it more and more isotropic.

7] Texture patterns in case of Fe - 28% Al - 5% Cr - 5% Zr - 0.05% C alloy, differ across the thickness direction and material is anisotropic across the thickness direction. Surface seems to have a nearly random grain orientation while interior is strongly textured. Annealing treatments seem to be ineffective to remove or lessen this anisotropy across thickness direction.

REFERENCES

[1] V. K. Sikka, S. Viswanathan and C. G.Mckamey, "Development and Commercialization Status of Fe_3Al based Intermetallic Alloys" *Oak Ridge National Laboratory*, 1993.

[2] C. G. Mckamey and D. H. Pierce, *Scripta Metallurgica et Materialia*, 28 (1993), 1173 - 1176.

[3] N. S. Stolaff and R. G. Davies, *Acta Metallurgica*, Vol. 12, May (1964), 473 -485.

[4] L.Anthonyand B. Fultz, *Acta Metallurgica et Materialia*, 43 (1995), 3385 - 3891.

[5] W. Justusson, V. F.Zackay and E. R. Morgan, *Transactions of the ASM*, Vol. 49 (1957), 905 - 92.

[6] I. Baker, H. Xiao, O. Klein, C. Nelson and J. D. Whittenberger, *Acta metall. mater.*, Vol.43, (1995), 1723 - 1730.

[7] M. J. Marcinkowski, M. E. Taylor, F. X.Kayser, *Journal of Materials Science*, 10 (1975), 406 - 414.

[8] W. Mao and Z. Sun, *Scripta Metallurgica et. Materialia*, 29 (1993), 217 - 220.

[9] D. Raabe, *Materials Letters*, 19(1994), 75 - 78.

[10] B.D. Cullity, "*Elements of X-ray Diffraction*", Addison - Wesley, 2nd Edision (1978).

[11] R. L. Lawson, D.K.Matlock, C. Krauss, *Metallography*, 13 (1980), 71.

[12] C.T. Liu, C. G. Mckamey,and E.H.Lee, *Scripta Metallurgica et Materialias*, Vol. 24 (1990) 385 - 390.

[13] H.Xiao and I. Baker, *Acta Metallurgica et. Materialia*, Vol.43 (1995), 391 - 396.

[14] K.Yashimi, S.Handa and M. H. Yoo, *Acta Metallurgica et Materialia*, 43 (1995), 4141 - 4151.

[15] H. J. Leamy, F. X. Kayser, M. J. Marcinkowski, *Acta Metallurgica*, (1969), 779 - 798.

[16] X. Wang and J. V. Wood, *Powder Metallurgy*, Vol. 38 (1995), 59.

[17] D. - Q. Yi, C. - H. li, J. - H. Wang, R.Warren, I. Olefjord, *Materials Science and Technology*, Vol. 11, July (1995), 650 - 655.

[18] Robert A.Buckley, Howard Jones, Prakash, C. Michael Sellars, *ISIJ International*, Vol. 31 (1991), 1113 -1126.

[19] W. Yan, *Scripta Metallurgica*, Vol. 21 (1991), 1511

[20] Gautam Ghosh, "Aluminium -Iron - Chromium", *Ternary Alloys: A Comprehensive Compendium of Evaluated Constitutional Data and Phase Diagram*, Edited by G. Petrow and G.Effenberg, Vol.4..

[21] Zoya M.Alakseeva, Aluminium - Iron - Zirconium, *Ternary Alloys: A Comprehensive Compendium of Evaluated Constitutional Data and Phase Diagram*, Edited by G. Petrow and G.Effenberg, Vol.4..

[22] O. Kubaschewski, *Iron - Binary Phase diagrams*, 1982, Springer - Verlag Berlin/Heidelberg, FRG, p.6.

[23] M. G. Mendiratta, S. K.Ehlers, D. K.Chatterjee and H. A.Lipsitt., *Met. Trans. A*, Vol. 18A (1987), 283.

[24] M. J. Marcinkowski, *Electron Microscopy and Strength of Materials*, eds. G. Thomas and J. Washburn, Interscience Publishers, John Wiley and Sons, New York, 1963, p.333.

[25] R. T. Fortrum and D.E. Mikola, *Mater. Sci. Eng.*, Vol. 91 (1987), 223.

[26] C. G. Mckamay and J. A. Hosten, *Met. Trans. A*, Vol.20A (1989),751.

[27] H. Inouye, MRS Symp. Proc., *High Temperature Ordered Intermetallic Alloys*, eds. C. C. Koch, C.T.Liu and N. S. Stoloff, MRS, Pittsburgh, 1985, p.255.

[28] D. G. Morris, M. M. Dadras' and M. A. Morris, *Acta Metall. Mater.*, 41 (1993), 97 - 111.

[29] G. E. Fuchosand, N. S.Stoloff, *Acta Metallurgica*, Vol. 36 (1988).

[30] B. H. Rabin and R. N. Wright, *Metallurgical Transactions A*, Vol. 23A (1992), 35 - 40.

[31] C. G. Mckamay, J. A. Horton and C. T. Liu, MRS Symp. Proc, *High Temperature Ordered Intermetallic Alloys - II*, eds. N.S. Stoloff, C. C. Koch, C. T. Liu and O. Izumi, MRS, Pittsburg, 1987, p.321.

[32] S. Hana, S. Watanbe, T. Sato and O.rumi, *Scripta Met.*, Vol. 15 (1981), 1345.

[33] Y.Umakoshi, M. Yamagudi, Y. Namba and K. Murakami, *Acta Met.*, Vol. 24 (1976), 89.

[34] C. G. Mckamay, C. T.Liu, S. A. David, J.A. Horton and J. V. Calhcart, *Fossil Energy Mat. Prog. Confg. Proc.*, ORNL/FMP - 87/4,August 1987, p.683.

[35] S. H. Wang, C.T.Liu, D. P. Pope and J. O. Steigher: *High Temperature Aluminides and Intermetallics.*

[36] B. G. Gieseke, D.J. Alexander, V. K.Sikka and R. H. Baldwin, *Scripta Metallurgica et. Materialia*, Vol.29 (1993), 129 - 134.

[37] P.G. Sanders, V. K. Sikka, C. R. Howell and R. H. Baldwin, *Scripta Metallurgica et. Materialia*, Vol. 25 (1991), 2365 - 2369.

[38] K. T. Park and E. Goo, *Acta Metall. Mater.*, Vol. 39 (191), 307 - 3035.

[39] A. E. Vidoz, D. P. Lazarevic and R. W. Cahn, *Acta Metallurgica*, Vol. 11 (1963), p. 17.

[40] H. Omato and P. A. Beek, *Met. Trans.*, Vol. 2 (1971), p.569.

[41] L. Zhuang, L. Buckenhout, J. Duszczyk, *Scripta Metallurgica et. Materialia*, Vol. 30(1994), 5 - 8.

[42] C. G. Mckamay, J. H. Devan, P. F.Tortorelli and V. K. Sikka, *J. Mater. Res.*, 6, (8) (1991), 1779 - 1800.